12-2006

Regularization of the Particle-Particle Interaction in the Nuclear Density Functional Theory

Piotr Jerzy Borycki

University of Tennessee - Knoxville

To the Graduate Council:

I am submitting herewith a dissertation written by Piotr Jerzy Borycki entitled "Regularization of the Particle-Particle Interaction in the Nuclear Density Functional Theory." I have examined the final electronic copy of this dissertation for form and content and recommend that it be accepted in partial fulfillment of the requirements for the degree of Doctor of Philosophy, with a major in Physics.

Witold Nazarewicz, Major Professor

We have read this dissertation and recommend its acceptance:

Elbio Dagotto, David Dean, Thomas Papenbrock, Lawrence Townsend

Accepted for the Council:

Carolyn R. Hodges

Vice Provost and Dean of the Graduate School

(Original signatures are on file with official student records.)

To the Graduate Council:
I am submitting herewith a dissertation written by Piotr Jerzy Borycki entitled "Regularization of the Particle-Particle Interaction in the Nuclear Density Functional Theory". I have examined the final electronic copy of this dissertation for form and content and recommend that it be accepted in partial fulfillment of the requirements for the degree of Doctor of Philosophy, with a major in Physics.

Witold Nazarewicz,

Major Professor

We have read this dissertation
and recommend its acceptance:

Elbio Dagotto

David Dean

Thomas Papenbrock

Lawrence Townsend

Accepted for the Council:

Linda Painter

Interim Dean of Graduate Studies

(Original signatures are on file with official student records.)

Regularization of the Particle-Particle Interaction in the Nuclear Density Functional Theory

A Dissertation
Presented for the
Doctor of Philosophy
Degree
The University of Tennessee, Knoxville

Piotr Jerzy Borycki
December 2006

Acknowledgments

First and foremost, I wish to thank my scientific advisor, Witold Nazarewicz, for all the support he gave during my Tennessee years. He was a real mentor - besides teaching how to solve HFB equations and truncate quasiparticle space without doing harm to myself, he also showed me a joy of physics and helped me to master various skills and abilities essential in academic life - and beyond; all in a warm and friendly manner.

Secondly, I would like to thank my close collaborators, Jacek Dobaczewski and Mario Stoitsov, for the numerous interactions. They made me a smarter physisist - but also a better person. In case of Mario - occasionally better fed as well.

Writing this thesis would have been also more difficult without scientific and social support of all people of good will I encountered here in Tennessee. Andrzej Baran, Robert Grzywacz, Nicolas Michel, Janusz Skalski, Andrzej Staszczak, and all other friends too numerous to list - thank you all!

Last but not least, I would like to thank my family, especially my wife, for all the patience with me during the long years apart as I was having fun as a PhD student.

Thank you all!

Abstract

In this work we show how to regularize the ultraviolet divergences appearing in the local pairing term of the energy density functional. Our approach, entirely rooted in the framework of the Density Functional Theory, is based on the regularization of local densities and currents and can be applied to various classes of energy density functionals. We demonstrated, that for the particular choice of the pairing term of energy density functional, our procedure gives the same regularization scheme to the one obtained earlier by the means of the pairing gap regularization.

We also investigated the non-unitarity of the Bogoliubov tranformation due to the energy cutoff in the quasiparticle space. We developed and tested the method of restoring the unitarity of the Bogoliubov transformation. We demonstrated that by applying this method one can perform HFB calculations for significantly lower cutoff energies, without losing accuracy.

Contents

List of Figures

Chapter 1

Motivation and General Introduction

1.1 Nuclear Structure and the Frontier of Exotic Beams Physics

The ultimate goal of nuclear structure is to 'build a unified and comprehensive microscopic framework in which bulk nuclear properties, nuclear excitations, and nuclear reactions can all be described' [1]. During the last 60+ years our understanding of nuclear dynamics has become extensive, but it is still far from being complete, and many fundamental questions remain to be answered microscopically. Among them are [1]:

- How do protons and neutrons make complex nuclei?
- How do simple patterns emerge from nuclear many-body dynamics?
- What is the equation of state[1] of nucleonic matter?

Comprehensive low-energy theory of nuclei would help us to understand the structure of atomic nucleus and answer some crucial questions in other areas of science and technology [1]:

- Detailed understanding of certain nuclear reactions is necessary in order to explain the elemental abundances in the universe and nucleosynthesis processes, as well as star evolution.
- Neutron stars are among the most fascinating astrophysical objects. In order to understand their properties and dynamics, a better understanding of physics of the bulk nuclear matter is required.
- Better understanding of nuclear structure will improve radioisotope-related medical technologies.
- Knowledge of nuclear structure and dynamics is crucial for a reliable description of the aging process of nuclear weapons 'in the era without testing'.
- A more complete understanding of nuclear reactions may enable us to design a new generation of nuclear fission reactors, which are safer and produce less waste.

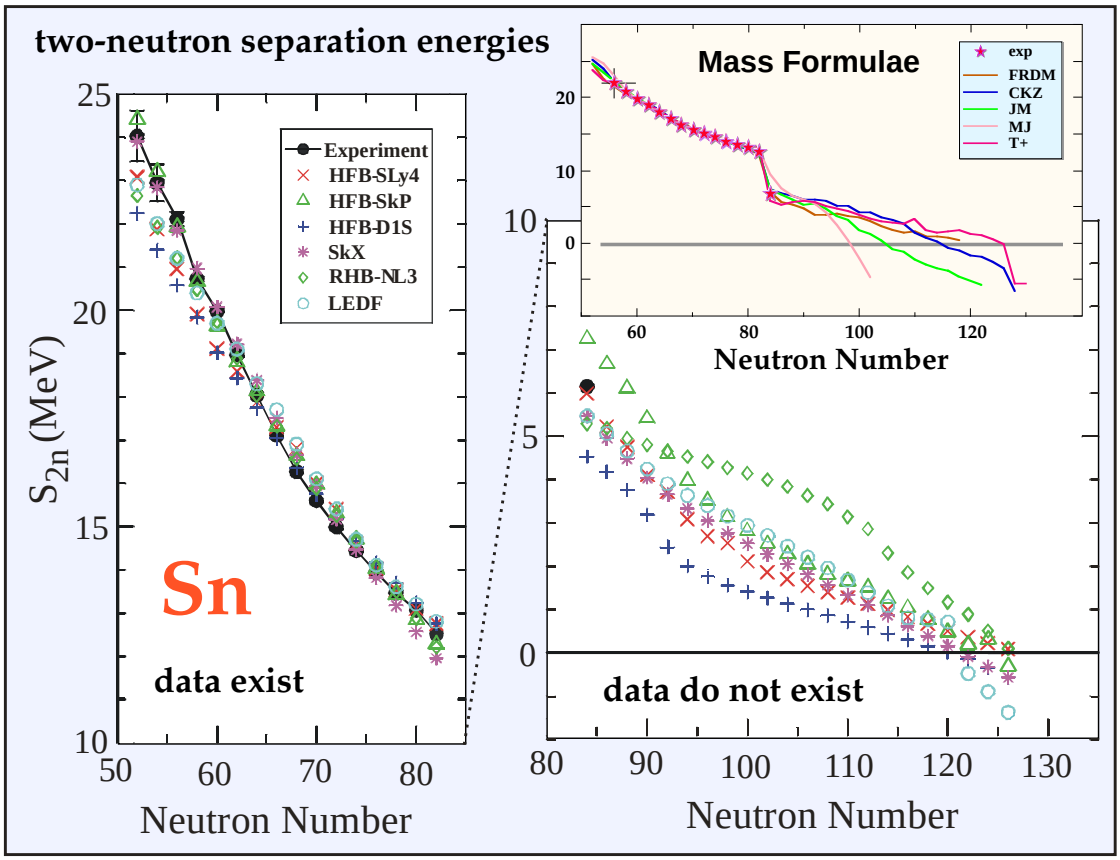

Figure 1.1: Comparison between two neutron separation energies for various Energy Density Functionals (left and lower-right panels), mass formulae (upper-right panel) and experimental data for Sn nuclei. Figure courtesy of W. Nazarewicz.

Until recently, nuclear theory has been dominated by macroscopic and microscopic models, with numerous phenomenologically adjusted parameters. As a result, these models, while giving consistent results for known nuclei in the vicinity of the valley of stability, where experimental data are abundant, often give different predictions for exotic nuclei. A typical example of this situation is illustrated in Fig. 1.1. One can see that various parameterizations of the nuclear energy density functional (EDF) reproduce experimental data well, but give different predictions in the neutron-rich region where there are no experimental data available. However, due to the microscopic character of nuclear Density Functional Theory (DFT), various parameterizations of EDF offer more consistent predictions and comparable root-mean-square (rms) errors for known nuclei compared to purely phenomenological macroscopic mass formulae (see upper-right panel of Fig 1.1). The limited ability of nuclear models to extrapolate may be explained by a very incomplete understanding of some phe-

[1] Equation of state (EOS) (after [2]) - a mathematical relationship between the values of pressure, volume, and temperature of a given substance in thermodynamical equilibrium.

nomena critical to nuclear dynamics; such as nuclear pairing, density and isospin dependence of energy functional, and interplay between collective and single particle degrees of freedom in exotic nuclei.

Consequently, considerable experimental effort is concentrated on gathering data for nuclei with large isospin. Experiments are very challenging because these nuclei are not accessible using well-known techniques employing reactions involving stable target and projectile nuclei. New experimental methods are being developed, which involve two consecutive reactions (secondary beam concept). The first reaction produces the so-called secondary, short-lived beam that is directed at a second target. For example, experiments using exotic beams and the development of radioactive beam techniques constitute a major part of the scientific agenda at the Holifield Radioactive Ion Beam Facility (HRIBF) at the Oak Ridge National Laboratory (ORNL). Moreover, a new generation of experimental facilities such as RIKEN (Japan), GSI (Germany), and RIA (USA) are being designed and built. Experiments at these high-performance laboratories will provide an excellent insight into nuclear dynamics in the unknown regions of the nuclear chart. At the same time, progress in few- and many-body nuclear structure will help us to constrain and improve modern interactions and functionals.

1.2 Brief Overview of the Nuclear Many-Body Problem

The atomic nucleus is a fascinating many-body system that is difficult to solve. Although various powerful many-body methods have been developed for nucleonic systems, their applicability often possess a challenge.

First of all, the atomic nucleus is a finite system that consists of two kinds of strongly interacting Fermions – neutrons and protons. Although for medium-mass and heavy nuclei the number of particles, $A \sim 10^2$, is too large for most *ab-initio* techniques to be computationally feasible, it is too small for a description that can ignore the finite-size effects.

Nucleons in nuclei are effective degrees of freedom for the strong interaction and are strongly correlated. The dynamics of the strong interaction may be described using Quantum Chromo-Dynamics (QCD), which is non-perturbative for energies below $\Lambda_{QCD} \approx 200\,\mathrm{MeV}$. Low-energy approaches to QCD, such as the lattice-QCD, have not yet been successful in providing a low-energy nuclear interaction. Consequently, a derivation of the nuclear interaction coming from the underlying fundamental theory does not exist and even the relevance of nucleonic degrees of freedom is not obvious. More information about constructing the effective nuclear interaction based on the chiral Effective Field Theory (EFT) and on nuclear scattering data can be found in Refs. [3–11].

Finding the ground state and excitations energies *ab-initio* is not feasible for any but the lightest nuclei. Therefore, different approaches are used for heavier systems. Methods used in the low-energy nuclear many-body problem can be roughly classified as (see also Fig. 1.2):

- *Ab-initio* methods [12–15], computationally feasible only for very light systems (e.g. dimension of diagonalized matrices $1.1 \cdot 10^9$ in calculations of ^{11}B [14]). On the other hand, these methods only have limited theoretical uncertainties related to the method themselves, and provide excellent insights into the nuclear dynamics and interaction.

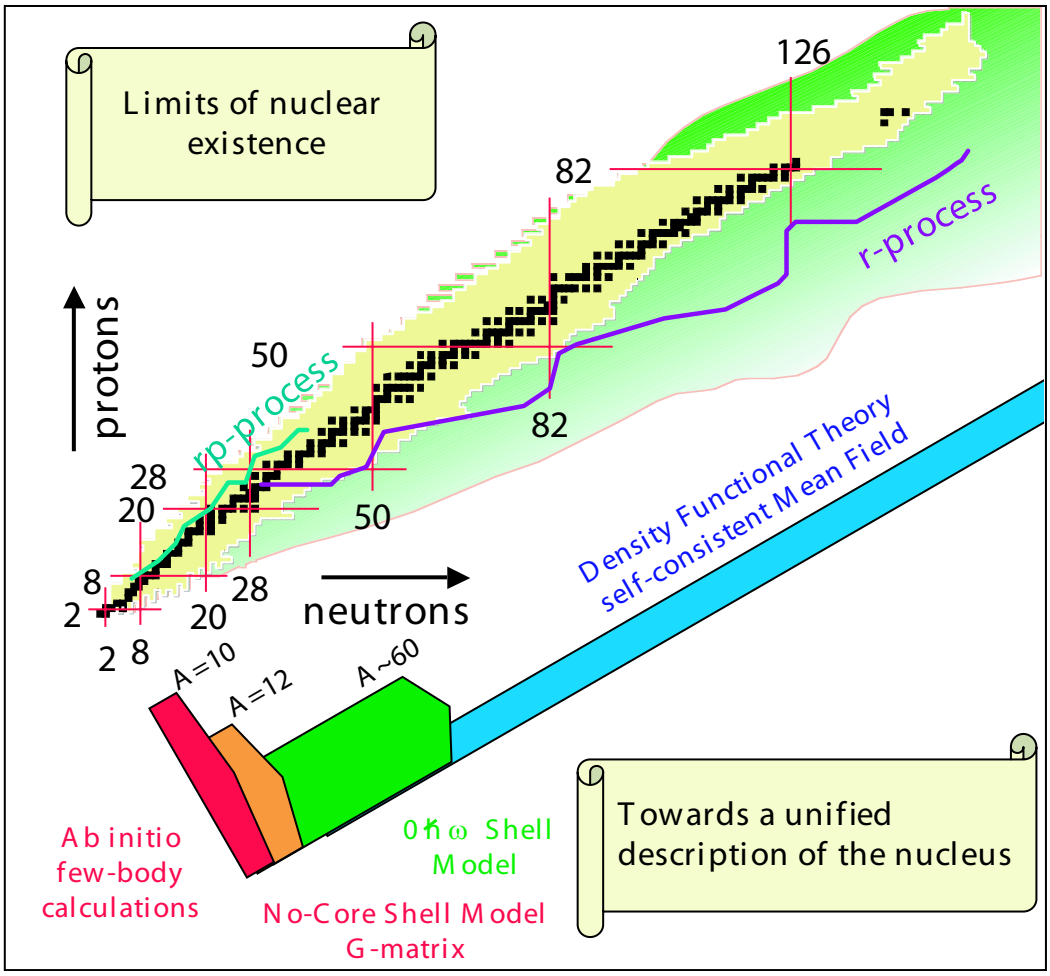

Figure 1.2: Theoretical approaches used in the low-energy nuclear structure and their limitations. Figure courtesy of W. Nazarewicz.

- Shell Model approach [16–20], in which the choice of the configuration space and interaction is coupled. The interaction may be obtained by finding the G-matrix, or parameterized for a given model space. However, for heavier systems far from the shell closures, shell model approaches involve diagonalization of huge matrices (i.e. dimension in m-scheme $\sim 10^9$ for ^{60}Zn [20] in the $p-f$ shell model space). Consequently various numerical techniques have been developed and applied, such as the Lanczos method [21], factorization algorithms like Density Matrix Renormalization Group (DMRG) [22–25], and the Monte Carlo approach [26].

- Nuclear Density Functional Theory (DTF) is the framework used in this work and will be discussed in some detail in the following chapters.

- The approaches above can be considered as microscopic; they are based on quantum mechanical description of interacting Fermions. In certain applications, macroscopic,

microscopic-macroscopic, and semi-classical methods, such as optical [27] or liquid drop [28,29] models, are applied, especially in heavy-ion reactions studies where complicated reaction dynamics and a huge number of reaction channels make microscopic modeling difficult.

Chapter 2

Nuclear Density Functional Theory

2.1 Hohenberg-Kohn-Sham Formulation

Since its development in the 1960s, the Hohenberg-Kohn-Sham formulation of the Density Functional Theory took its place among the most commonly used many-body techniques in quantum chemistry, physics of correlated electronic systems, and low-energy nuclear physics.

Theorem 2.1.1 (Hohenberg-Kohn [30]) *For a non-degenerate ground state of a many-body system, the ground state energy is a unique and universal functional of the particle density.*

The Hohenberg-Kohn theorem states that there exists a unique and universal density functional that will allow calculating ground state energy, but the theory does not provide a prescription for its construction. Moreover, DFT in the Hohenberg-Kohn formulation provides no link between particle density and the many-body wave function.

The most commonly used DFT formalism is that by Kohn and Sham [31]. They showed that the density to be used in the Hohenberg-Kohn functional, as long as is varies slowly, may be constructed using product states, the so-called natural orbitals, and correlation of the many-body wave function for the system is not necessary. Variational minimalization of the energy density functional over densities corresponding to product states gives the so-called Kohn-Sham equations - which are formally identical to the Hartree-Fock-Bogoliubov (HFB) equations.

2.2 Nuclear Mean-Field Theory and Beyond

In the Hartree-Fock-Bogoliubov theory the expectation value of the Hamiltonian is variationally minimized over a set of trial wave functions represented by product states. As a result, one obtains HFB equations [32] (in condensed matter physics called Bogoliubov-de Gennes [33] equations):

$$[H, \mathcal{R}] = 0, \tag{2.1}$$

with $\mathcal{R}$ being the generalized density matrix and H the HFB Hamiltonian in the space of particles and holes (see appendix B.3 for details). In the HFB formalism, the system of M interacting particles, with corresponding particle creation and annihilation operators $\{a^\dagger, a\}$

is replaced with the system of M uncorrelated quasiparticles with corresponding quasiparticle creation and annihilation operators $\{\beta^\dagger, \beta\}$. The unitary transformation between particle and quasiparticle operators is called the Bogoliubov transformation. Quasiparticles move in the mean-field generated by the densities, and the densities in turn are calculated using quasiparticle wave functions. Hence, Hartree-Fock and Hartree-Fock-Bogoliubov approaches are also known are Self-Consistent Mean-Field models. Quantum correlations to the ground state energy and correlated many-body wave function can be calculated using perturbation theory on the top of the HFB solution.

Among commonly used methods of including selected classes of correlations is the Generator Coordinate Method (GCM). The GCM energy and wave function can be found by solving the Hill-Wheeler equation [34–36]:

$$\sum_{q'} \mathbb{H}_{qq'} f_{q'} = E_q \sum_{q'} \mathbb{I}_{qq'} f_{q'}, \tag{2.2}$$

where matrix elements of the Hamiltonian and norm kernels $\mathbb{H}_{qq'}$ and $\mathbb{I}_{qq'}$ are:

$$\mathbb{H}_{qq'} = \langle q|\hat{H}|q'\rangle, \tag{2.3}$$
$$\mathbb{I}_{qq'} = \langle q|q'\rangle. \tag{2.4}$$

GCM and other approximate methods of configuration mixing and projection are usually used in order to:

- Restore the rotational invariance by projecting the deformed wave function (in the intrinsic frame of reference) onto the good angular momentum in the laboratory frame of reference [37–39].
- Calculate quantum fluctuations effects associated with collective motion (see, e.g. Refs. [39–41]).
- Restore the particle number symmetry broken in HFB calculations, as HFB wave functions are in general not eigenstates of the particle number operator ([42–44], see also Refs. [45, 46]).
- Restore the translational invariance by projecting onto the zero center-of-mass momentum [47–49].

It should be noted here that symmetry restoration using GCM method is a Projection After Variation (PAV) approach and the resulting state is not variationally minimized. However, Variation After Projection (VAP) techniques are usually very computationally intensive.

2.3 DFT and HFB

Even though the total HFB energy can always be written as a density functional for a given Hamiltonian, and DFT variational minimization yields equations formally identical to HFB equations, there are major differences between these formalisms:

1. The HFB wave function is a quasiparticle product state to which the beyond-mean-field correlations must be added. On the other hand, natural orbitals in DFT are just abstract constructs used to determine densities, and all correlations effects are supposed to be incorporated into the EDF.

2. For a given Hamiltonian, any eigenstate can be calculated using HFB (and beyond mean-field methods), while in the DFT only stationary points of the potential energy surface are well defined.

3. In the HFB framework, the underlying Hamiltonian yields a limited class of density dependent terms in the corresponding Energy Density Functional. Moreover, there exist connections between time-even particle-hole, time-odd particle-hole, and pairing terms in the EDF. Such constrains do not apply for EDF in the Density Functional Theory.

2.4 DFT for Electrons and Nucleons

The formal differences between HFB and DFT frameworks described in section 2.3 are particularly important in nuclear applications. While Density Functional Theory is one of the most commonly used approaches in atomic, condensed matter, and nuclear physics, there are some important differences that make application of DFT in the electronic and nucleonic systems significantly different:

1. For electronic systems, correlations are generated by well-known electromagnetic interactions, while effective inter-nucleon interactions are weakly understood at low energies.

2. Kohn-Sham theorem 2.1.1 applies to systems with non-degenerate ground states. For electronic systems, this is assured by the existence of the external potential due to the ionic lattice. The nucleus is a self-bound system in which many symmetries are spontaneously broken. Since there is no underlying Hamiltonian in the DFT framework, symmetry restoration and configuration mixing in DFT becomes a serious conceptual problem.

3. Separation of the scales between ionic lattice and electronic degrees of freedom for electronic systems allows the application of adiabatic techniques. On the other hand, there is no separation in scales between single-particle and collective degrees of freedom in the atomic nucleus and application of adiabatic techniques is questionable.

More information about the nuclear DFT can be found in Refs. [50–53].

2.5 The Skyrme Functional

The Skyrme functional originates from the Skyrme interaction [54–58] and is a second order local momentum expansion of the general short range spin-dependent two-body interaction

v_{12} [57]:

$$\begin{aligned} v_{12} &= t_0\left(1+x_0P_\sigma\right)\delta(\boldsymbol{r_1}-\boldsymbol{r_2}) + \frac{1}{2}t_1\left[\delta(\boldsymbol{r_1}-\boldsymbol{r_2})k^2 + k'^2\delta(\boldsymbol{r_1}-\boldsymbol{r_2})\right] + \\ &+ t_2\boldsymbol{k'}\delta(\boldsymbol{r_1}-\boldsymbol{r_2})\boldsymbol{k} + iW_0\left(\boldsymbol{\sigma_1}+\boldsymbol{\sigma_2}\right)\cdot\left(\boldsymbol{k'}\times\delta(\boldsymbol{r_1}-\boldsymbol{r_2})\boldsymbol{k}\right), \end{aligned} \tag{2.5}$$

to which the contact three body term v_{123} [57] is added:

$$v_{123} = t_3\delta(\boldsymbol{r_1}-\boldsymbol{r_2})\delta(\boldsymbol{r_2}-\boldsymbol{r_3}). \tag{2.6}$$

In Eq. (2.5) P_σ is a spin-exchange operator, $\boldsymbol{\sigma}$ are Pauli matrices, with $\boldsymbol{k} = (\boldsymbol{\nabla}_{\boldsymbol{r_1}} - \boldsymbol{\nabla}_{\boldsymbol{r_2}})/2i$ acting to the right and $\boldsymbol{k'} = -(\boldsymbol{\nabla}_{\boldsymbol{r_1}} - \boldsymbol{\nabla}_{\boldsymbol{r_2}})/2i$ acting to the left. The contact three-body interaction (2.6) can be associated with the density-dependent two body interaction [57]:

$$v_{123} \approx \frac{1}{6}t_3(1+P_\sigma)\delta(\boldsymbol{r_1}-\boldsymbol{r_2})\rho\left(\frac{\boldsymbol{r_1}+\boldsymbol{r_2}}{2}\right). \tag{2.7}$$

Parameters t_i, x_i, and W_0, are usually adjusted to fit a select set of experimental data (i.e. binding energies and radii of some magic nuclei) and properties of the infinite nuclear matter, such as saturation density, incompressibility, and binding energy per nucleon. There are different parameterizations of the Skyrme functional commonly used in calculations (see, i.e. Refs. [41, 59–62]).

The particle-hole component of the HFB energy density for even-even nuclei associated with the interaction (2.5, 2.6) reads [57]:

$$\begin{aligned} \mathcal{H} &= \frac{\hbar^2}{2m}\tau + \frac{t_0}{2}\left[\left(1+\frac{x_0}{2}\right)\rho^2 - \left(x_0+\frac{1}{2}\right)\left(\rho_n^2+\rho_p^2\right)\right] + \frac{t_1+t_2}{4}\rho\tau + \\ &+ \frac{t_2-t_1}{8}\left(\rho_n\tau_n+\rho_p\tau_p\right) + \frac{t_2-3t_1}{16}\rho\nabla^2\rho + \frac{3t_1+t_2}{32}\left(\rho_n\nabla^2\rho_n+\rho_p\nabla^2\rho_p\right) + \\ &+ \frac{t_1-t_2}{16}\left(J_n^2+J_p^2\right) + \frac{t_3}{4}\rho_n\rho_p\rho - \frac{W_0}{2}\left(\rho\boldsymbol{\nabla J} + \rho_n\boldsymbol{\nabla J_n} + \rho_p\boldsymbol{\nabla J_p}\right) + \mathcal{H}_{Coulomb}, \end{aligned} \tag{2.8}$$

where $\mathcal{H}_{Coulomb}$ is the Coulomb term. For odd- neutron or proton number nuclei, or in the description of rotational states, non-zero time-odd terms in the EDF must be included. In this work, we concentrate on even-even nuclei for which time-odd densities and currents vanish. One can also see the Skyrme functional as a result of the local Density Matrix Expansion [63,64], replacing the weak non-locality of EDF with its local gradient expansion.

For the three-body contact interaction (2.6), energies of isoscalar monopole and isovector dipole resonances are too large [60]. These energies are lower when the linear density dependence in term (2.7) is replaced with a fractional power of density ρ^γ, with $\gamma \approx 1/6 - 1/3$ [60]. Such a non-integer power density dependence in the EDF ($\gamma = N/3$ with N integer) appear in calculations for diluted Fermi gases [65–67] and in Effective Field Theory [68–70]. Such a EDF can not be generated by a many-body Hamiltonian in the HFB approach.

As more exotic nuclei close to the drip line[1] are becoming accessible experimentally and energy functionals are getting more sophisticated, some theoretical aspects considered in the

[1] Drip line (after [2]) - a locus in the chart of $N-Z$ nuclei that separates the last particle-bound nucleus in an isotopic chain (either in neutron rich or proton rich nuclei) from particle unbound nuclei.

past as unimportant and/or too involved computationally, gain importance. The exponential increase of computational power available in the last decades makes many techniques feasible.

For strongly-bound nuclei, the average pairing gap,

$$\bar{\Delta} = -\frac{1}{N}\int d^3\boldsymbol{r_1} d^3\boldsymbol{r_2} \sum_{\sigma_1\sigma_2} \tilde{h}(\boldsymbol{r_1}\sigma_1, \boldsymbol{r_2}\sigma_2)\rho(\boldsymbol{r_2}\sigma_2, \boldsymbol{r_1}\sigma_1), \tag{2.9}$$

is much smaller than the absolute value of the Fermi energy, μ, and pairing is often treated as a small correction [71]. The Bardeen-Cooper-Schrieffer (BCS) [72] approximation is often used to calculate the pairing contribution to the total energy and pairing gap using Hartree-Fock wave functions. However, for the weakly bound nuclei, $\bar{\Delta} \sim |\mu|$, and pairing cannot be treated as a small correction. In this case particle-particle (p-p) and particle-hole (p-h) channels of the interaction should be described within the same framework. In the nuclear Density Functional Theory, EDF is a functional of particle density and abnormal density (see appendix B.3 for details). As a result of variational minimalization of such a functional one obtains the HFB equations.

In most HFB applications, pairing interaction is assumed to be either in the form of the finite-range Gogny force [73] or the zero-range, possibly density-dependent, delta force [71, 74–76]. The Gogny interaction in the pairing channel can be viewed as a regularized contact interaction, with regularization fixed through the finite range. The resulting pairing field is nonlocal, though. The pairing term of EDF may be also derived from the underlying Hamiltonian [61]. However, only a fraction of the nuclear pairing originates from the many-body interaction [77, 78], because some of the nuclear pairing is induced; i.e. it results from coupling to collective excitations. Consequently, one usually adjusts couplings of the particle-hole and particle-particle terms of the EDF independently.

The Skyrme Hartree-Fock-Bogoliubov method, within the framework of Density Functional Theory is one of the few theoretical approaches used for nuclei throughout the nuclear chart. Modern Skyrme functionals reproduce all experimentally known nuclear masses with the rms error $\sim$ 700 keV [79, 80]. More information about Skyrme-HFB formalism can be found in Refs. [47, 52, 59–61, 81] and the pairing interaction in nuclei is discussed in Refs. [71, 82].

2.6 Energy Cutoff in Skyrme-HFB

Theories employing local densities are simpler than those with non-local densities, and allow for functionals to be improved in a systematic way. The price paid for simplicity is high: ultraviolet divergences appear. To remove them, one has to discretize and apply a cutoff procedure within a given space of single-particle (s.p.) states [61, 71], and when the dimension of this space increases, the pairing gap diverges for any given strength of the interaction. Pairing strength has to be readjusted for each s.p. space. Thus the energy cutoff and the pairing strength together define the pairing interaction, and this definition can be understood as a phenomenological introduction of finite range [71, 83]. Such a procedure is usually referred to as the renormalization of the contact pairing force. It is performed in the spirit of the Effective Field Theory, where contact interactions are used to describe low energy phenomena, while the coupling constants are readjusted for any given energy cutoff to account for neglected high energy effects.

Another way of removing ultraviolet divergences is showed in Refs. [83–92], where the energy density functional with the pairing term

$$\mathcal{H}_{pair}[\rho, \tilde{\rho}] = g[\rho]\tilde{\rho}^2 \tag{2.10}$$

is regularized.

The problem of the ultraviolet divergence for the zero-range pairing interaction (2.10) has been approached by:

- Removing the divergence by regularization of the scattering problem [83].
- Regularizing the gap equation by either dimensional regularization [84] or subtracting the diverging component using the Thomas-Fermi approximation [85–90].
- Treating the pairing divergence as an in-medium effects and renormalizing two-body propagators [91, 92].

All these approaches yield similar or equivalent results.

Chapter 3

This Work

3.1 Research Overview

In the first part of this work we study the character of ultraviolet divergences appearing in local densities for a given EDF. We demonstrate how to construct regularized functionals by regularization of all densities appearing in the EDF.

References [85–90] provide a regularization scheme for the pairing term (2.10), in which pairing strength becomes cutoff energy dependent. This method has been applied successfully to different systems that use the zero-range pairing interaction is used. Examples include the infinite nuclear matter [87], spherical [89, 93] and deformed [94] nuclei, and trapped fermionic atoms [95, 96]. The pairing regularization scheme also provides very similar results, and a better understanding of the phenomenological pairing renormalization approach [94].

Just as the Skyrme functional is a second order local gradient expansion of the general non-local density functional in the particle-hole channel, the pairing functional (2.10) is the lowest order term in a similar expansion of the particle-particle channel. In some calculations more involved forms of the pairing term of the EDF are used (see, i.e. Ref. [97]). These terms cannot be regularized using any of methods listed above.

In the second part of this work we investigate the consequences stemming from the fact that applying the cutoff procedure causes the resulting Bogoliubov transformation to become rectangular. However, in derivations of the HFB equations the generalized density matrix is assumed to be projective, and the projectivity of $\mathcal{R}$ results from the unitarity of the Bogoliubov transformation. As a consequence, the particle density and the abnormal density develop non-Hermitian components. These components are usually neglected in practical calculations, but their importance has never been verified. In this work we propose a two-step method of solving the HFB equations, with a second step that guarantees the unitarity of the Bogoliubov transformation.

The HFB and Skyrme-HFB formalisms have been explained in a great detail in many papers (see e.g. Refs. [47,52,61,71]) and are briefly introduced in Appendix B. The notation in this work is consistent with that used in Ref. [61]. In chapter 4 we discuss the formalism of the regularized Skyrme-HFB. The problem of the non-unitarity of the Bogoliubov transformation in HFB calculations is discussed in chapter 5. Finally, the perspectives and summary are contained in chapter 6, with section 6.1 including results from the work in

progress. Certain relations used in formalism and technical aspects of the numerical implementation are discussed in the appendices. Some of the results presented in this work have been published in Refs. [94, 98, 99].

In the course of the PhD studies, the author was involved in other projects, which are not directly related to the topic of this thesis. One of them is the problem of the pseudospin symmetry [100, 101]. We investigated [102] the pseudospin symmetry as a dynamical symmetry of a many-body potential and found that even though pseudospin partner orbitals are significantly shifted in energy, their wave functions fulfill relations resulting from the symmetry. Moreover, even though pseudospin symmetry has a relativistic origin, symmetry breaking effects for wave functions obtained in non-relativistic and relativistic self-consistent calculations, and in a harmonic oscillator model, are comparable.

3.2 Numerical Implementation

In our study, we use SLy4 [62] and SkP [61] parameterizations of the Skyrme density functionals in the p-h channel. These parameterizations are commonly used in realistic HFB calculations. In the p-p channel we use the contact density-dependent force, which leads to a pairing energy density of the form [74]:

$$\mathcal{H}_{pair}(\mathbf{r}) \quad = \quad g(\boldsymbol{r})\tilde{\rho}(\boldsymbol{r})^2 = \frac{1}{2}V_0\left[1 - V_1\frac{\rho(\boldsymbol{r})}{\rho_0}\right]\tilde{\rho}(\boldsymbol{r})^2, \tag{3.1}$$

where $\rho_0 = 0.16\,\mathrm{fm}^{-3}$. For $V_1 = 0$ the resulting pairing interaction is called volume pairing, while $V_1 = 1/2$ corresponds to the so-called mixed pairing (Ref. [103] and references quoted therein).

In this work we have performed numerical calculations using two numerical codes solving the HFB equations:

- HFBRAD [104] – solves the HFB equations in the spherically symmetric coordinate basis. Unless stated otherwise, the maximum angular momenta used in calculations were $j_{\max} = 39/2$ for neutrons and $j_{\max} = 25/2$ for protons.
- HFBTHO [105] – diagonalizes the HFB problem in the axially symmetric transformed harmonic oscillator (HO) basis. Unless stated otherwise, we use $N_{osc} = 20$ HO shells in the basis.

In the course of this work some programming was involved:

- For pairing regularization, relevant subroutines were added to HFBTHO.
- Using code HFBTHO as a basis, a numerical code performing the two-step procedure ensuring the unitarity of the Bogoliubov transformation was written.
- Using HFB quasiparticle wave functions and some of the subroutines from HFBTHO, a numerical code performing configuration mixing for quadrupole q_{20} collective coordinate was written.

Chapter 4

Regularized Skyrme-HFB

4.1 Formalism

For a given energy density functional, the energy is variationally minimized with particle number constraints imposed for neutrons, N, and protons, Z,

$$\delta \int \mathcal{H}_r[\rho(z_1,z_2),\tilde{\rho}(z_1,z_2)]dz_1dz_2 \Big| \begin{array}{l} \mathrm{Tr}\rho_1 = N \\ \mathrm{Tr}\rho_2 = Z \end{array} = 0, \tag{4.1}$$

where $z_i = (\boldsymbol{r_i}, \sigma_i, t_i)$, $\boldsymbol{r_i}$ is the spatial coordinate, σ_i is the spin, and t_i is the isospin. In Eq. (4.1) ρ is the particle density and $\tilde{\rho}$ is the abnormal density defined by:

$$\rho(\boldsymbol{r_2}\sigma_2 t_2, \boldsymbol{r_1}\sigma_1 t_1) = \langle\Phi|a^\dagger_{\boldsymbol{r_1}\sigma_1 t_1} a_{\boldsymbol{r_2}\sigma_2 t_2}|\Phi\rangle, \tag{4.2}$$

$$\tilde{\rho}(\boldsymbol{r_2}\sigma_2 t_2, \boldsymbol{r_1}\sigma_1 t_1) = -2\sigma_1\langle\Phi|a_{\boldsymbol{r_1}-\sigma_1 t_1} a_{\boldsymbol{r_2}\sigma_2 t_2}|\Phi\rangle, \tag{4.3}$$

where a and $a^\dagger$ are respectively the particle annihilation and creation operators. Variational minimization (4.1) over a class of product states, yields HFB equations, which in coordinate space read [47, 61]:

$$\int dz_1 \begin{bmatrix} h_\mu(z_2,z_1) & \tilde{h}(z_2,z_1) \\ \tilde{h}(z_2,z_1) & -h_\mu(z_2,z_1) \end{bmatrix} \begin{bmatrix} \varphi_{1i}(z_1) \\ \varphi_{2i}(z_1) \end{bmatrix} = E_i \begin{bmatrix} \varphi_{1i}(z_2) \\ \varphi_{2i}(z_2) \end{bmatrix}, \tag{4.4}$$

where E_i is the quasiparticle energy, h_μ is the single-particle Hamiltonian, and $\tilde{h}$ is the pairing Hamiltonian:

$$h_\mu(z_2,z_1) = \frac{\delta\mathcal{H}_r[\rho,\tilde{\rho}]}{\delta\rho}(z_1,z_2) - \mu(t_2)\delta_{\sigma_1\sigma_2}\delta_{t_1t_2}, \tag{4.5}$$

$$\tilde{h}(z_2,z_1) = \frac{\delta\mathcal{H}_r[\rho,\tilde{\rho}]}{\delta\tilde{\rho}}(z_1,z_2). \tag{4.6}$$

The two-component solution (φ_1, φ_2) of the HFB equations is called the HFB quasiparticle wave function.

Matrix elements of the particle density that are non-diagonal in the isospin originate in the proton-neutron pairing interaction. For $N \neq Z$ nuclei this interaction can be neglected

(see, e.g., Ref. [106]) and in most practical calculations the nuclear wave function is a product of the proton and neutron wave functions. The resulting particle density is diagonal in isospin:

$$\rho(\boldsymbol{r_2}\sigma_2 t_2, \boldsymbol{r_1}\sigma_1 t_1) = \rho_{t_2}(\boldsymbol{r_2}\sigma_2, \boldsymbol{r_1}\sigma_1)\delta_{t_1 t_2}, \tag{4.7}$$

$$\tilde{\rho}(\boldsymbol{r_2}\sigma_2 t_2, \boldsymbol{r_1}\sigma_1 t_1) = \tilde{\rho}_{t_2}(\boldsymbol{r_2}\sigma_2, \boldsymbol{r_1}\sigma_1)\delta_{t_1 t_2}. \tag{4.8}$$

In order to keep the notation compact, we will assume the particle density to be diagonal in isospin and omit the isospin index henceforth, keeping in mind that in calculations all single-particle densities and fields must be calculated for protons and neutrons separately.

Consider the local energy density:

$$\mathcal{H}_r[\rho_r, \tau_r, \tilde{\rho}_r, \tilde{\tau}_r], \tag{4.9}$$

where index r denotes physical (or *regularized*) particle density ρ_r, abnormal density $\tilde{\rho}_r$, kinetic density τ_r, and abnormal kinetic density $\tilde{\tau}_r$:

$$\rho_r = \rho + F_\rho[\rho, \tau, \tilde{\rho}, \tilde{\tau}], \tag{4.10}$$

$$\tilde{\rho}_r = \tilde{\rho} + F_{\tilde{\rho}}[\rho, \tau, \tilde{\rho}, \tilde{\tau}], \tag{4.11}$$

$$\tau_r = \tau + F_\tau[\rho, \tau, \tilde{\rho}, \tilde{\tau}], \tag{4.12}$$

$$\tilde{\tau}_r = \tilde{\tau} + F_{\tilde{\tau}}[\rho, \tau, \tilde{\rho}, \tilde{\tau}], \tag{4.13}$$

where unregularized densities are defined in terms of the upper φ_1 and lower φ_2 components of the quasiparticle wave functions as:

$$\rho(\boldsymbol{r_2}\sigma_2, \boldsymbol{r_1}\sigma_1) = \sum \varphi_{2i}(\boldsymbol{r_2}\sigma_2)\varphi^*_{2i}(\boldsymbol{r_1}\sigma_1), \tag{4.14}$$

$$\tilde{\rho}(\boldsymbol{r_2}\sigma_2, \boldsymbol{r_1}\sigma_1) = -\sum \varphi_{1i}(\boldsymbol{r_2}\sigma_2)\varphi^*_{2i}(\boldsymbol{r_1}\sigma_1), \tag{4.15}$$

$$\tau(\boldsymbol{r_2}\sigma_2, \boldsymbol{r_1}\sigma_1) = \sum \boldsymbol{\nabla}_{\boldsymbol{r_2}}\varphi_{2i}(\boldsymbol{r_2}\sigma_2)\boldsymbol{\nabla}_{\boldsymbol{r_1}}\varphi^*_{2i}(\boldsymbol{r_1}\sigma_1), \tag{4.16}$$

$$\tilde{\tau}(\boldsymbol{r_2}\sigma_2, \boldsymbol{r_1}\sigma_1) = -\sum \boldsymbol{\nabla}_{\boldsymbol{r_2}}\varphi_{1i}(\boldsymbol{r_2}\sigma_2)\boldsymbol{\nabla}_{\boldsymbol{r_1}}\varphi^*_{2i}(\boldsymbol{r_1}\sigma_1). \tag{4.17}$$

In Eqs. (4.10-4.13) we assume that the regulators F_α are functionals of ρ, τ, $\tilde{\rho}$, $\tilde{\tau}$, and functions of the cutoff energy. In Eqs. (4.14-4.17) the summation is all over quasiparticle wave functions with the corresponding quasiparticle energy positive, $E_i > 0$, and equivalent energy [61],

$$\bar{e}_i = \left[1 - 2\int d^3\boldsymbol{r}|\varphi_{2i}(\boldsymbol{r})|^2\right] E_i + \mu, \tag{4.18}$$

below the cutoff energy $\epsilon_{\rm cut}$.

For ED (4.9) Hamiltonians h_μ and $\tilde{h}$ read:

$$h_\mu = -\boldsymbol{\nabla}_{\boldsymbol{r_2}}\frac{\delta\mathcal{H}_r}{\delta\tau}\boldsymbol{\nabla}_{\boldsymbol{r_1}} + \frac{\delta\mathcal{H}_r}{\delta\rho} - \mu = h - \mu = -\boldsymbol{\nabla}_{\boldsymbol{r_2}}B\boldsymbol{\nabla}_{\boldsymbol{r_1}} + U - \mu, \tag{4.19}$$

$$\tilde{h} = -\boldsymbol{\nabla}_{\boldsymbol{r_2}}\frac{\delta\mathcal{H}_r}{\delta\tilde{\tau}}\boldsymbol{\nabla}_{\boldsymbol{r_1}} + \frac{\delta\mathcal{H}_r}{\delta\tilde{\rho}} = -\boldsymbol{\nabla}_{\boldsymbol{r_2}}\tilde{B}\boldsymbol{\nabla}_{\boldsymbol{r_1}} + \tilde{U}. \tag{4.20}$$

The schematic ED (4.9) we discuss does not include a spin-orbit term, because due to relative smallness of the corresponding coupling constant for cutoff energies used in low-energy

nuclear physics, the associated cutoff dependence is negligible. Thus it will be discussed in detail later in the text.

The quasiparticle Hilbert space can be roughly divided into three subspaces:

1. Particle subspace - where quasiparticle wave functions have an almost pure particle character:
$$\int |\varphi_{1i}(\boldsymbol{r})|^2 d^3\boldsymbol{r} \approx 0. \tag{4.21}$$
One can assume that all states with equivalent energy $\bar{e}_i < \mu - 3\bar{\Delta}$ belong to the particle subspace.

2. Pairing subspace - where in quasiparticle wave functions have a non-vanishing particle and hole component
$$\int \varphi_{1i}(\boldsymbol{r})\varphi^*_{2i}(\boldsymbol{r}) d^3\boldsymbol{r} \neq 0. \tag{4.22}$$
Due to the Coulomb and centrifugal barriers, some resonant quasiparticle states with corresponding equivalent energy, even several MeV above the Fermi level, are partially occupied, and are important for nuclear dynamics. Consequently, these states, along with states in the vicinity of the Fermi surface, belong to the pairing subspace, which includes quasiparticle states with equivalent energies approximately such that $\mu - 3\bar{\Delta} < \bar{e}_i < \mu + 15\,\mathrm{MeV}$.

3. Hole space - where quasiparticle wave functions have an almost pure hole character:
$$\int |\varphi_{2i}(\boldsymbol{r})|^2 d^3\boldsymbol{r} \approx 0. \tag{4.23}$$
The particle subspace is dominated by bound and resonant states, for which shell effects are crucial, but there are mostly non-resonant unbound states in hole space. Their density of states and wave functions can be approximated by semiclassical methods.

In Skyrme-HFB calculations in the coordinate space, particle and pairing subspaces, and some states from hole space must be included in the truncated model space. The resulting cutoff energy used in calculations should be no less than 50 MeV (see e.g. Refs. [71, 98]).

For each density ρ_α, where $\{\rho_\alpha\} = \{\rho, \tau, \tilde{\rho}, \tilde{\tau}\}$, one can perform regularization by:

1. Identification of the character of ultraviolet divergence.

2. Evaluation of contributions to the divergent component $\delta\rho_{\alpha,div}$ for i-th quasiparticle state
$$\delta\rho^{\epsilon_i}_\alpha = \delta\rho^{\epsilon_i}_{\alpha,div} + \delta\rho^{\epsilon_i}_{\alpha,r}. \tag{4.24}$$

3. Regularization of the density by removing contributions leading to divergence corresponding to states below cutoff energy
$$\rho^{\epsilon_{\mathrm{cut}}}_{\alpha,r} = \rho^{\epsilon_{\mathrm{cut}}}_\alpha - \sum_{\epsilon_i < \epsilon_{\mathrm{cut}}} \delta\rho_{\alpha,div}(\epsilon_i). \tag{4.25}$$

Regulator F_{ρ_α} is, therefore, given as (4.25, 4.10-4.13):

$$F_{\rho_\alpha} = -\sum_{\epsilon_i<\epsilon_{\rm cut}} \delta\rho^{\epsilon_i}_{\alpha,div}. \tag{4.26}$$

Regularized densities are assumed here to be finite and independent of the unphysical parameters of the numerical implementation such as the cutoff energy $\epsilon_{\rm cut}$. Consequently, our goal is to (i) construct HFB densities and currents using the complete Hilbert space of wave functions, (ii) identify and remove all divergences, and (iii) evaluate densities and currents for a finite energy cutoff that is high enough to provide convergence. The cutoff independence of the densities guarantees that the EDF is also independent of cutoff energy:

$$\frac{d}{d\epsilon_{\rm cut}}\mathcal{H}_r = 0. \tag{4.27}$$

4.1.1 Ultraviolet Divergence in Local Densities

Using the Thomas-Fermi approximation for Hamiltonians h, $\tilde{h}$ of the form (4.19, 4.20), quasiparticle wave functions with corresponding equavalent energy high can be written as:

$$\varphi_{1E_{\boldsymbol{k}\sigma}}(\boldsymbol{r}) \approx \frac{-(2\pi)^{-3/2}\alpha(\boldsymbol{r})e^{i\boldsymbol{k}(\boldsymbol{r})\boldsymbol{r}}\chi(\sigma)}{\sqrt{\left[\beta(\boldsymbol{r})-E_{\boldsymbol{k}\sigma}\right]^2+\alpha^2}}, \tag{4.28}$$

$$\varphi_{2E_{\boldsymbol{k}\sigma}}(\boldsymbol{r}) \approx \frac{(2\pi)^{-3/2}\left(\beta(\boldsymbol{r})-E_{\boldsymbol{k}\sigma}\right)e^{i\boldsymbol{k}(\boldsymbol{r})\boldsymbol{r}}\chi(\sigma)}{\sqrt{\left[\beta(\boldsymbol{r})-E_{\boldsymbol{k}\sigma}\right]^2+\alpha(\boldsymbol{r})^2}}, \tag{4.29}$$

where

$$\alpha(\boldsymbol{r}) = \tilde{B}(\boldsymbol{r})k(\boldsymbol{r})^2+\tilde{U}(\boldsymbol{r}), \tag{4.30}$$

$$\beta(\boldsymbol{r}) = B(\boldsymbol{r})k(\boldsymbol{r})^2+U(\boldsymbol{r})-\mu, \tag{4.31}$$

and $\chi(\sigma)$ is the spinor component of the quasiparticle wave function. Quasiparticle energy and momentum $k(\boldsymbol{r})$ are related through:

$$E_{\boldsymbol{k}\sigma} \approx \sqrt{B(\boldsymbol{r})^2k(\boldsymbol{r})^4+\left[\tilde{B}(\boldsymbol{r})k(\boldsymbol{r})^2+\tilde{U}(\boldsymbol{r})\right]^2}. \tag{4.32}$$

In the Thomas-Fermi approximation, one can locally approximate the wave function with plain waves, but the wave vector for a given wave function is coordinate dependent.

Equations (4.28, 4.29) yield that for $\tilde{B}\neq 0$, single particle high-momentum,

$$Bk^2 \gg |\mu-U|, \qquad \tilde{B}k^2 \gg \tilde{U}, \tag{4.33}$$

contribution to the particle density can be approximated as:

$$\delta\rho^{E_{\boldsymbol{k}\sigma}}(\boldsymbol{r}) \approx \frac{1}{8\pi^3}\left[1+\frac{\tilde{B}(\boldsymbol{r})^2}{\left(\sqrt{B(\boldsymbol{r})^2+\tilde{B}(\boldsymbol{r})^2}-B(\boldsymbol{r})\right)^2}\right]^{-1}. \tag{4.34}$$

Such an energy-independent non-zero contribution to the particle density would correspond to a significant occupation probability for all states, including those with extremely high energy. As this is unphysical, we assume:

$$B \gg \tilde{B}. \tag{4.35}$$

Under condition (4.35), Eqs. (4.28-4.29) reduce to:

$$\varphi_{1E_{\boldsymbol{k}\sigma}}(\boldsymbol{r}) \approx -\frac{1}{(2\pi)^{3/2}} e^{i\boldsymbol{k}\boldsymbol{r}} \chi(\sigma), \tag{4.36}$$

$$\varphi_{2E_{\boldsymbol{k}\sigma}}(\boldsymbol{r}) \approx \frac{1}{(2\pi)^{3/2}} \frac{\tilde{B}(\boldsymbol{r})k^2 + \tilde{U}(\boldsymbol{r})}{2B(\boldsymbol{r})k^2} e^{i\boldsymbol{k}\boldsymbol{r}} \chi(\sigma). \tag{4.37}$$

From (4.36,4.37) it follows that high-momentum contributions to densities:

$$\delta\rho_\alpha^{k_1 k_2} = \sum_\sigma \sum_{k=k_1}^{k_2} \delta\rho_\alpha^{E_{\boldsymbol{k}\sigma}}, \tag{4.38}$$

can be approximated as (4.14-4.17):

$$\delta\rho^{k_1 k_2} = \frac{1}{4\pi^2}\left[\frac{\tilde{B}^2}{B^2} S_1^{k_1 k_2} + \frac{2\tilde{B}\tilde{U}}{B^2} S_{-1}^{k_1 k_2} + \frac{\tilde{U}^2}{B^2} S_{-3}^{k_1 k_2}\right], \tag{4.39}$$

$$\delta\tilde{\rho}^{k_1 k_2} = -\frac{1}{2\pi^2}\left[\frac{\tilde{B}}{B} S_1^{k_1 k_2} + \frac{\tilde{U}}{B} S_{-1}^{k_1 k_2}\right], \tag{4.40}$$

$$\delta\tau^{k_1 k_2} = \frac{1}{4\pi^2}\left[\frac{\tilde{B}^2}{B^2} S_3^{k_1 k_2} + \frac{2\tilde{B}\tilde{U}}{B^2} S_1^{k_1 k_2} + \frac{\tilde{U}^2}{B^2} S_{-1}^{k_1 k_2}\right], \tag{4.41}$$

$$\delta\tilde{\tau}^{k_1 k_2} = -\frac{1}{2\pi^2}\left[\frac{\tilde{B}}{B} S_3^{k_1 k_2} + \frac{\tilde{U}}{B} S_1^{k_1 k_2}\right], \tag{4.42}$$

where

$$S_n^{k_1 k_2}(\boldsymbol{r_1}, \boldsymbol{r_2}) = |\boldsymbol{r_1} - \boldsymbol{r_2}|^{-n-2} \int_{k_1|\boldsymbol{r_1}-\boldsymbol{r_2}|}^{k_2|\boldsymbol{r_1}-\boldsymbol{r_2}|} q^n \sin(q) dq \tag{4.43}$$

and

$$\lim_{\boldsymbol{r_1}\to\boldsymbol{r_2}} S_n^{k_1 k_2}(\boldsymbol{r_1}, \boldsymbol{r_2}) \sim \begin{cases} \ln k_2 - \ln k_1 & n = -2 \\ k_2^{n+2} - k_1^{n+2} & n \neq -2 \end{cases}. \tag{4.44}$$

Equations (4.26, 4.39-4.42) yield:

$$\tilde{B}F_{\tilde{\tau}} + 2BF_\tau + \tilde{U}F_{\tilde{\rho}} = 0. \tag{4.45}$$

More generally, if for a given ED the maximum orders of derivatives in densities present is D_{ph} (D_{pp}) in the p-h (p-p) channel, and derivative order of a density ρ_α ($\tilde{\rho}_\alpha$) in the p-h (p-p) channel is d, the high momentum contributions to a given local density are proportional to:

$$\delta\rho_\alpha \sim S_{-2(D_{ph}-D_{pp})+1+d}^{k_1 k_2}, \tag{4.46}$$

$$\delta\tilde{\rho}_\alpha \sim S_{-(D_{ph}-D_{pp})+1+d}^{k_1 k_2}. \tag{4.47}$$

Therefore, high-momentum contributions to densities ρ_α and $\tilde{\rho}_\alpha$, corresponding to maximum derivative order in the p-h and p-p channels, have the same functional dependence on momentum:

$$\delta\rho_\alpha \sim \delta\tilde{\rho}_\alpha \sim S^{k_1 k_2}_{-D_{ph}+2D_{pp}+1}. \tag{4.48}$$

These high-energy contributions diverge logarithmically with momentum k_2 for $D_{pp} = D^0_{pp}$, with

$$D^0_{pp} = \frac{D_{ph} - 3}{2}, \tag{4.49}$$

and for $D_{pp} < D^0_{pp}$ all densities in EDF converge. Densities with ultraviolet divergences of higher order than logarithmic appear for EDF with $D_{pp} > D^0_{pp}$.

High energy contributions to local densities (4.39-4.42) are plotted in Fig. 4.1. As quasiparticle states from particle subspace and pairing subspace contribute to particle densities, and only those from the pairing subspace contribute to abnormal densities, the relative high energy contributions to abnormal densities are larger.

Figure 4.1 shows that high-momentum contributions to ρ are large for energies $50\,\mathrm{MeV} > \epsilon^{k_2}_{\mathrm{cut}} > 200\,\mathrm{MeV}$. Therefore, for cutoff energies $50\,\mathrm{MeV} < \epsilon_{\mathrm{cut}} < 200\,\mathrm{MeV}$ we conclude that particle density dependents is weakly on ϵ_{cut} and particle density regulator is approximately zero:

$$F_\rho \approx 0. \tag{4.50}$$

Contributions to densities in the low-energy spectrum calculated in the full SkP functional are smaller than those obtained with the volume pairing (see Fig. 4.1). This corresponds to the observation [107] that for negative potential and positive kinetic terms in the p-p channel, the pairing Hamiltonian

$$\tilde{h} \approx \tilde{B}k^2 + \tilde{U} \tag{4.51}$$

becomes $\tilde{h} \approx 0$ for

$$k_0^2 = -\tilde{U}/\tilde{B}. \tag{4.52}$$

Hence quasiparticles with $k \approx k_0$ are almost exactly eigenfunctions of the p-h Hamiltonian and their contributions to the abnormal density is negligible.

The cutoff independence of the particle density (approximation (4.50)) is illustrated in Fig. 4.2. One can see, that contributions to the particle density coming from the high energy states with $\epsilon_i > 60\,\mathrm{MeV}$ do not exceed a factor of 10^{-4} of the saturation density. The difference between particle densities evaluated for different values of the cutoff energy constitutes not only contributions from quasiparticle states with corresponding equivalent energies between given values of the cutoff energy, but also reflects the change in all quasiparticle wave functions. Therefore, it may become negative, even though the local density is positively defined, as illustrated in Fig. 4.2 for $r \approx 5\,\mathrm{fm}$.

Ultraviolet Divergence in Spin-Orbit Terms

High energy contributions to spin-current density,

$$\boldsymbol{J}(\boldsymbol{r_2}\sigma_2, \boldsymbol{r_1}\sigma_1) = \frac{i}{2}\sum \left[\varphi_{2i}(\boldsymbol{r_2}\sigma_2)\nabla_{\boldsymbol{r_1}}\varphi^*_{2i}(\boldsymbol{r_1}\sigma_1) - \nabla_{\boldsymbol{r_2}}\varphi_{2i}(\boldsymbol{r_2}\sigma_2)\varphi^*_{2i}(\boldsymbol{r_1}\sigma_1)\right] \langle\sigma_2|\boldsymbol{\sigma}|\sigma_1\rangle, \tag{4.53}$$

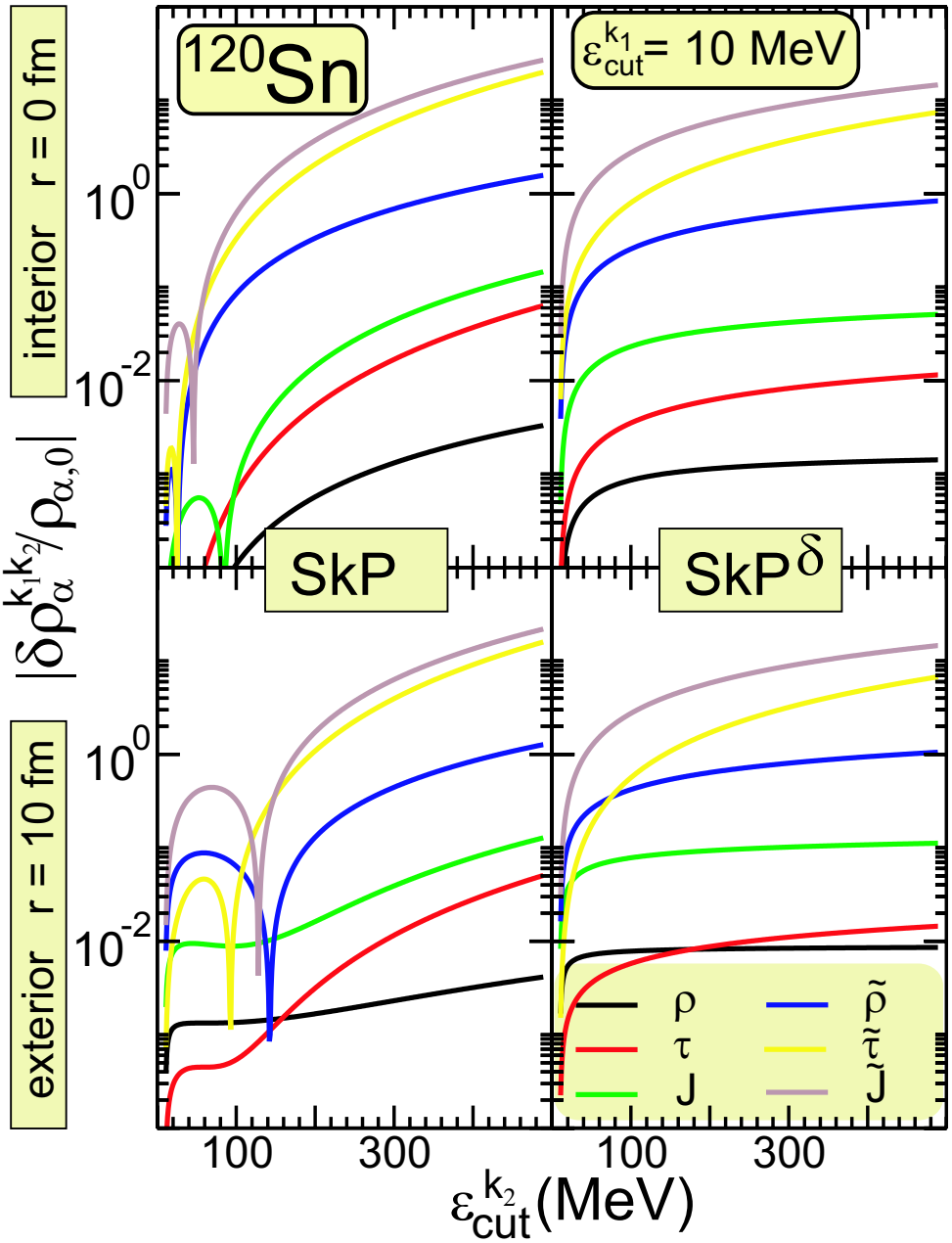

Figure 4.1: The ratio between the absolute value of the approximate high energy neutron contributions to local densities $\delta\rho_\alpha^{k_1k_2}$ (4.39-4.42, 4.55-4.56) with $\{\rho_\alpha\} = \{\rho, \tau, J, \tilde{\rho}, \tilde{\tau}, \tilde{J}\}$ and the maximum value of respective densities calculated for $\epsilon_{\rm cut}^{k_1} = 10\,$MeV, as a function of $\epsilon_{\rm cut}^{k_2}$. SkP parameterization of the Skyrme functional is used in the p-h channel. The pairing functional derived from the Skyrme interaction for SkP parameterization (left panels) and volume pairing (right panels) were used. The calculations were carried out for ^{120}Sn. In this nucleus proton pairing is zero. Presented results correspond to the center of nucleus - $r = 0$ (top panels) and the nuclear exterior - $r = 10\,$fm (bottom panels) for $\epsilon_{\rm cut}^{k_1} = 10\,$MeV.

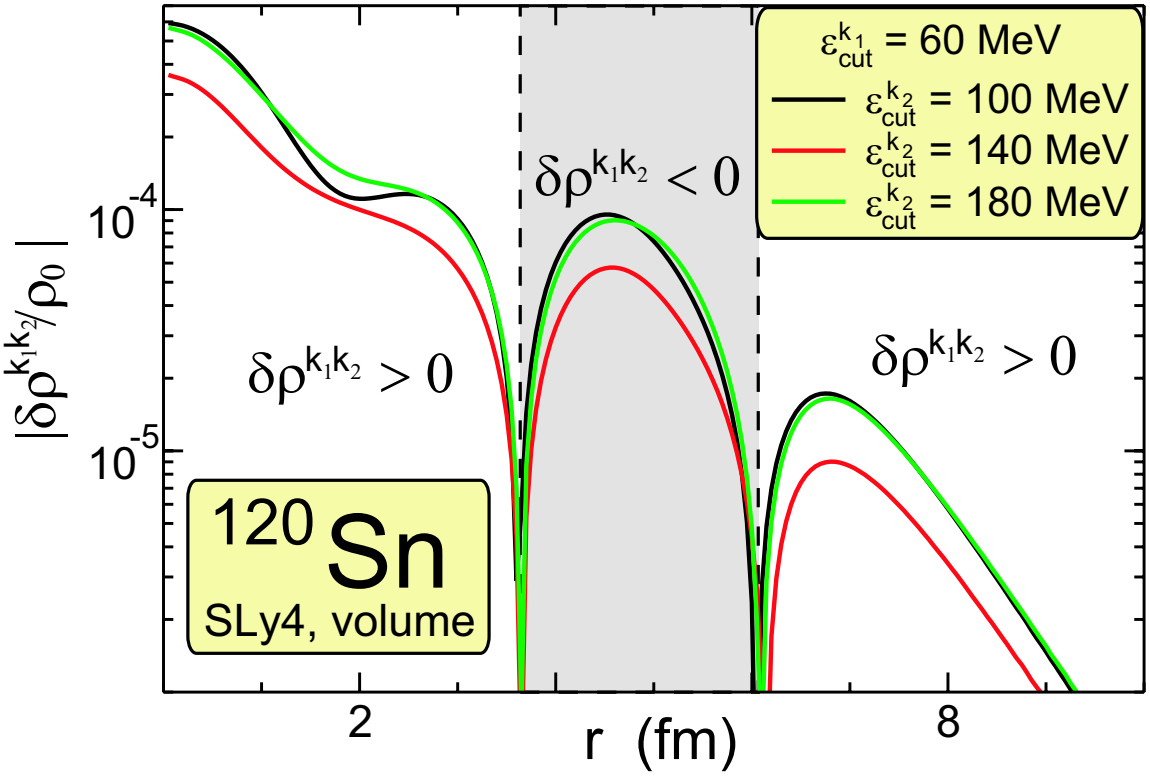

Figure 4.2: The ratio between the high energy contribution to the particle density, $|\delta\rho^{k_1k_2}|$, and its value in the center of nucleus for $\epsilon^{k_1}_{\rm cut} = 60\,$MeV for different values of $\epsilon^{k_2}_{\rm cut}$. The HFB+SLy4 calculations were carried out for ^{120}Sn.

and abnormal spin-current density,

$$\tilde{\boldsymbol{J}}(\boldsymbol{r_2}\sigma_2,\boldsymbol{r_1}\sigma_1) = -\frac{i}{2}\sum\left[\varphi_{1i}(\boldsymbol{r_2}\sigma_2)\nabla_{\boldsymbol{r_1}}\varphi^*_{2i}(\boldsymbol{r_1}\sigma_1) - \nabla_{\boldsymbol{r_2}}\varphi_{1i}(\boldsymbol{r_2}\sigma_2)\varphi^*_{2i}(\boldsymbol{r_1}\sigma_1)\right]\langle\sigma_2|\boldsymbol{\sigma}|\sigma_1\rangle, \tag{4.54}$$

may be approximated by:

$$\delta J^{k_1k_2} = \frac{1}{4\pi^2}\left[\frac{\tilde{B}^2}{B^2}S_2^{k_1k_2} + \frac{2\tilde{B}\tilde{U}}{B^2}S_0^{k_1k_2} + \frac{\tilde{U}^2}{B^2}S_{-2}^{k_1k_2}\right], \tag{4.55}$$

$$\delta\tilde{J}^{k_1k_2} = -\frac{1}{2\pi^2}\left[\frac{\tilde{B}}{B}S_2^{k_1k_2} + \frac{\tilde{U}}{B}S_0^{k_1k_2}\right]. \tag{4.56}$$

These contributions are plotted in Fig. 4.1. One can see that for the spin-current density, high energy contributions are very small, such that $\delta J^{k_1k_2}/J_0 \ll 10^{-2}$ for $50\,\text{MeV} < \epsilon_{\rm cut} < 200\,\text{MeV}$. On the other hand, Fig. 4.1 illustrates that the abnormal spin-current strongly depends on the cutoff energy.

The divergence in the spin-current density is of a lower order than that of the kinetic density, and for cutoff energies used in the low-energy nuclear structure calculations and

rather weak coupling constants, no additional regularization is necessary. Therefore, regularization expressions will still be approximately valid when the spin-orbit term is included in the functional. If particular, for $\tilde{B} = 0$, there is only a logarithmic divergence in the spin-current density and it is not practical to remove it.

On the other hand, ultraviolet divergence appearing in the abnormal spin-current density is of the higher order, $\delta\tilde{J} \sim S_0^{k_1 k_2}$, and consequently, regularization would be necessary if corresponding terms were included in the functional.

4.1.2 Regularized Skyrme-HFB

The Skyrme ED [55,57,108] is local in the coordinate space. For local energy densities, HFB equations give (see appendix C.1 for details):

$$\begin{aligned}&\left[\tilde{B}(\boldsymbol{r})\left(\frac{1}{4}\nabla_{\boldsymbol{r}}^2 - \nabla_{\boldsymbol{x}}^2\right) + \tilde{U}(\boldsymbol{r})\right]\left[\mathcal{F}_{\epsilon_{\rm cut}}(\boldsymbol{r},\boldsymbol{x}) - \rho(\boldsymbol{r},\boldsymbol{x})\right]\Big|_{\boldsymbol{x}=0} = \\ &= -\left[B(\boldsymbol{r})\left(\frac{1}{4}\nabla_{\boldsymbol{r}}^2 - \nabla_{\boldsymbol{x}}^2\right) + U(\boldsymbol{r}) - \mu\right]\tilde{\rho}(\boldsymbol{r},\boldsymbol{x})\Big|_{\boldsymbol{x}=0}\end{aligned} \tag{4.57}$$

where the completeness function $\mathcal{F}_{\epsilon_{\rm cut}}$ is defined as:

$$\mathcal{F}_{\epsilon_{\rm cut}}(\boldsymbol{r_2},\boldsymbol{r_1}) = \sum_{\epsilon_i<\epsilon_{\rm cut}}\left[\varphi_{1i}(\boldsymbol{r_2}\sigma)\varphi_{1i}^*(\boldsymbol{r_1}\sigma) + \varphi_{2i}(\boldsymbol{r_2}\sigma)\varphi_{2i}^*(\boldsymbol{r_1}\sigma)\right], \tag{4.58}$$

where the relative coordinates $(\boldsymbol{r},\boldsymbol{x})$ are

$$\boldsymbol{r} = \frac{1}{2}(\boldsymbol{r_1}+\boldsymbol{r_2}), \tag{4.59}$$

$$\boldsymbol{x} = \boldsymbol{r_2}-\boldsymbol{r_1}. \tag{4.60}$$

All eigenstates of a linear operator form a complete basis in the Hilbert space. Therefore, when the truncation procedure is not applied:

$$\lim_{\epsilon_{\rm cut}\to\infty}\mathcal{F}_{\epsilon_{\rm cut}}(\boldsymbol{r_2},\boldsymbol{r_1}) = \delta(\boldsymbol{r_2}-\boldsymbol{r_1}). \tag{4.61}$$

Therefore, one can write:

$$\mathcal{F}_{\epsilon_{\rm cut}}(\boldsymbol{r_2},\boldsymbol{r_1}) = \delta(\boldsymbol{r_2}-\boldsymbol{r_1}) - \sum_{\epsilon_i\geq\epsilon_{\rm cut}}\varphi_{1i}(\boldsymbol{r_2})\varphi_{1i}^*(\boldsymbol{r_1}) - \left[\rho^{\infty}(\boldsymbol{r_2},\boldsymbol{r_1}) - \rho^{\epsilon_{\rm cut}}(\boldsymbol{r_2},\boldsymbol{r_1})\right], \tag{4.62}$$

where $\rho^{\epsilon_{\rm cut}}$ corresponds to the density, ρ, calculated for the given cutoff energy $\epsilon_{\rm cut}$. However, as discussed above:

$$\rho^{\infty}(\boldsymbol{r},\boldsymbol{r}) = \rho^{\epsilon_{\rm cut}}(\boldsymbol{r},\boldsymbol{r}). \tag{4.63}$$

Moreover, for a large equivalent energy (see Eqs. (4.28, 4.29)):

$$h_\mu \gg \tilde{h}, \qquad |\varphi_{1i}| \gg |\varphi_{2i}|, \tag{4.64}$$

and one can approximate:

$$\tilde{h} = 0, \qquad \varphi_{2i} = 0. \tag{4.65}$$

Therefore, $\varphi_{1i}(\boldsymbol{r_1})$ is approximately an eigenfunction of the Hamiltonian h (4.19), with the corresponding eigenvalue $e_i \approx E_i + \mu \approx \bar{e}_i$:

$$\begin{aligned} \varphi_{1i}(\boldsymbol{r_1}) &\approx \varphi_i(\boldsymbol{r_1}), & (4.66) \\ \int h(\boldsymbol{r_2}, \boldsymbol{r_1})\varphi_i(\boldsymbol{r_1}) d^3\boldsymbol{r_1} &= e_i \varphi_i(\boldsymbol{r_2}), & (4.67) \end{aligned}$$

and since eigenvectors of a linear operator form a complete basis, the completeness function $\mathcal{F}_{\epsilon_{\rm cut}}$ (4.62) may be written as

$$\mathcal{F}_{\epsilon_{\rm cut}}(\boldsymbol{r_2}, \boldsymbol{r_1}) = \sum_{\epsilon_i < \epsilon_{\rm cut}} \varphi_i(\boldsymbol{r_2})\varphi_i^*(\boldsymbol{r_1}). \quad (4.68)$$

Green's function $G(\boldsymbol{r_1}, \boldsymbol{r_2}; e)$ of the Hamiltonian h can be written in the spectral representation as:

$$G(\boldsymbol{r_2}, \boldsymbol{r_1}; e) = \sum_i \frac{\varphi_i^*(\boldsymbol{r_1})\varphi_i(\boldsymbol{r_2})}{e - e_i}. \quad (4.69)$$

For $\boldsymbol{x} = 0$ Eq. (4.57) yields:

$$\tilde{\rho} = \frac{\tilde{B}}{B}\left[\rho - \mathcal{F}_{\epsilon_{\rm cut}}\right] + \left[\tilde{U} - \frac{\tilde{B}}{B}(U - \mu)\right] G_\mu^*, \quad (4.70)$$

where

$$G_\mu^*(\boldsymbol{r}) = G(\boldsymbol{r}, \boldsymbol{r}; \mu) + \bar{G}(\boldsymbol{r}, \boldsymbol{r}; \mu), \quad (4.71)$$

and $\bar{G}$ is a solution of equation:

$$\int d^3\boldsymbol{r_3}\left[h(\boldsymbol{r_1}, \boldsymbol{r_3}) - \mu\delta(\boldsymbol{r_1} - \boldsymbol{r_3})\right]\bar{G}(\boldsymbol{r_3}, \boldsymbol{r_2}, \mu) = \rho(\boldsymbol{r_1}, \boldsymbol{r_2}), \quad (4.72)$$

that does not depend on the cutoff energy $\epsilon_{\rm cut}$.

4.2 Regularization Within the Thomas-Fermi Approximation

The Thomas-Fermi approximation [47, 109, 110] is a semiclassical approach, where wave functions are approximated with eigenstates of the momentum operator and the momentum is related to the energy and local value of the potential. As a consequence, the Green's function in the Thomas Fermi approximation is a free particle Green's function at the energy renormalized by the value of the local potential:

$$G_\epsilon^{TF}(\boldsymbol{r}, \boldsymbol{x}) = G_{\epsilon - U(\boldsymbol{r})}^{free}(\boldsymbol{r}, \boldsymbol{x}). \quad (4.73)$$

Therefore, using the Thomas-Fermi approximation, Green's function (4.69) may be written as:

$$\begin{aligned} G_\mu(\boldsymbol{r}, \boldsymbol{x}) &= \frac{1}{(2\pi)^3 B(\boldsymbol{r})} \lim_{\gamma \to 0} \int_0^{k_{\rm cut}(\boldsymbol{r})} \frac{d^3\boldsymbol{k} \exp(i\boldsymbol{k}\boldsymbol{x})}{k_F^2(\boldsymbol{r}) - k^2 + i\gamma} = \\ &= \frac{1}{2\pi^2 B(\boldsymbol{r}) x} \lim_{\gamma \to 0} \int_0^{k_{\rm cut}(\boldsymbol{r})} \frac{k dk \sin(kx)}{k_F^2(\boldsymbol{r}) - k^2 + i\gamma}, \end{aligned} \quad (4.74)$$

where

$$k_F^2(\boldsymbol{r}) = \frac{\mu - U(\boldsymbol{r})}{B(\boldsymbol{r})}, \tag{4.75}$$

$$k_{\rm cut}(\boldsymbol{r}) = \sqrt{\frac{\epsilon_{\rm cut} + \mu - U(\boldsymbol{r})}{B(\boldsymbol{r})}}. \tag{4.76}$$

Using the residue theorem, one can express integral (4.74) as:

$$G_\mu(\boldsymbol{r}, \boldsymbol{x}) = \frac{1}{2\pi^2 B(\boldsymbol{r}) x}\left[\mathcal{P}\int_0^{k_{\rm cut}(\boldsymbol{r})} \frac{k dk \sin(kx)}{k_F^2(\boldsymbol{r}) - k^2} + i\pi \sum {\rm Res}\left(\frac{k\sin(kx)}{k_F^2(\boldsymbol{r}) - k^2}\right)\right], \tag{4.77}$$

where Res() corresponds to residuum of integral kernel laying on the integration contour. There is only one residuum at $k = k_F$ for real k_F, and

$$\sum {\rm Res}\frac{k\sin(kx)}{k_F^2(\boldsymbol{r}) - k^2} = -\frac{\sin(k_F x)}{2}. \tag{4.78}$$

The principal value of the integral in Eq. (4.77) may be written as:

$$\begin{aligned}
&\frac{1}{2\pi^2 B x}\mathcal{P}\int_0^{k_{\rm cut}} \frac{k\sin(kx)\,dk}{k_F^2 - k^2} = \\
&= -\frac{1}{Bx^2}\Big\{ {\rm Ci}\left((-k_F + k_{\rm cut})x\right)\sin(k_F x) + {\rm Si}\left((-k_F + k_{\rm cut})x\right)\cos(k_F x) - \\
&-{\rm Ci}\left((k_F + k_{\rm cut})x\right)\sin(k_F x) + {\rm Si}\left((k_F + k_{\rm cut})x\right)\cos(k_F x)\Big\},
\end{aligned} \tag{4.79}$$

where Ci() stands for the cosine integral function and Si() is the sine integral function.

The completeness function may be evaluated using the Thomas-Fermi approximation as:

$$\mathcal{F}_{\epsilon_{\rm cut}} = \frac{1}{2\pi^2}\frac{\sin(k_{\rm cut}x) - k_{\rm cut}x\cos(k_{\rm cut}x)}{x^3}. \tag{4.80}$$

Finally, equations (4.77, 4.80, 4.72) can be written for $x \to 0$ as:

$$\lim_{x\to 0} G_\mu = \begin{cases} \frac{-1}{2\pi^2 B}\left(k_{\rm cut} - \frac{k_F}{2}\left(\ln\frac{k_{\rm cut}+k_F}{k_{\rm cut}-k_F} - i\pi\right)\right) & k_F^2 \geq 0 \\ \frac{-1}{2\pi^2 B}\left(k_{\rm cut} - |k_F|{\rm atan}\frac{k_{\rm cut}}{|k_F|}\right) & k_F^2 < 0 \end{cases}, \tag{4.81}$$

$$\lim_{x\to 0}\mathcal{F}_{\epsilon_{\rm cut}} = \frac{k_{\rm cut}^3}{6\pi^2}, \tag{4.82}$$

$$\bar{G}_\mu(\boldsymbol{r}, 0) = \int \frac{d^3\boldsymbol{x'}\exp(i\boldsymbol{k_F}\boldsymbol{x'})}{x'}\rho(\boldsymbol{r}, \boldsymbol{x'}). \tag{4.83}$$

The cubic $\sim k_{\rm cut}^3$ ultraviolet divergence, generated by $\tilde{\tau}$, is more difficult to regularize than the linear $\sim k_{\rm cut}$ divergence generated by $\tilde{\rho}$.

The typical behavior of the completeness function $\mathcal{F}_{\epsilon_{\rm cut}}$ for different values of the cutoff energy is shown in Fig. 4.3, and approximation (4.82) is tested in Fig. 4.4. Both figures show that the Thomas-Fermi approximation reproduces the exact results, not only for the

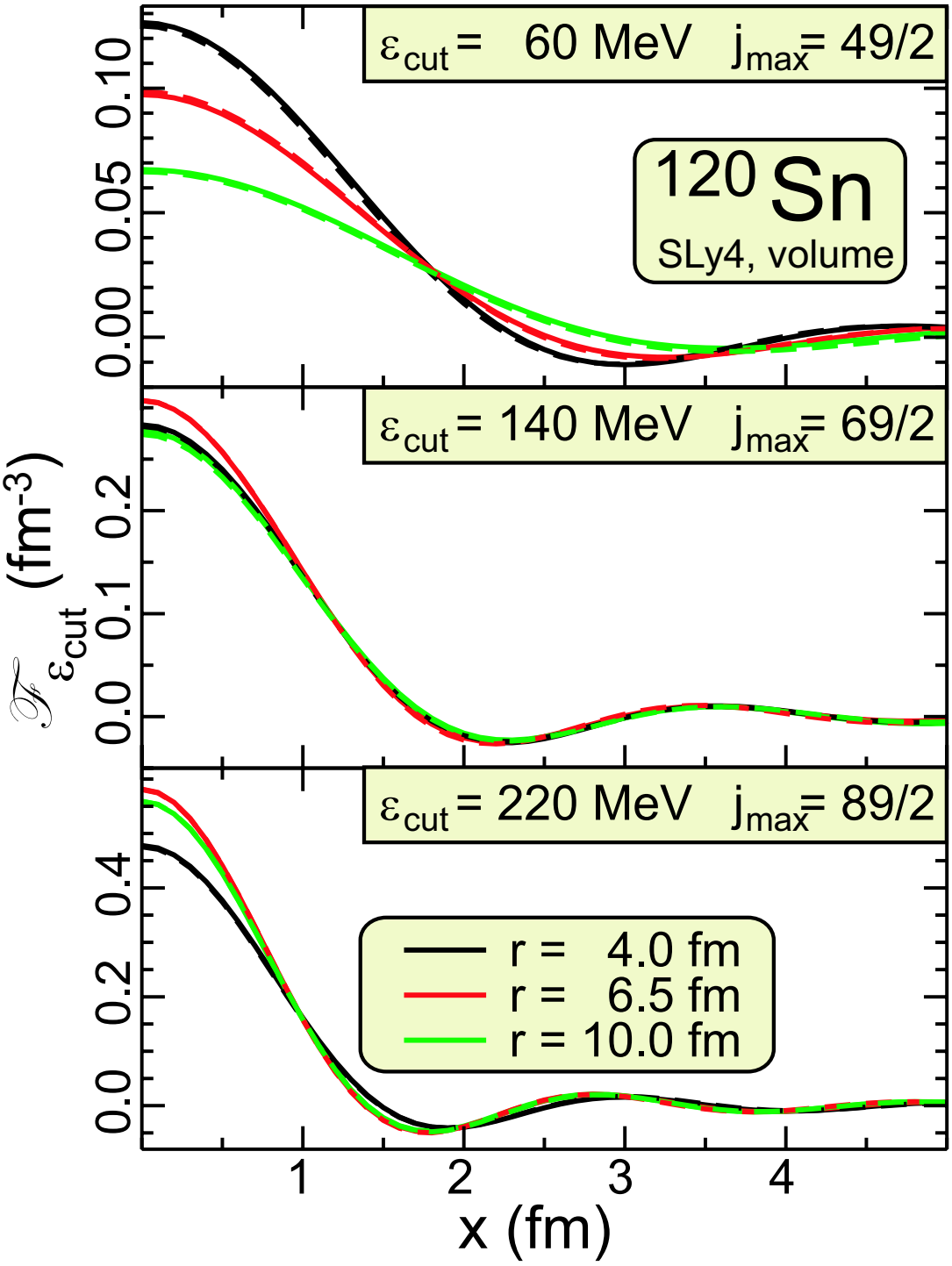

Figure 4.3: A comparison between the completeness function in the Thomas-Fermi approximation (dashed lines; Eq. 4.80) and the HFB (solid lines; Eq. 4.58) completeness function for neutrons in ^{120}Sn. HFB calculations for different values of the maximum angular momentum $j_{\max}$ were performed using the SLy4 parameterization of the Skyrme functional in the p-h channel, and volume pairing.

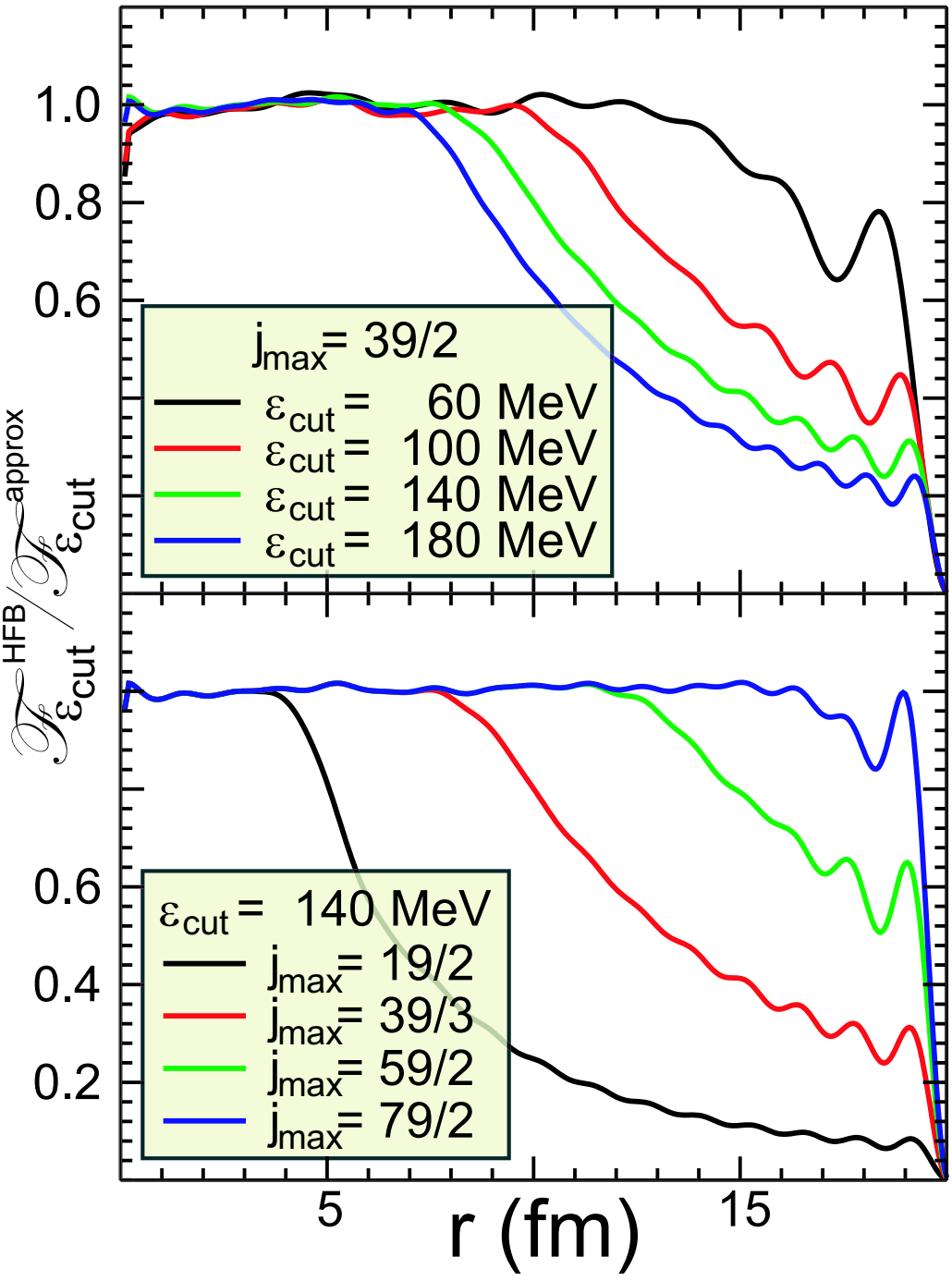

Figure 4.4: The ratio between $\mathcal{F}_{\epsilon_{\rm cut}}(r,0)$ from HFB calculations and Thomas-Fermi approximation (4.82) for neutrons in ^{120}Sn. The upper (lower) panel shows results for the maximum angular momentum $j_{\rm max}$ fixed (varying) and the cutoff energy varying (fixed) . The SLy4 parameterization of the Skyrme functional and volume pairing are used.

local completeness function, $\mathcal{F}_{\epsilon_{\rm cut}}(r,0)$, but also at large values of x. In the upper panel of Fig. 4.4 one can see that for large values of cutoff energy and r there is a significant discrepancy between the HFB results and the approximate expression (4.82). This results from the finite value of the maximum angular momentum, $j_{\rm max}$, allowed in spherical HFB calculations (see the lower panel of Fig. 4.4).

The Green's function, G_μ, and completeness function, $\mathcal{F}_{\epsilon_{\rm cut}}$, can be written for infinitely high cutoff energy as:

$$G_\mu(\boldsymbol{r}, x \to 0) = -\frac{1}{4\pi B}\frac{\exp(ik_F x)}{x} \approx -\frac{1}{4\pi B}\left(\frac{1}{x} + ik_F\right), \tag{4.84}$$

$$\mathcal{F}_{\epsilon_{\rm cut}}(\boldsymbol{r}, x \to 0) = \delta(\boldsymbol{x}). \tag{4.85}$$

The regulator $F_{\tilde\rho}$, which constitutes the divergent component of the abnormal density $\tilde\rho$ (4.70), is:

$$F_{\tilde\rho} = \frac{\tilde B}{B}\left[\mathcal{F}_{\epsilon_{\rm cut}} + (U-\mu)\,G^r_\mu\right] - \tilde U G^r_\mu, \tag{4.86}$$

where

$$G^r_\mu = G_\mu + \frac{ik_F}{4\pi B}. \tag{4.87}$$

Using Eqs. (4.57, 4.70) one can write:

$$-\tilde B\mathcal{F}''_{\epsilon_{\rm cut}} + \tilde U\mathcal{F}_{\epsilon_{\rm cut}} + \tilde B F_\tau = B F_{\tilde\tau} - (U-\mu)\,F_{\tilde\rho}, \tag{4.88}$$

where

$$\mathcal{F}''_{\epsilon_{\rm cut}}(\boldsymbol{r_1}, \boldsymbol{r_2}) = \nabla_{\boldsymbol{r_2}}\nabla_{\boldsymbol{r_1}}\mathcal{F}_{\epsilon_{\rm cut}}(\boldsymbol{r_1}, \boldsymbol{r_2}). \tag{4.89}$$

The second derivative $\mathcal{F}''_{\epsilon_{\rm cut}}$ may be evaluated using the Thomas-Fermi approximation:

$$\mathcal{F}''_{\epsilon_{\rm cut}} = \frac{3(k^2_{\rm cut}x^2-2)\sin(k_{\rm cut}x)}{2\pi^2x^5} - \frac{k_{\rm cut}x(k^2_{\rm cut}x^2-6)\cos(k_{\rm cut}x)}{2\pi^2x^5}, \tag{4.90}$$

and for small values of x $\mathcal{F}''_{\epsilon_{\rm cut}}$ becomes:

$$\lim_{x\to 0}\mathcal{F}''_{\epsilon_{\rm cut}} = \frac{k^5_{\rm cut}}{10\pi^2} = \frac{3k^2_{\rm cut}}{5}\lim_{x\to 0}\mathcal{F}_{\epsilon_{\rm cut}}. \tag{4.91}$$

It follows from (4.41, 4.42) that the ratio

$$\frac{\tilde B F_\tau}{B F_{\tilde\tau}} \sim \frac{\tilde B^2}{B^2} \tag{4.92}$$

is small (4.35) and Eq. (4.88) reads:

$$F_{\tilde\tau} = \frac{\tilde B}{B}\left[\left(\frac{U-\mu}{B} - \frac{3k^2_{\rm cut}}{5}\right)\mathcal{F}_{\epsilon_{\rm cut}} + \frac{(U-\mu)^2}{B}G^r_\mu\right] + \frac{\tilde U}{B}\left[\mathcal{F}_{\epsilon_{\rm cut}} - (U-\mu)\,G^r_\mu\right]. \tag{4.93}$$

Finally, the regulator $F_{\tilde\tau}$ can be found using Eq. (4.45):

$$F_\tau = -\frac{\tilde U\tilde B}{B^2}\mathcal{F}_{\epsilon_{\rm cut}} + \frac{\tilde U^2}{2B}G^r_\mu - \frac{\tilde B^2}{2B^2}\left[\left(\frac{U-\mu}{B} - \frac{3k^2_{\rm cut}}{5}\right)\mathcal{F}_{\epsilon_{\rm cut}} + \frac{(U-\mu)^2}{B}G^r_\mu\right]. \tag{4.94}$$

4.2.1 Regularized Skyrme-HFB: Examples and Self-Consistency

The density regulators depend on mean-fields U, $\tilde{U}$, B, and $\tilde{B}$:

$$U = \frac{\delta\mathcal{H}_r}{\delta\tilde{\rho}_r}\frac{\delta F_{\tilde{\rho}}}{\delta\rho} + \frac{\delta\mathcal{H}_r}{\delta\tau_r}\frac{\delta F_{\tau}}{\delta\rho} + \frac{\delta\mathcal{H}_r}{\delta\tilde{\tau}_r}\frac{\delta F_{\tilde{\tau}}}{\delta\rho}, \tag{4.95}$$

$$\tilde{U} = \frac{\delta\mathcal{H}_r}{\delta\tilde{\rho}_r}\left(1+\frac{\delta F_{\tilde{\rho}}}{\delta\tilde{\rho}}\right) + \frac{\delta\mathcal{H}_r}{\delta\tau_r}\frac{\delta F_{\tau}}{\delta\tilde{\rho}} + \frac{\delta\mathcal{H}_r}{\delta\tilde{\tau}_r}\frac{\delta F_{\tilde{\tau}}}{\delta\tilde{\rho}}, \tag{4.96}$$

$$B = \frac{\delta\mathcal{H}_r}{\delta\tilde{\rho}_r}\frac{\delta F_{\tilde{\rho}}}{\delta\tau} + \frac{\delta\mathcal{H}_r}{\delta\tau_r}\left(1+\frac{\delta F_{\tau}}{\delta\tau}\right) + \frac{\delta\mathcal{H}_r}{\delta\tilde{\tau}_r}\frac{\delta F_{\tilde{\tau}}}{\delta\tau}, \tag{4.97}$$

$$\tilde{B} = \frac{\delta\mathcal{H}_r}{\delta\tilde{\rho}_r}\frac{\delta F_{\tilde{\rho}}}{\delta\tilde{\tau}} + \frac{\delta\mathcal{H}_r}{\delta\tau_r}\frac{\delta F_{\tau}}{\delta\tilde{\tau}} + \frac{\delta\mathcal{H}_r}{\delta\tilde{\tau}_r}\left(1+\frac{\delta F_{\tilde{\tau}}}{\delta\tilde{\tau}}\right), \tag{4.98}$$

which in turn depend on those regulators. Consequently, one obtains a set of partial differential equations which must be solved self-consistently.

Let us consider a model ED:

$$\mathcal{H}_r[\rho,\tau_r,\tilde{\rho}_r,\tilde{\tau}_r] = b[\rho]\tau_r + \tilde{b}[\rho]\tilde{\tau}_r^{n_{\tilde{\tau}}} + g[\rho]\tilde{\rho}_r^{n_{\tilde{\rho}}} + \mathcal{H}_{pot}[\rho]. \tag{4.99}$$

For $n_{\tilde{\tau}} = 0$ and $n_{\tilde{\rho}} \neq 0$, regulators F_τ and $F_{\tilde{\rho}}$ are depend on ρ and $\tilde{\rho}$, and Eqs. (4.86, 4.94, 4.96, 4.97) give:

$$\left[n_{\tilde{\rho}} g G_\mu^r \left(\tilde{\rho}+F_{\tilde{\rho}}\right)^{n_{\tilde{\rho}}-1} + F_{\tilde{\rho}}\right]\left(1+\frac{\delta F_{\tilde{\rho}}}{\delta\tilde{\rho}}\right) = 0, \tag{4.100}$$

and

$$\tilde{U} = -\frac{F_{\tilde{\rho}}}{G_\mu^r}, \qquad B = b, \qquad F_\tau = \frac{F_{\tilde{\rho}}^2}{2bG_\mu^r}. \tag{4.101}$$

For $n_{\tilde{\rho}} = 0$, regulators F_τ and $F_{\tilde{\tau}}$ become functionals of ρ and $\tilde{\tau}$, and one can write:

$$\left[\gamma\frac{n_{\tilde{\tau}}\tilde{b}}{b}\left(\tilde{\tau}+F_{\tilde{\tau}}\right)^{n_{\tilde{\tau}}-1} - F_{\tilde{\tau}}\right]\left(1+\frac{\delta F_{\tilde{\tau}}}{\delta\tilde{\tau}}\right) = 0, \tag{4.102}$$

where

$$\gamma = \left(\frac{U-\mu}{B} - \frac{3k_{\rm cut}^2}{5}\right)\mathcal{F}_{\epsilon_{\rm cut}} + \frac{(U-\mu)^2}{B}G_\mu^r, \tag{4.103}$$

$$\tilde{B} = \frac{bF_{\tilde{\tau}}}{\gamma}, \qquad B = b, \qquad F_\tau = \frac{F_{\tilde{\tau}}^2}{2\gamma}. \tag{4.104}$$

Let us consider two simple analytically solvable cases.

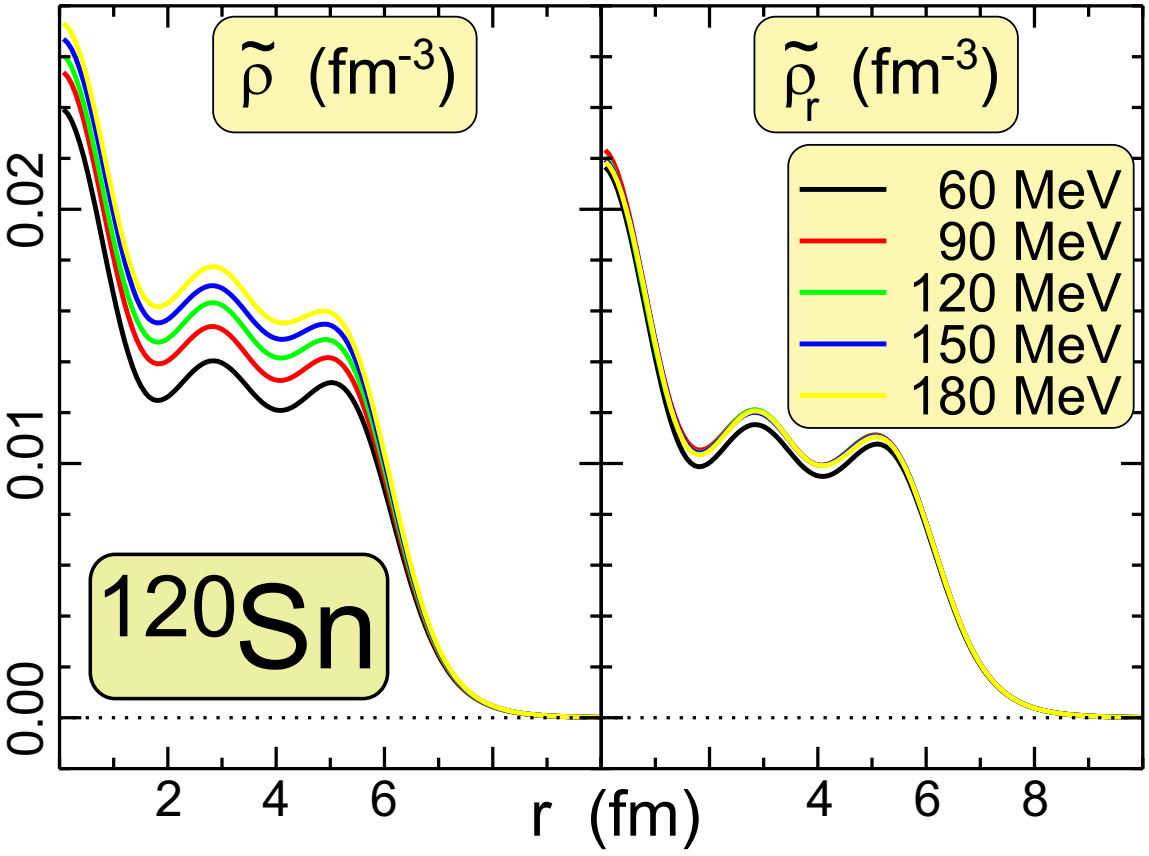

Figure 4.5: The unregularized $\tilde{\rho}$ (left panel) and regularized $\tilde{\rho}_r$ (right panel) abnormal neutron density for $n_{\tilde{\rho}} = 1$, $n_{\tilde{\tau}} = 0$ (see Eq. (4.99)), for different values of cutoff energy. Calculations were carried out for ^{120}Sn within the HBF+SLy4 model.

Academic Case: $n_{\tilde{\tau}} = 0$, $n_{\tilde{\rho}} = 1$

In this case one obtains:

$$F_{\tilde{\rho}} = -gG^r_\mu, \tag{4.105}$$

$$\mathcal{H}_r = b\tau + g\tilde{\rho} - \frac{1}{2}g^2 G^r_\mu + \mathcal{H}_{pot}, \tag{4.106}$$

$$h = -\boldsymbol{\nabla}_{\boldsymbol{r_2}} b \boldsymbol{\nabla}_{\boldsymbol{r_1}} + \tau\frac{\delta b}{\delta\rho} + \frac{\delta\mathcal{H}_{pot}}{\delta\rho} + \tilde{\rho}_r\frac{\delta g}{\delta\rho} - \frac{1}{2}g^2\frac{\delta G^r_\mu}{\delta\rho}, \tag{4.107}$$

$$\tilde{h} = g. \tag{4.108}$$

In order for the pairing field to be localized, we use a density dependent pairing strength:

$$g = g_0\rho. \tag{4.109}$$

The resulting regularized abnormal density is practically cutoff independent (see the right panel of Fig. 4.5) and variations of the total energy with respect to the cutoff energy are

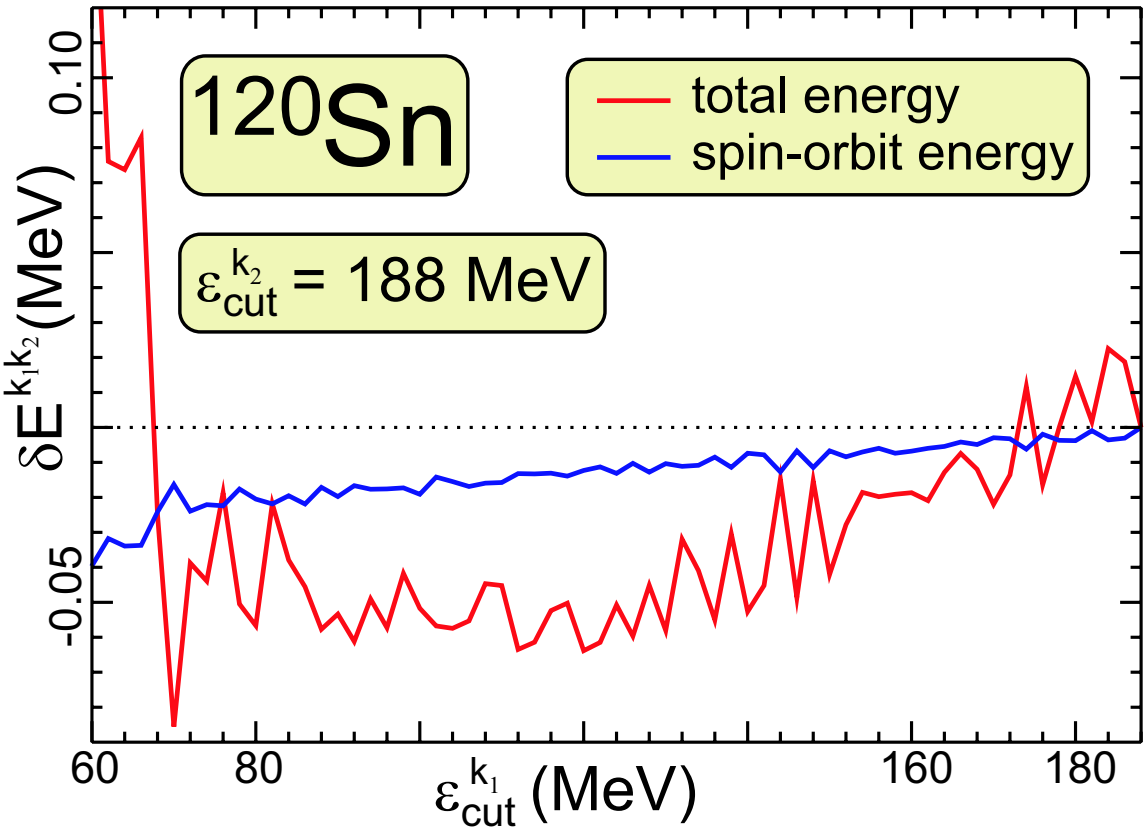

Figure 4.6: Variation of the total energy (red line) and the spin-orbit component (blue line) for $n_{\tilde{\rho}} = 1$ and $n_{\tilde{\tau}} = 0$ (see Eq. (4.99)). Calculations were carried out for ^{120}Sn within the HBF+SLy4 model.

small (see Fig. 4.6). Figure 4.6 also illustrates the variations in the spin-orbit term of the Skyrme functional. Since for the cutoff energy in the range between $60-190$ MeV, spin-orbit energy varies by no more than 50 keV, we can conclude that no further regularization of the spin-current is necessary.

Physical Case: $n_{\tilde{\tau}} = 0$, $n_{\tilde{\rho}} = 2$

Here, the regulator $F_{\tilde{\rho}}$ (4.86) is proportional to $\tilde{\rho}$,

$$F_{\tilde{\rho}} = \frac{-2gG_\mu^r}{1+2gG_\mu^r}\tilde{\rho}, \tag{4.110}$$

and the energy density and Hamiltonians h, $\tilde{h}$ are:

$$\mathcal{H}_r = B\tau + \mathcal{H}_{pot} + g_{eff}\tilde{\rho}^2, \tag{4.111}$$

$$h = -\boldsymbol{\nabla}_{\boldsymbol{r_2}} b \boldsymbol{\nabla}_{\boldsymbol{r_1}} + \tau\frac{\delta b}{\delta\rho} + \frac{\delta\mathcal{H}_{pot}}{\delta\rho} + \tilde{\rho}^2\frac{\delta g_{eff}}{\delta\rho}, \tag{4.112}$$

$$\tilde{h} = 2g\tilde{\rho}_r = 2g_{eff}\tilde{\rho}, \tag{4.113}$$

where

$$g_{eff} = \left(\frac{1}{g} + 2G^r_\mu\right)^{-1} = \begin{cases} \left(\frac{1}{g} - \frac{1}{\pi^2 B}\left(k_{\rm cut} - \frac{k_F}{2}\ln\frac{k_{\rm cut}+k_F}{k_{\rm cut}-k_F}\right)\right)^{-1} & k_F^2 \geq 0 \\ \left(\frac{1}{g} - \frac{1}{\pi^2 B}\left(k_{\rm cut} + |k_F|\text{atan}\frac{|k_F|}{k_{\rm cut}}\right)\right)^{-1} & k_F^2 < 0 \end{cases} . \quad (4.114)$$

In terms of the effective pairing strength, g_{eff}, regulators $F_{\tilde{\rho}}$ and F_τ can be written as:

$$F_{\tilde{\rho}} = \left(\frac{g_{eff}}{g} - 1\right)\tilde{\rho}, \quad (4.115)$$

$$F_\tau = -\frac{g_{eff}\,(g_{eff} - g)}{gB}\tilde{\rho}^2. \quad (4.116)$$

Therefore, for the pairing term of the EDF given by Eq. (2.10), regularization is equivalent to replacing pairing strength g with the effective cutoff-dependent pairing strength g_{eff}. The same regularization scheme was introduced in Refs. [85–87], in which the pairing gap equation was regularized.

Self-Consistency in the Regularized Skyrme-HFB

As illustrated above, for pairing terms $\mathcal{H}_{pair} = g\tilde{\rho}$ and $\mathcal{H}_{pair} = g\tilde{\rho}^2$, regularization of the functional yields mean-field potentials independent of the cutoff energy (see Eqs. (4.108, 4.113)). However, for an arbitrary energy density functional this is not guaranteed. For example, for ED:

$$\mathcal{H}_r[\rho, \tau_r, \tilde{\rho}_r] = b[\rho]\tau_r + g_1[\rho]\tilde{\rho}_r + g_2[\rho]\tilde{\rho}_r^2 + \mathcal{H}_{pot}[\rho], \quad (4.117)$$

the resuling pairing mean field,

$$\tilde{h} = \frac{g_1 + 2g_2 G^r_\mu \tilde{\rho}}{1 + 2g_2 G^r_\mu} = 2g_2\tilde{\rho}_r - \frac{g_1}{1 + 2g_2 G^r_\mu}, \quad (4.118)$$

depends on $\epsilon_{\rm cut}$ for $g_1 g_2 \neq 0$. Therefore, even though divergent components $\delta\rho_{\alpha,div}$ are removed, the finite components $\rho_{\alpha,r}$ would still depend on the cutoff, as they are constructed from eigenfunctions of the cutoff dependent Hamiltonian.

4.3 Pairing Renormalization vs. Regularization Schemes

4.3.1 Pairing Renormalization Procedure

Within the HFB theory, the energy cutoff can be applied either to the s.p. or to the quasiparticle spectrum (4.18). The first option is used when the HFB equations are solved within a restricted s.p. space. However, the s.p. energies play only an auxiliary role in the HFB method, and the cutoff applied to the quasiparticle spectrum is more justified. Due to the similarity between equivalent s.p. energies and s.p. energies, one takes into account only those quasiparticle states for which $\bar{e}_n$ is less than the assumed cutoff energy $\epsilon_{\rm cut}$.

It was shown [71] that for a fixed pairing strength, pairing energies depend significantly on the energy cutoff. Within the renormalization scheme employed in this work, we use

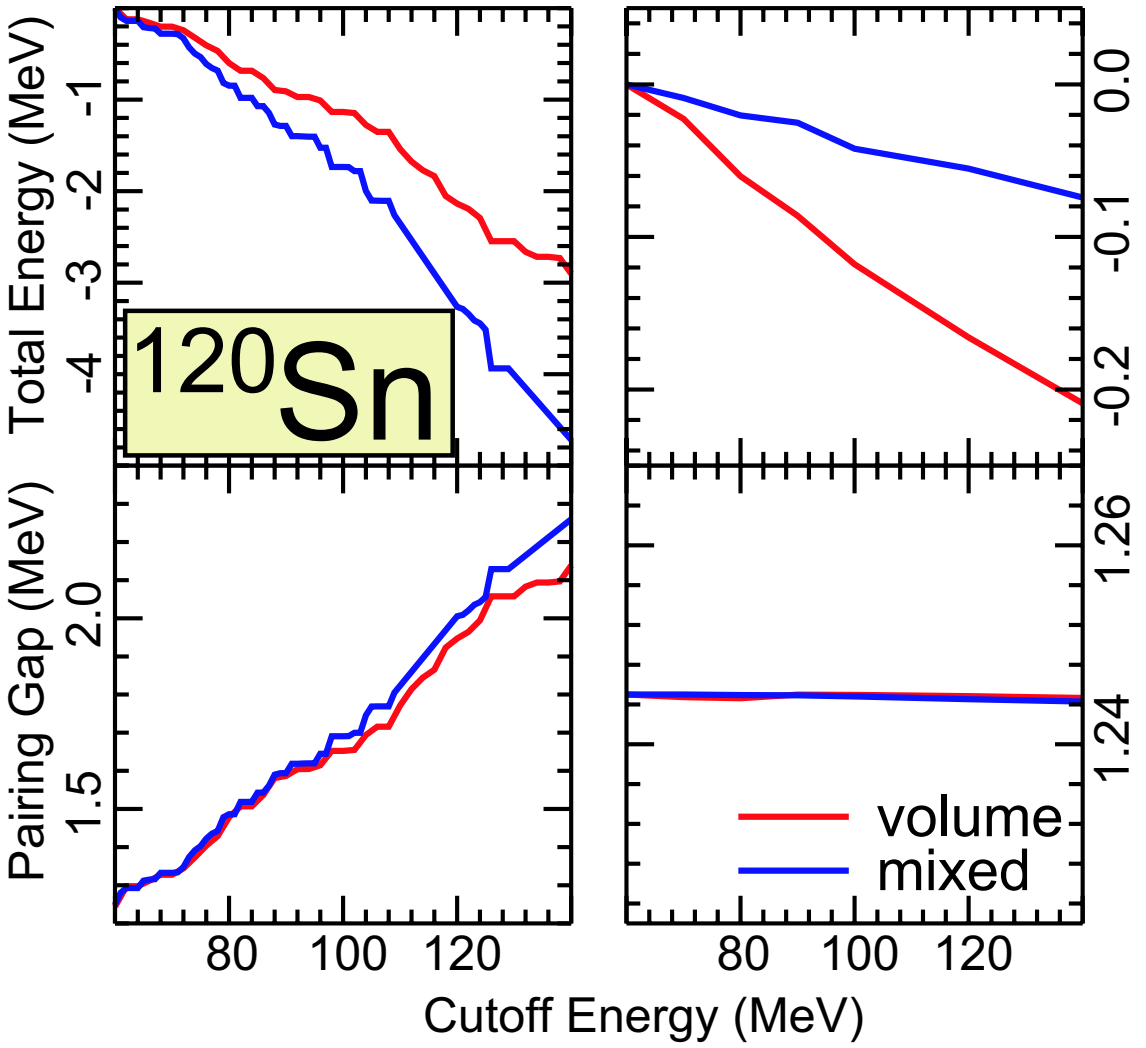

Figure 4.7: The total energy (top) and neutron pairing gap (bottom) in ^{120}Sn without (left) and with (right) pairing renormalization applied. Results are shown for volume (red) and mixed (blue) pairing. The total energy is plotted relative to the values obtained for the cutoff energy of $\epsilon_{\rm cut}$=60 MeV.

the prescription of adjusting the pairing strength to obtain a fixed average neutron pairing gap $\bar{\Delta}$ in ^{120}Sn equal to the experimental value of 1.245 MeV [61]. Such a procedure almost eliminates the dependence of the HFB energy on the cutoff [71].

Figure 4.7 illustrates the importance of the pairing renormalization procedure in the case of ^{120}Sn. Due to the constraint on the pairing strength, the neutron average pairing gap stays constant, while the resulting total energy changes with the cutoff energy by a few hundred keV. On the other hand, without pairing renormalization applied, the total energy and the average neutron gap vary significantly with increasing dimension of the quasiparticle space. In this case, the total energy changes by several MeV.

4.3.2 Pairing Regularization - Results

In Ref. [88] a different regularization scheme has been proposed that involves truncation below and above the Fermi level. However, the HFB calculations in the quasiparticle basis should be performed for a cutoff energy of 50 MeV and higher [71]. Since the magnitude of the self-consistent mean field U is also about 50 MeV, both methods are equivalent at the high cutoff energy. In order to obtain results independent of $\epsilon_{\rm cut}$, the Thomas-Fermi approximation requires the value of $\epsilon_{\rm cut}$ to be high enough that $k_{\rm cut}$ (4.76) is real everywhere.

Self consistent mean field U is given as:

$$U = \frac{\delta}{\delta\rho}\mathcal{H}_r = \frac{\delta}{\delta\rho}\mathcal{H}_{p-h} + \frac{\delta}{\delta\rho}\mathcal{H}_{pair}. \tag{4.119}$$

The density dependence of the pairing part of the ED gives so-called pairing rearrangement term (second term in Eq. 4.119). For the EDF (4.111) the rearrangement term is (see Appendix C.2):

$$\frac{\delta}{\delta\rho}\mathcal{H}_{pair} = \tilde{\rho}^2\left[\frac{\partial g_{eff}}{\partial g}\frac{\delta g}{\delta\rho} + \frac{\partial g_{eff}}{\partial k_F}\frac{\delta k_F}{\delta\rho} + \frac{\partial g_{eff}}{\partial k_{\rm cut}}\frac{\delta k_{\rm cut}}{\delta\rho}\right]. \tag{4.120}$$

The first term in Eq. (4.120) is similar to the usual rearrangement term associated with the explicit density dependence of the effecive interaction, while the other two terms associated with the regularization procedure are entirely new. It is easy to check that all the terms appearing in Eq. (4.120) are continuous at the classical turning point $k_F(\boldsymbol{r}) = 0$.

The total energy and the average neutron pairing gap in ^{120}Sn, with the pairing regularization procedure applied, are shown in Fig. 4.8. The pairing strength V_0 is kept constant; it reproduces the neutron pairing gap for ^{120}Sn at the cutoff energy of $\epsilon_{\rm cut}$ =60 MeV.

In the left panels of Fig. 4.8, we show results obtained in the HO basis and the results from the solution of the HFB equations in coordinate space are displayed in the right panels. One can correlate the coordinate-space and HO representations by introducing an 'effective box size' $R \approx \sqrt{2N_{osc}\hbar/m\omega}$ [71], where N_{osc} is the number of harmonic oscillator shells. Using this formula, the basis of 20 HO shells corresponds to a box radius of about 14.5 fm. Figure 4.8 demonstrates that the regularization procedure is stable with respect to the cutoff energy. Moreover, one obtains reasonable results already for fairly low cutoff energies of about 40 MeV. Variations in the total energy in coordinate-space calculations do not exceed 40 keV, while they are about 150 keV in the HO expansion. The latter does not decrease significantly with N_{osc}.

The differences in applying the pairing regularization procedure in the coordinate-space and HO calculations can be explained by the different way the quasiparticle space is expanded in both approaches. The particle density ρ is defined by the lower components of the quasiparticle wave functions, which are localized within the nuclear interior. On the other hand, the abnormal density is defined by the products of the upper and lower components of the quasiparticle wave function. The upper components of the quasiparticle wave function are not localized for the quasiparticle energies that are greater than the modulus of the chemical potential. Therefore, contrary to the normal density, the abnormal density strongly depends on the completeness of the s.p. basis outside the nuclear interior.

In the coordinate-space calculations, the box boundary conditions provide discretization of the spectrum for the non-localized quasiparticle. On the other hand, all the HO basis

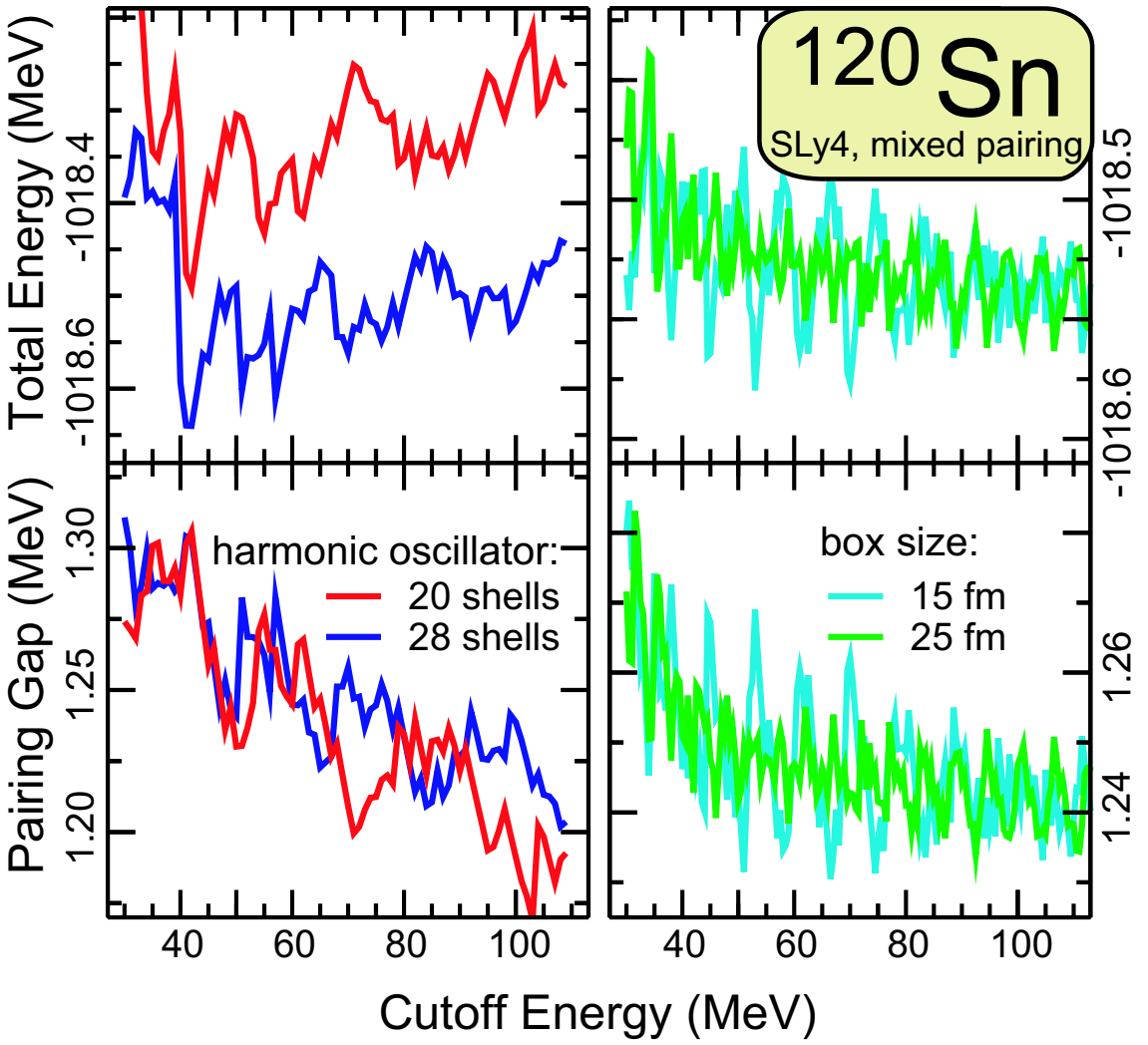

Figure 4.8: Total energy (top) and neutron pairing gap (bottom) in ^{120}Sn for the two values of N_{osc} (left), and using two box sizes (right). Calculations were performed using the mixed pairing interaction.

states are localized. Results of stability with respect to the cutoff energy for the coordinate-space and HO calculations are, therefore, different. As far as the description of nonlocalized states is concerned, the coordinate-space method is superior to the HO expansion method.

Fluctuations in the total energy, shown in Fig. 4.8, coincide with $2j+1$-folded degenerate angular-momentum multiplets of states in spherical nuclei that enter the pairing window with increasing cutoff energy. This can be confirmed by performing a similar analysis for a deformed nucleus, where the magnetic degeneracy is lifted. Such results are shown for deformed ^{110}Zr in comparison with spherical ^{120}Sn in Fig. 4.9. One can see that the fluctuations of the total energy in ^{110}Zr are down to about 40 keV. It is worth noting that even though mean-field symmetries and resulting degeneracies increase the magnitude of fluctu-

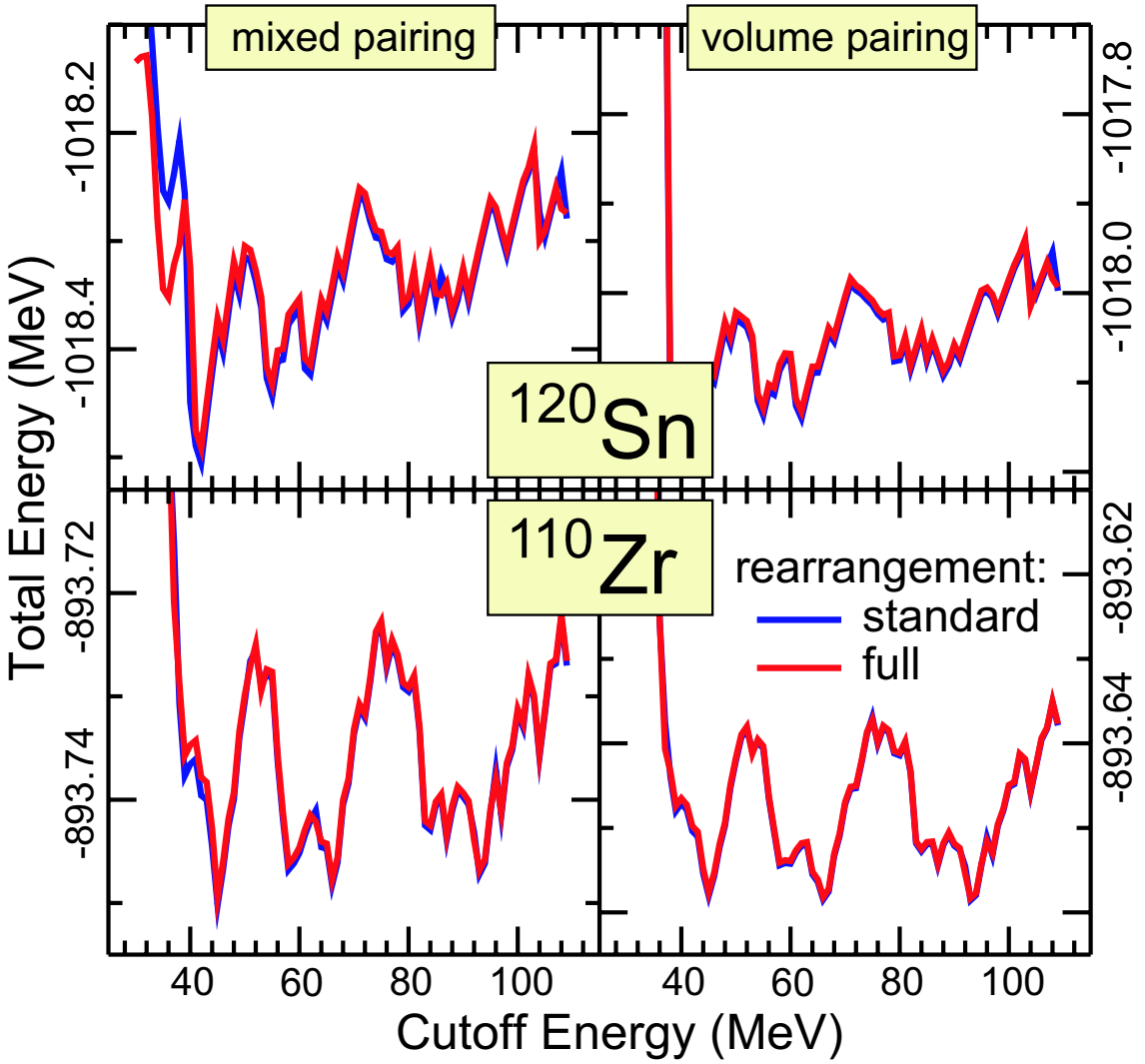

Figure 4.9: Total energy of spherical ^{120}Sn (top) and deformed ^{110}Zr (bottom) obtained with pairing regularization (red lines) for mixed pairing (left) and volume pairing (right). The results obtained without the rearrangement terms resulting from the variation of $k_{\rm cut}$ and k_F are also shown (blue lines).

ations, the most important factor is the continuum discretization scheme used in a given numerical implementation.

The steep increase of the total energy at cutoff energies below 30 MeV results from neglecting quasiparticle states with significant occupation probability. This effect is more severe for mixed pairing than for volume-pairing calculations due to the surface-peaked character of mixed pairing fields. The stability with respect to the cutoff energy is similar in both cases.

We have also tested the importance of the rearrangement terms (see appendix C.2)

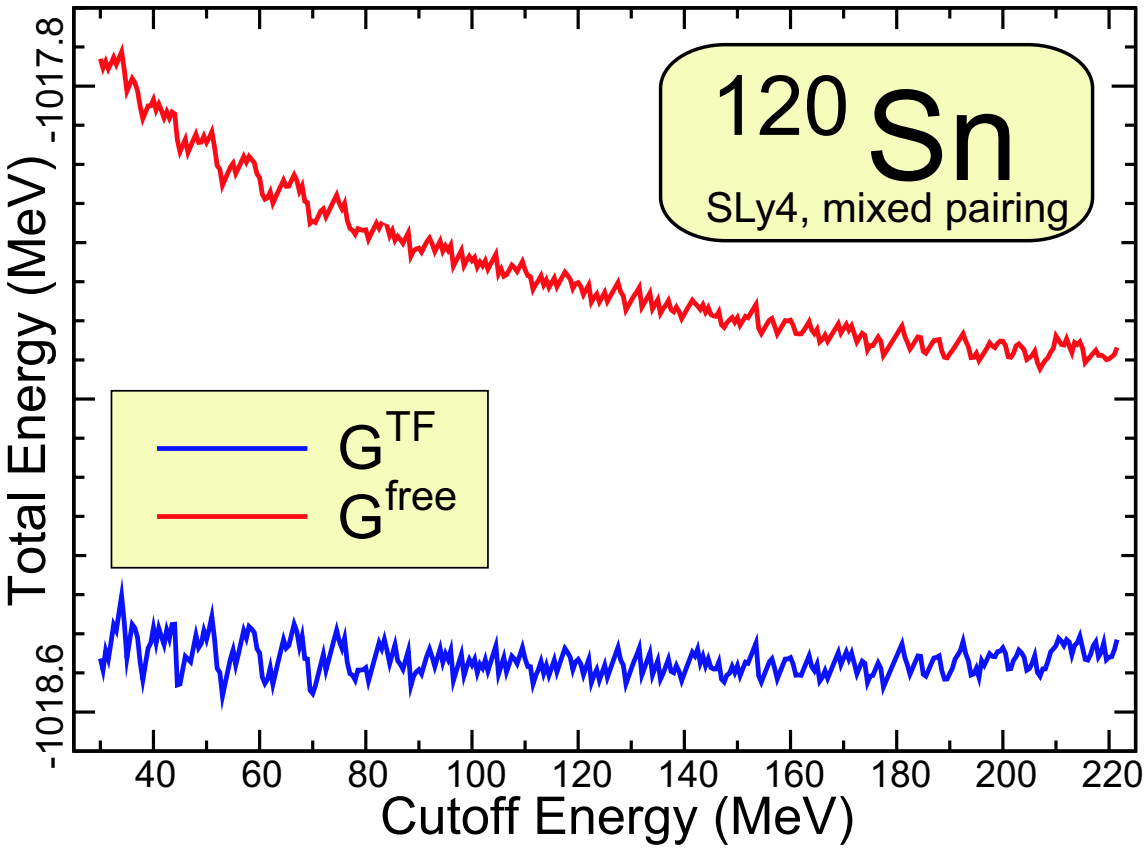

Figure 4.10: Two pairing regularization schemes applied to the case of ^{120}Sn: the Thomas-Fermi approximation (blue line) and the free particle Green's function (red line). Coordinate-space calculations were performed in a 15 fm box.

arising as a result of the regularization procedure. The blue lines in Fig. 4.9 show results obtained without taking into account the second and third term of Eq. (4.120). These terms lead to changes in the total energy of a few keV and can be safely neglected.

Finally, we have tested the Thomas-Fermi approximation used in the pairing regularization procedure. Instead of adopting the Thomas-Fermi ansatz, one can perform regularization using the free particle Green's function [83]. As illustrated in Fig. 4.10, the convergence of the latter method is very slow, therefore the Thomas-Fermi method is clearly superior.

4.3.3 Link Between the Pairing Renormalization and Regularization Procedures

The renormalized and regularized pairing calculations are based on two different effective interactions. Consequently, their results should be comparable only to the degree that their effective pairing strengths g_{eff} are similar. By expanding Eq. (4.114) at very high cutoff

energies ($k_F/k_{\rm cut} << 1$), one obtains:

$$g_{eff}(\boldsymbol{r}) \approx \left(1 - \frac{M^*(\boldsymbol{r})g(\boldsymbol{r})}{2\pi^2\hbar^2}k_{\rm cut}(\boldsymbol{r})\right)^{-1} g(\boldsymbol{r}), \tag{4.121}$$

which has the form of $g_{eff} = \alpha g$. For the volume pairing, the proportionality factor α is ρ-dependent through the weak density dependence of the effective mass M^*. For the mixed pairing, it also depends on ρ through the density dependence of g.

Therefore, the renormalization procedure may be considered as a fair approximation to the regularization for volume pairing, but not for mixed pairing or, more generally, for any density-dependent pairing. This approximate equality of the effective pairing strengths for the pairing regularization and renormalization explains remarkable stability of the total energy in the phenomenological pairing renormalization treatment (see Fig. 4.7), and why results obtained for the volume pairing are more stable than those in the mixed pairing variant.

This effect can be clearly seen in Fig. 4.11. The ratio between the effective pairing strengths in the regularization and renormalization methods is much closer to unity for the volume pairing than for the mixed pairing in the region of space, where the pairing energy density is maximal.

4.3.4 Pairing Renormalization and Regularization Procedures - Comparison of Results

In this section, we present a comparison between pairing renormalization and regularization procedures applied to a large number of nuclei. As representative cases, we discuss the results obtained for the drip-to-drip line isotopic chains of spherical Sn nuclei and for deformed Dy nuclei. Calculations are performed for the volume and/or mixed pairing interactions by using the HFB+THO approach. The isotopic chains include all particle-bound even-even nuclei, including the drip line systems. The stability of the regularization procedure is primarily determined by the equivalent energies around the cutoff energy. Therefore, the quality of results is comparable for stable nuclei and weakly bound systems.

Spherical Nuclei

Figures 4.12 and 4.13 display differences between the pairing renormalization and regularization procedures for the Sn isotopes. Calculations are performed with both volume and mixed pairing interactions. For the two-neutron separation energies, the maximum difference between the renormalization and regularization schemes is about 100 (300) keV for the volume (mixed) pairing. In the neutron gap, the corresponding difference is about 50 (100) keV, and in nuclear radii (not displayed) it is practically negligible (about 0.01 fm). The largest differences show up in the pairing energies – about 1 (3) MeV for the volume (mixed) pairing; however, total energy differences are much smaller – about 400 (800) keV.

Analyzing the total energies obtained in both methods, Fig. 4.12 shows that the pairing renormalization procedure gives systematically more binding. The differences are negligible for stable nuclei and nuclei near the proton drip line. They increase in mid-shell nuclei near the two-neutron drip line where the pairing effects are the largest, and then decrease towards the closed-shell nucleus ^{176}Sn located just at the two-neutron drip line. In general,

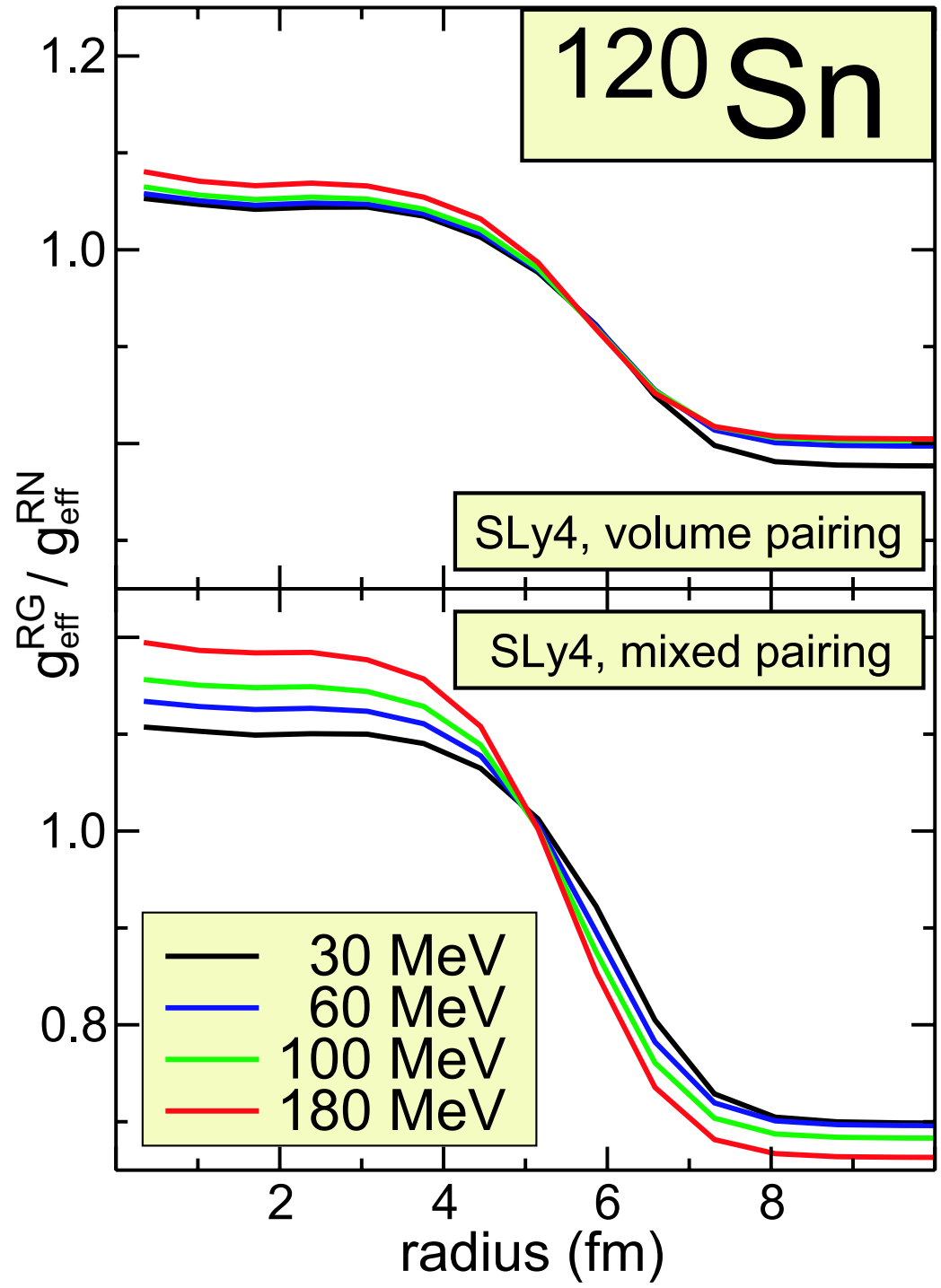

Figure 4.11: Ratio between the effective pairing strengths for pairing regularization and renormalization, $g_{eff}^{RG}/g_{eff}^{RN}$, for the volume (upper panel) and mixed pairing (lower panel) in ^{120}Sn for several values of $\epsilon_{\rm cut}$.

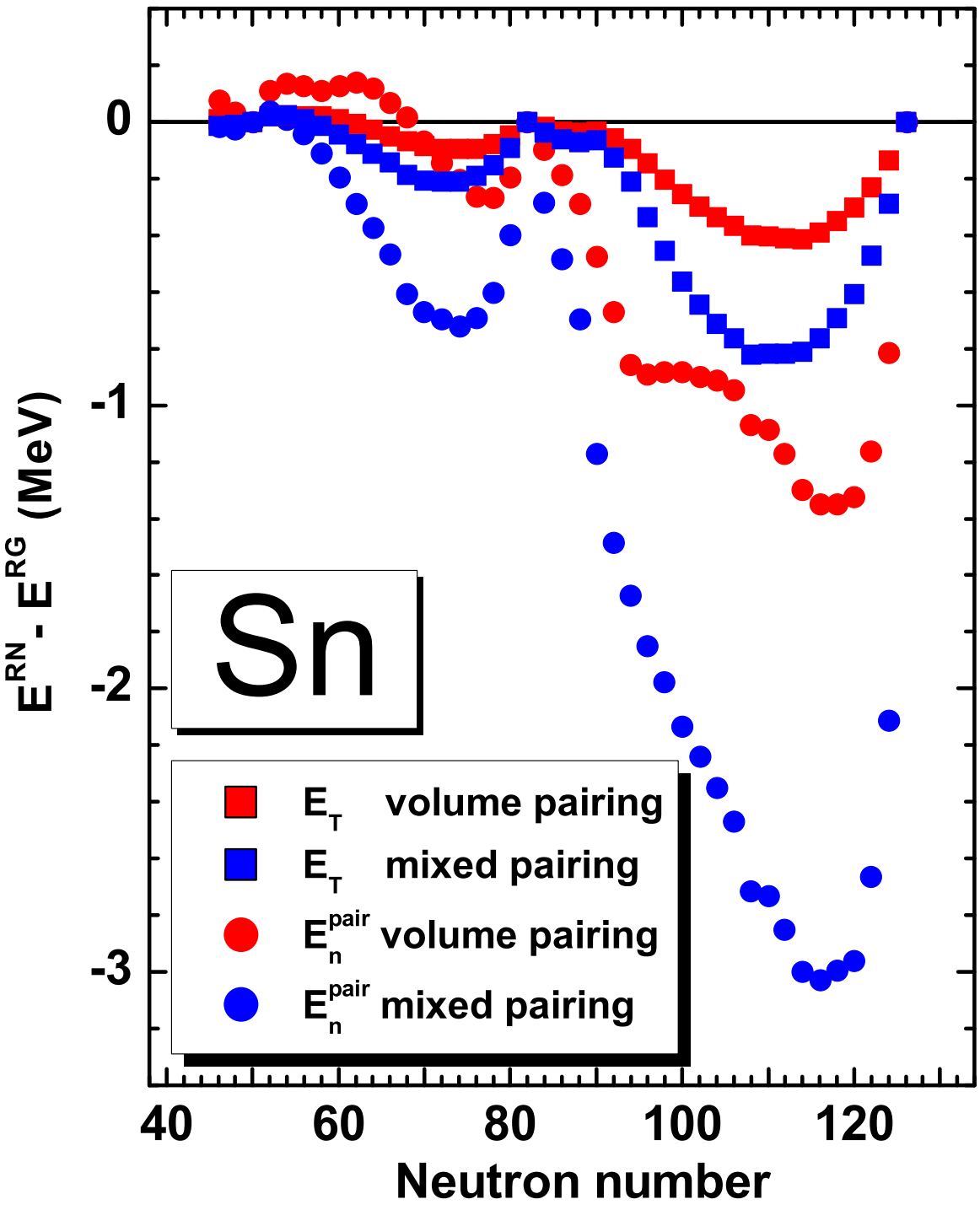

Figure 4.12: Differences between pairing renormalization (RN) and regularization (RG) procedures for total energies E_T and neutron pairing energies E_n^{pair}. The HFB+THO calculations are performed for the chain of the spherical Sn isotopes using the SkP Skyrme parameterization.

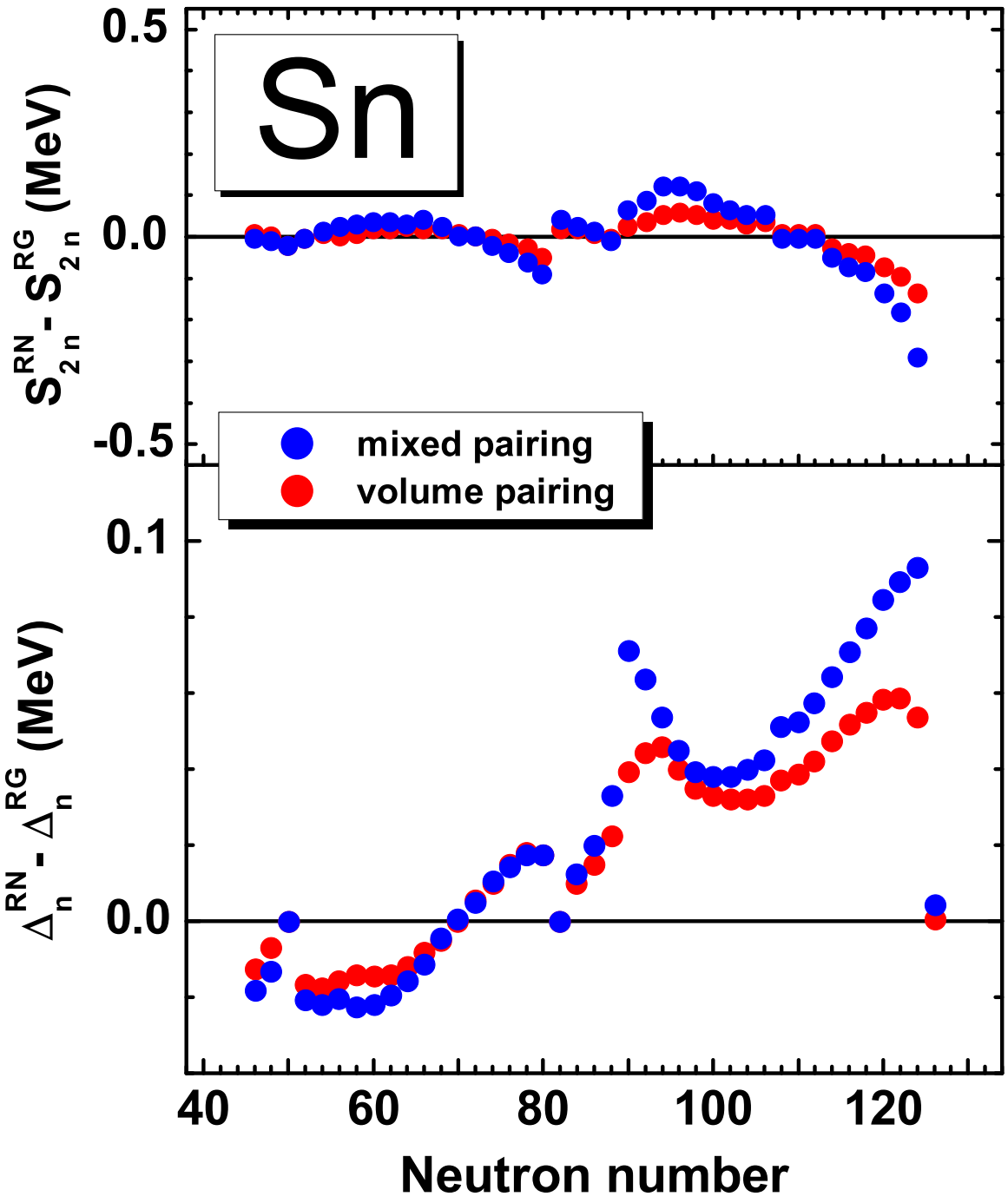

Figure 4.13: Differences between pairing renormalization (RN) and regularization (RG) procedures for two neutron separation energies (upper), and the average neutron gaps (lower). The HFB+THO calculations are performed for the chain of the spherical Sn isotopes using the SkP Skyrme parameterization.

both procedures give more similar results in the case of volume pairing than in the case of mixed pairing.

Recently, the pairing regularization procedure has been analyzed in the context of relativistic mean-field approximation [93]. In order to simulate the finite range contribution to the nuclear matter pairing gap coming from the Gogny pairing force, it was necessary to introduce strong density dependence in the pairing strength of the contact interaction.

Using the regularization procedure and calculating the Sn chain with both volume and newly constructed (surface) contact interaction, the authors of Ref. [93] have found differences in pairing energies of the order of 20 MeV in the neutron-rich nuclei around ^{148}Sn. In our work, for the same nuclei, the differences in pairing energies between volume and mixed pairing variants do not exceed 2.6 MeV. This comparison shows that the density-dependent contact interaction proposed in Ref. [93] is questionable for finite nuclei, despite its agreement with the finite-range Gogny pairing force in the infinite nuclear matter.

Deformed Nuclei

We applied the pairing renormalization and regularization procedures for the chain of deformed Dy isotopes. Differences between both sets of results are shown in Figs. 4.14 and 4.15. We show only the results with the mixed pairing since, as in the spherical nuclei, the differences between both procedures are larger.

As seen in Fig. 4.14, most of the nuclei considered are well deformed, and the deformations are practically the same within both procedures. Despite the fact that the maximum difference in the pairing energy is around 3 MeV (not shown), other quantities are very similar. The maximum difference in the total energy is about 360 keV, in the two-neutron separation energy – 160 keV, in the pairing gaps – 110 keV, and in the rms radii (not shown) – less than 0.005 fm.

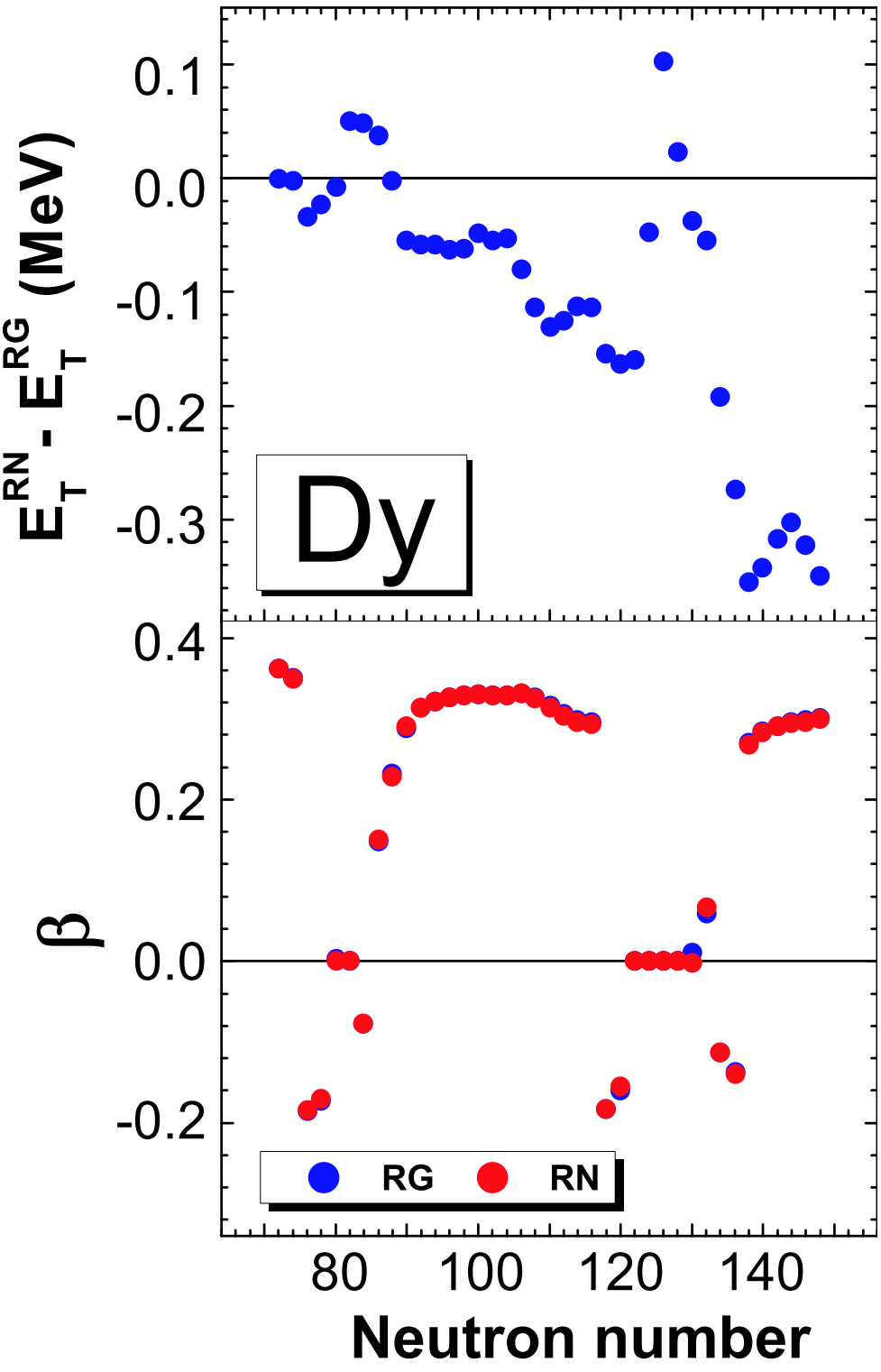

Figure 4.14: Differences between the pairing renormalization (RN) and regularization (RG) procedures for total energies (upper). Self-consistent deformations are plotted in the lower panel. The HFB+THO calculations are performed for the chain of the deformed Dy isotopes using the SkP Skyrme parameterization and the mixed pairing interaction.

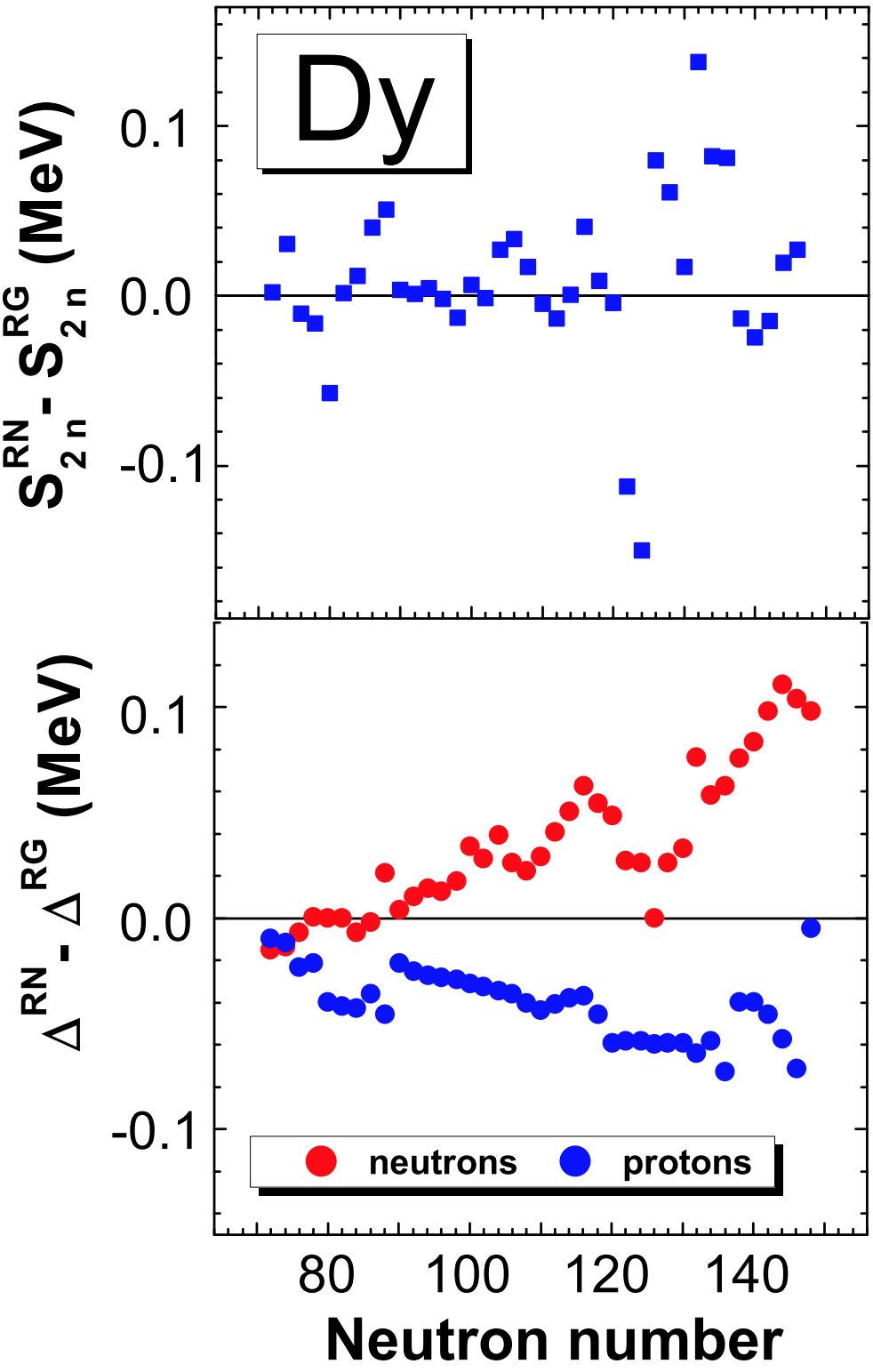

Figure 4.15: Similar to Fig. 4.14 except the two-neutron separation energies (upper) and average pairing gaps (lower) are plotted.

Chapter 5

The non-Unitarity of the Bogoliubov Transformation

Because an atomic nucleus is an open quantum system, the dimension of the single particle Hilbert space in the HFB framework is infinity. In actual calculations using a truncation scheme and discretization of single-particle continuum is necessary. The discretization is usually realized through either solving the HFB equations in a finite dimensional particle space (i.e. harmonic oscillator basis) or through appropriate boundary conditions in the coordinate space solution (i.e. Dirichlet or von Neumann boundary conditions at a certain box radius). Truncation is necessary due to the ultraviolet divergence of local densities discussed in chapter 4.

However, the application of these procedures implies different dimensions of particle and quasiparticle spaces and, therefore, makes the Bogoliubov transformation non-unitary. The unitarity of the Bogoliubov transformation leads to particle and abnormal densities that are Hermitian.

One can show that for the truncation of the quasiparticle space, there appears symmetric component in the pairing tensor κ. Following arguments of Dobaczewski *et al.* [111], we introduce matrix $\mathcal{P}$:

$$\mathcal{P} = \mathcal{A}\mathcal{A}^{\dagger} = \begin{bmatrix} P & Q \\ Q^{*} & P^{*} \end{bmatrix}, \tag{5.1}$$

where $\mathcal{A}$ is the Bogoliubov transformation matrix (see appendix B). Hermitian matrix P and symmetric matrix Q can be written in terms of Bogoliubov transformation matrices A and B as:

$$P = AA^{\dagger} + B^{*}B^{T}, \tag{5.2}$$

$$Q = AB^{\dagger} + B^{*}A^{T}. \tag{5.3}$$

For the complete Hilbert space, with no truncation procedure applied, the unitarity of the Bogoliubov transformation gives:

$$\mathcal{P} = 1. \tag{5.4}$$

On the other hand, as the truncation scheme is applied, one can show [111] that for M being the dimension of the particle space and $K \leq M$ - number of quasiparticle states in the

truncated space, there are k eigenstates of matrix P with corresponding eigenvalues $p_i = 1$, where

$$\max(0, 2K - M) \leq k \leq K. \tag{5.5}$$

The diagonalization also yields $M - 2K + k$ eigenstates of P corresponding to eigenvalue $p_i = 0$. Finally, there are $2(K - k)$ states with corresponding eigenvalues $0 < p_i < 1$, paired so that for every eigenvalue p_i there exists an eigenstate with corresponding eigenvalue $p_{\bar{i}} = 1 - p_i$. Diagonalization of the matrix Q gives $M - 2(K - k)$ eigenstates with corresponding eigenvalue $q_i = 0$. Eigenvalues for remaining $2(K - k)$ eigenstates are $0 < q_i < 1$, and may be related to relevant eigenvalues of P:

$$q_i = \sqrt{p_i\,(1 - p_i)}. \tag{5.6}$$

Since matrix Q can be written as:

$$Q = \kappa + \kappa^T, \tag{5.7}$$

the existence of the non-zero eigenvalues of Q means that the pairing tensor is no longer skew-symmetric, but it develops a symmetric component, which is equivalent to the development of the non-Hermitian component in the abnormal density $\tilde{\rho}$.

Figure 5.1 illustrates the maximum absolute value of matrix element of the non-Hermitian and Hermitian parts of the abnormal density

$$\frac{1}{2}\max\{|\tilde{\rho} \pm \tilde{\rho}^\dagger|\} \tag{5.8}$$

as functions of the cutoff energy $\epsilon_{\rm cut}$. One can see that for the cutoff energy of 50 MeV and above [71] used in HFB calculations in coordinate space, the former does not exceed 1% of the latter. Consequently, the dimension of the quasiparticle space that must be taken into account is much larger that is physically meaningful. Usually one simply disregards the non-Hermitian component in the abnormal density in the Skyrme-HFB calculations. However, such a non-zero component means that the state does not have Fermionic character.

The unitarity of the Bogoliubov transformation is also important, when calculating matrix elements of operators and overlaps between two different HFB states. This is necessary, for example, in GCM calculations leading to symmetry restoration and collective correlations (see i.e. Refs. [41, 112, 113]). However, this is difficult in the truncated space, because rectangular matrices cannot be inverted and for two different HFB states given by Bogoliubov transformations $\gamma = \mathcal{A}^\dagger c$, $\gamma' = \mathcal{A}'^\dagger c$, transformation $\gamma = \mathcal{A}^\dagger \mathcal{A}'^{\dagger\,-1}\gamma'$ is not well defined. On the other hand, for cutoff energy high enough, the occupation factor for quasiparticle states with corresponding equivalent energy above cutoff energy is small and, therefore, do not contribute significantly to either overlaps or matrix elements [112].

5.1 The Method of Restoration of the Unitarity of the Bogoliubov Transformation

In this work, we propose a method of restoring the unitarity of the Bogoliubov transformation, while keeping the number of quasiparticle states limited. Preliminary results of this project were presented in Ref. [98] and a more complete formal introduction to the method and results are in Ref. [111].

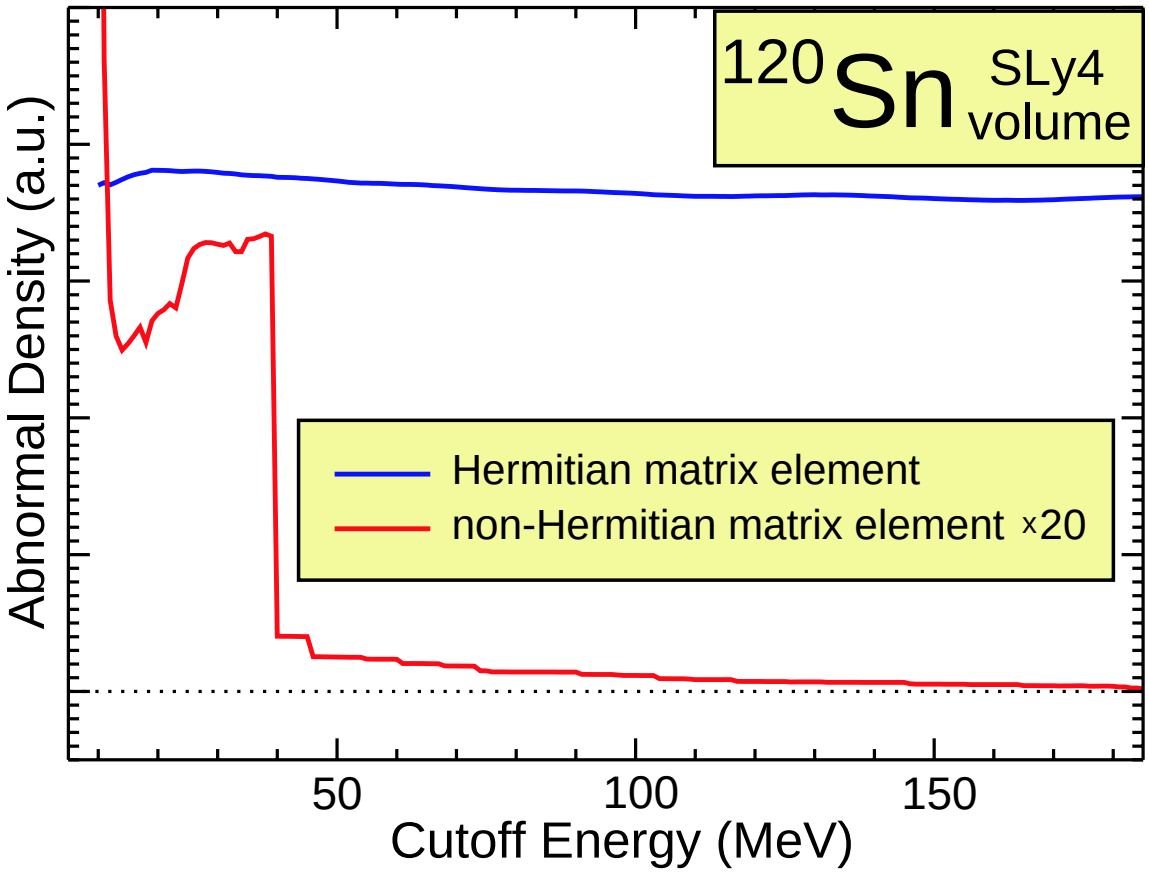

Figure 5.1: Maximum Hermitian and non-Hermitian component of the neutron abnormal density for ^{120}Sn as a function of the cutoff energy.

Our method ensures the Hermicity of the abnormal density and, at the same time, keeps the number of quasiparticle states limited. The approach is based on finding an optimal truncated particle space, dictated by a given quasiparticle truncation, in which the HFB equations are solved without any further cutoff. Full-space diagonalization of the HFB equations is necessary only to provide the aforementioned optimal basis. The proposed truncation scheme accommodates all the particle states that are needed within a given truncation of the quasiparticle space.

The Singular Value Decomposition (SVD) (see Appendix A) is an algebraic method which, by means of finding the so-called singular values, defines the new orthogonal singular basis, and orders its states according to their importance for decomposition of vectors in a rectangular matrix. In a M-dimensional space, the SVD of two sets of K orthogonal vectors, with one proportional to the other (i.e., BCS), gives K singular states corresponding to non-zero singular values. SVD of a set of $2K$ vectors, gives no more than $\min(2K, M)$ singular states corresponding to non-zero singular value. Moreover, since in the quasiparticle space canonical basis is usually defined as a basis spanned by eigenstates of the density matrix, which is quadratic in terms of the Bogoliubov matrix, φ_2, SVD provides a more precise

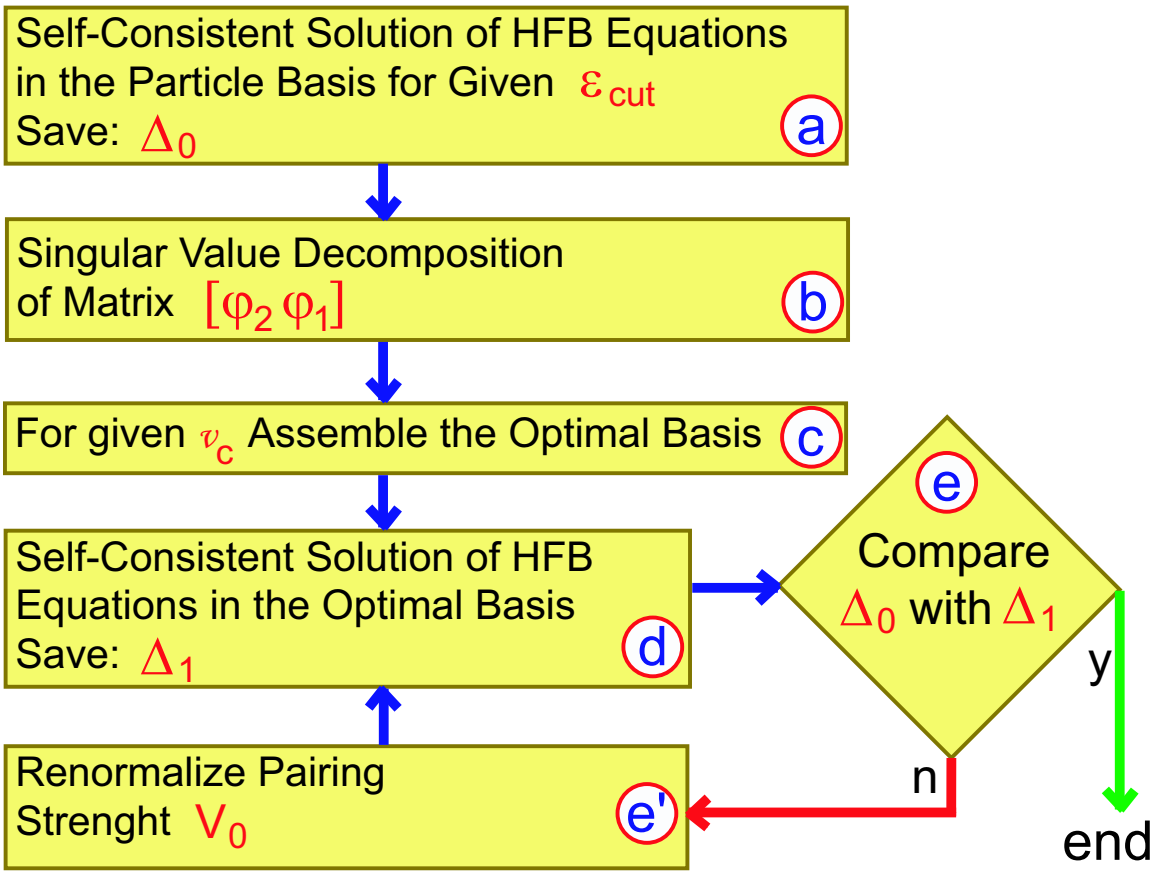

Figure 5.2: Diagram of the method used (explanation in the text).

method of determining canonical basis using quasiparticle wave functions.

We use SVD to decompose the combined matrix $[\varphi_2\varphi_1]$, where φ_2 and φ_1 are the rectangular Bogoliubov matrices corresponding to a non-unitary transformation, and assemble the optimal basis by taking only those particle states which have the corresponding singular values above a given SVD cutoff, v_c. Since for each value of the SVD cutoff the dimension of the resulting particle space is different, one has to readjust the pairing strength for any given value of v_c. We do it so that the pairing gap is the same in both steps: in the full-space solution obtained for a given energy cutoff and in the optimal basis solution.

Our calculations are carried out according to the following scheme (illustrated also in Fig. 5.2):

a. Self-consistent solution of the HFB equations in the full space for a given cutoff energy.

b. Singular Value Decomposition of the combined matrix $[\varphi_2\varphi_1]$ corresponding to the full-space solution.

c. Defining the optimal basis by keeping the SVD states with corresponding singular values above the SVD cutoff v_c.

d. Self-consistent solution of the HFB equations in the truncated particle space.

e. Fitting the pairing strength by repeating step d. with different pairing strengths, until the pairing gaps in the full and truncated spaces are equal.

5.2 Numerical Implementation and Results

By using the code HFBTHO [105], we performed the HFB calculations within the particle space of 20 harmonic oscillator shells, which leads to the single-particle energies of about 200 MeV.

Figure 5.3 illustrates the spectrum of singular values in the $\{\Omega\pi\} = \{1/2^+\}$ block, where Ω is a $z-$component of the angular momentum and π stands for parity, in a dripline nucleus ^{170}Sn for neutrons and protons. As ^{170}Sn is a magic nucleus, proton pairing is zero and every proton quasiparticle has either particle ($\varphi_{1i} = 0$) or hole ($\varphi_{2i} = 0$) character. Consequently, the number of non-zero vectors in the $[\varphi_2\varphi_1]$ matrix is equal to the number of quasiparticle states K. Moreover, due to the Fermionic commutation rules for quasiparticle operators, these vectors are orthonormal. Therefore, for magic nucleus there must be exactly K singular states with corresponding singular value $v_{i\leq K} = 1$ and for all remaining states $v_{i>K} = 0$, and this is illustrated in the lower panel of Fig. 5.3. The upper panel, on the other hand, shows the singular value spectrum for neutrons. One can clearly divide the spectrum into three regimes: almost K singular states with corresponding singular values $v_i \approx 1$, a few states with singular values $10^{-2} < v_i < 1$, and remaining singular states with corresponding singular values $v_i \leq 10^{-2}$.

The dependence of number of states in the optimal basis on the SVD cutoff is illustrated in Fig. 5.4. Similar to Fig. 5.3, the number of states in the optimal basis (solid) is very close to the dimension of the quasiparticle space for the given cutoff energy (dotted) for large values of the SVD cutoff and it increased with decreasing SVD cutoff.

Figure 5.5 illustrates the total HFB energy for the standard HFB method (stars) and modified method (curves) described above, for mixed (upper) and volume (lower) pairing. For $N_{sh} = 20$ the full single particle space corresponds to the highest equivalent energies below 200 MeV. Therefore, the highest cutoff energy results for both methods coincide. The importance of non-unitarity of the Bogoliubov transformation and cutoff schemes can be studied for lower cutoff energies. One can see that the optimal space method provides significant improvement of results for very low cutoff energy of $10 - 30$ MeV and results are closer to the full space solution for higher ϵ_{cut} as well. The increase in the total HFB energy for the standard method can be explained by the importance of states with significant occupation (especially high angular momentum states localized by the centrifugal barrier) with corresponding equivalent energy above ϵ_{cut} and the effects of the non-unitarity of the Bogoliubov transformation, since for such a low cutoff energy the non-Hermitian component of the abnormal density is large (see Fig. 5.1).

5.3 Pairing Regularization in the Truncated Space

As discussed above, pairing renormalization method is successful because it approximates a physically motivated pairing regularization approach. Using the two-step method introduced

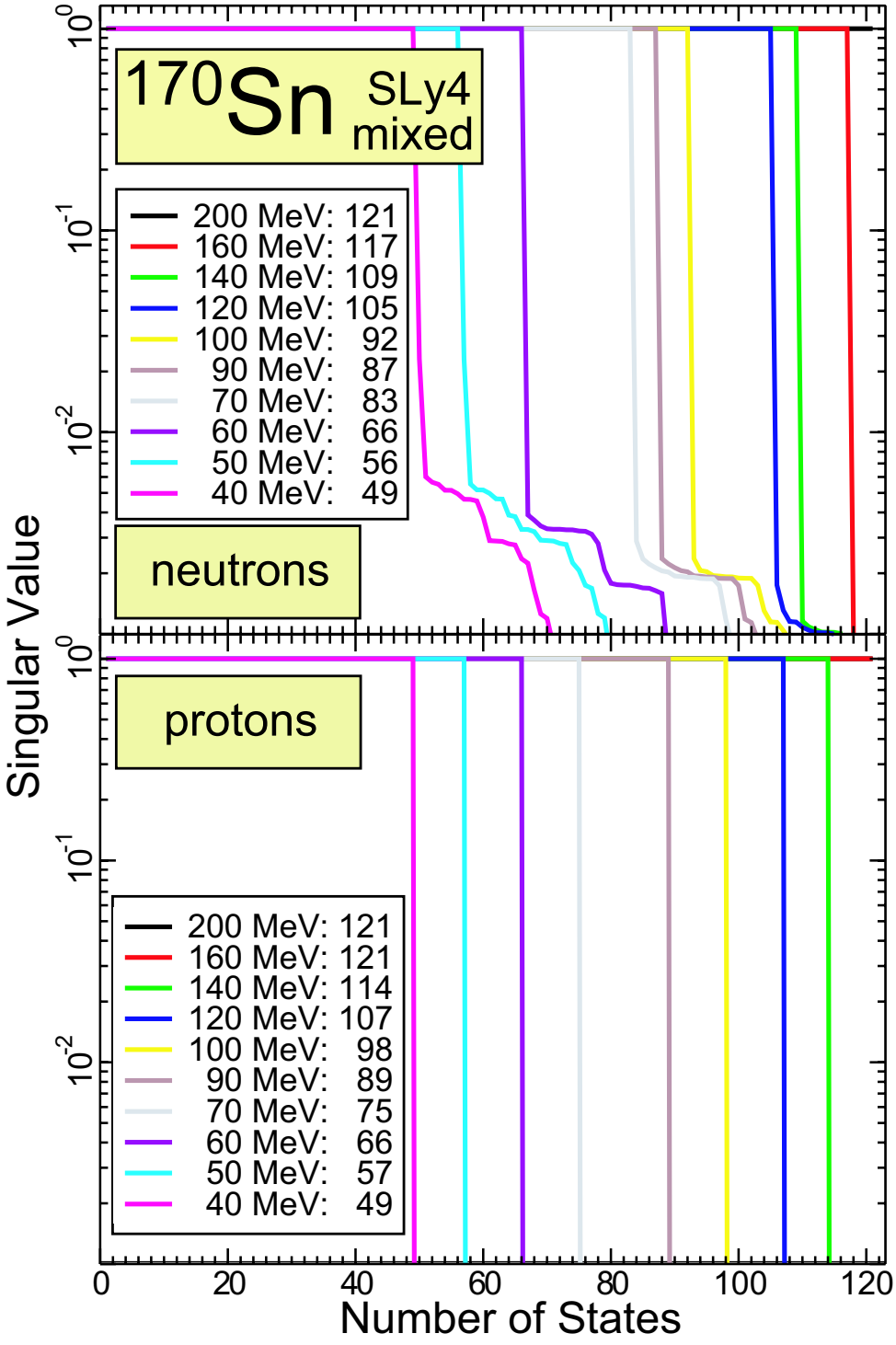

Figure 5.3: Singular values for a dripline nucleus ^{170}Sn neutrons (upper) and protons (lower) in the $\{\Omega\pi\} = \{1/2^+\}$ block for different values of cutoff energy. Numbers in the legend correspond to the dimension of the quasiparticle space for given cutoff energy. Calculations were performed using $N_{sh} = 20$ harmonic oscillator shells, SLy4 parameterization of the Skyrme functional and mixed pairing.

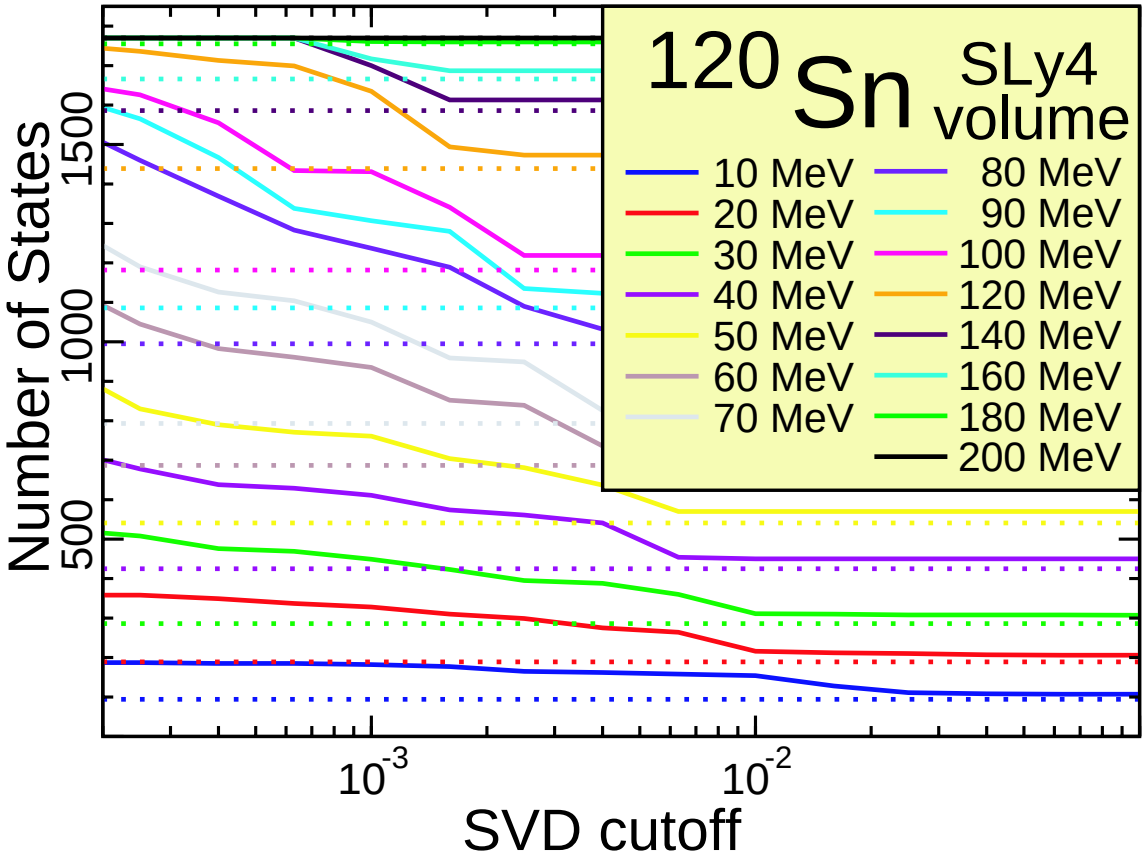

Figure 5.4: Number of states in the truncated basis as a function of the SVD cutoff for different cutoff energies. Dotted lined correspond to the dimension of the quasiparticle space in the standard HFB calculations for given cutoff energy. Calculations were performed using $N_{sh} = 20$ harmonic oscillator shells, SLy4 parameterization of the Skyrme functional and volume pairing.

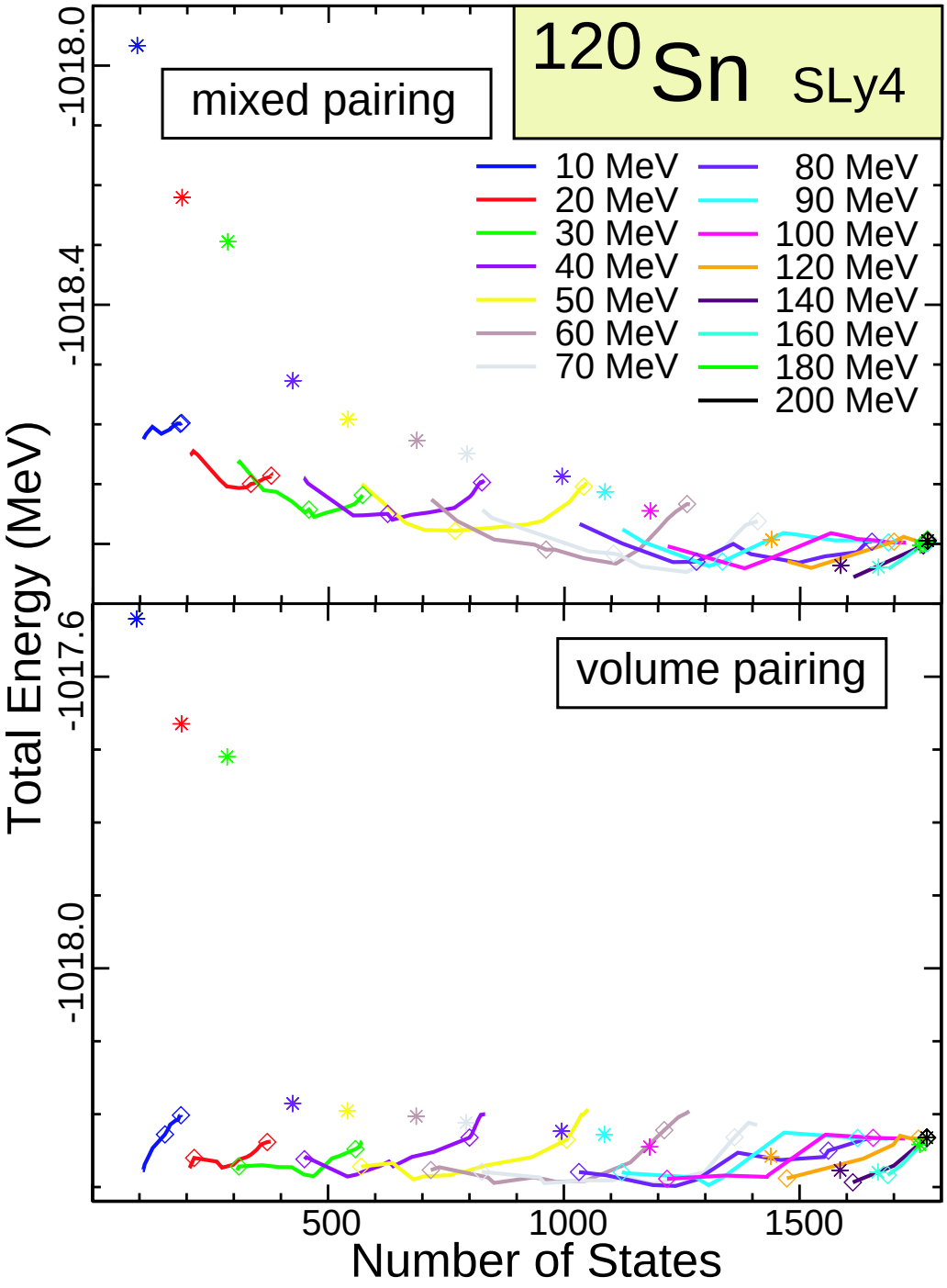

Figure 5.5: Total HFB energy for ^{120}Sn using the standard procedure (stars) and the two-step method for different values of the SVD cutoff (curves, diamonds correspond to $v_{\rm cut} = 10^{-3}$ and $v_{\rm cut} = 10^{-4}$) and different $\epsilon_{\rm cut}$. Calculations were performed using $N_{sh} = 20$ harmonic oscillator shells, SLy4 parameterization of the Skyrme functional and mixed (upper) and volume (lower) pairing.)

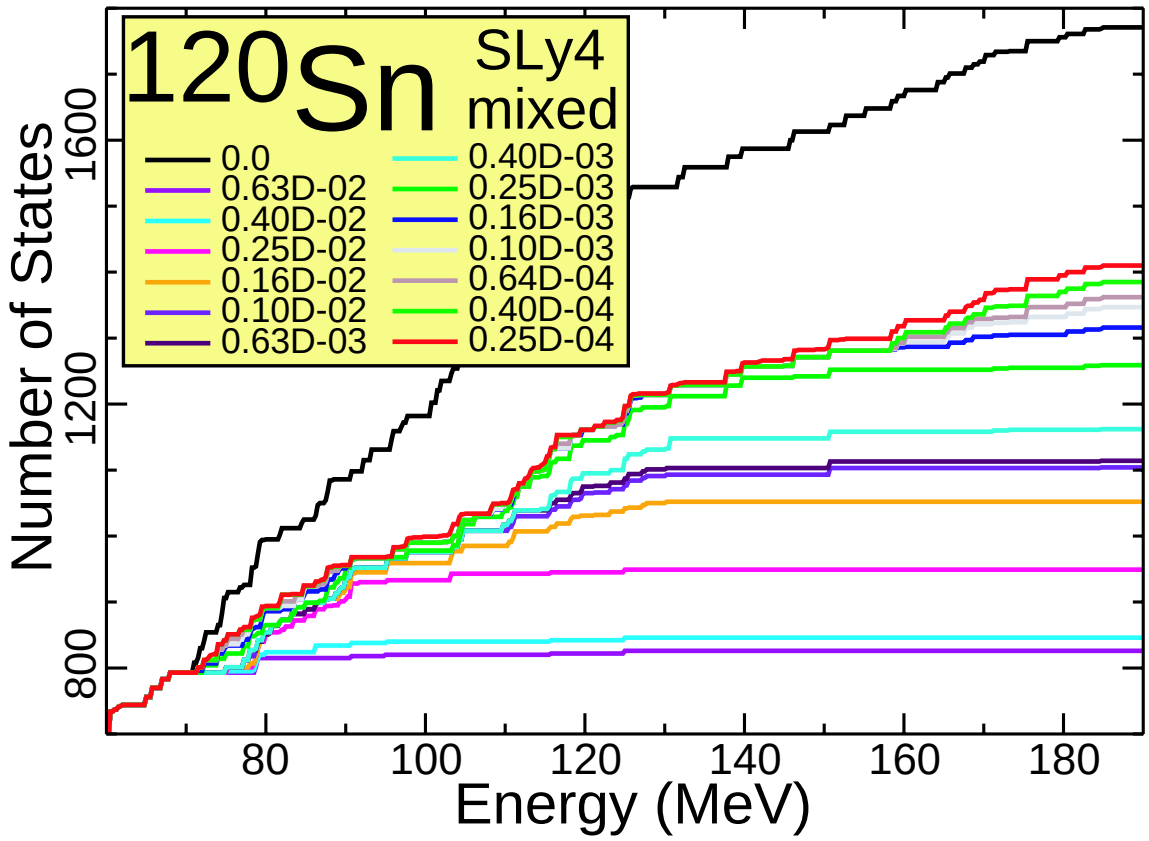

Figure 5.6: Number of states in the truncated basis as a function of the cutoff energy for as a function of the SVD cutoff. Calculations were performed using $N_{sh} = 20$ harmonic oscillator shells, SLy4 parameterization of the Skyrme functional and volume pairing.

in this work, we do not have the cutoff well defined in the second step of the method. This is illustrated in Fig. 5.6, where various values of the SVD cutoff give a practically identical density of states for equivalent energies below ϵ_{cut}, but for higher cutoff energy density of states strongly depends on v_c. Since the density of states does not correspond to any particular cutoff energy, these contributions are difficult to remove in a systematic fashion, and all results presented in this work are obtained using the pairing renormalization method. The necessity of repeating the second step several times in order to achieve the renormalized pairing functional, and the difficulties of applying more fundamental methods of removing the divergent component from densities, are major drawbacks of the presented method.

Chapter 6

Perspectives and Summary

6.1 Perspectives

The presence of quantum fluctuations, spontaneous symmetry breaking effects, and difficulties of including them in the nuclear DFT framework, make it necessary to improve results by evaluating the correlation and symmetry restoration effects implicitly using techniques like GCM, which are well defined in the Hamiltonian framework.

We investigate the importance of the ultraviolet divergence in local densities for the configuration mixing calculations and some of the preliminary results are illustrated in Fig. 6.1. As there is no Hamiltonian in the DFT approach, the path to evaluating the non-diagonal matrix elements of the Hamiltonian kernel (2.3) is uncertain.

In order to evaluate non-diagonal matrix elements of the Hamiltonian kernel (2.3), we use an ansatz [112] based on the Onishi formula for the matrix element of a many-body operator between two non-orthogonal product states [47]. Within this ansatz, Hamiltonian kernel is calculated as density functional of *transitional* or *mixed* densities:

$$\langle q|\hat{H}|q'\rangle = \langle q|q'\rangle \mathcal{H}[\rho^{10}_{qq'}, \tilde{\rho}^{10}_{qq'}, \tilde{\rho}^{01}_{qq'}], \tag{6.1}$$

where

$$\rho^{10}_{qq'}(\boldsymbol{r_2}\sigma_2, \boldsymbol{r_1}\sigma_1) = \frac{\langle q|a^\dagger_{\boldsymbol{r_1}\sigma_1} a_{\boldsymbol{r_2}\sigma_2}|q'\rangle}{\langle q|q'\rangle} \tag{6.2}$$

$$\tilde{\rho}^{10}_{qq'}(\boldsymbol{r_2}\sigma_2, \boldsymbol{r_1}\sigma_1) = \frac{-2\sigma_1\langle q|a_{\boldsymbol{r_1}-\sigma_1} a_{\boldsymbol{r_2}\sigma_2}|q'\rangle}{\langle q|q'\rangle} \tag{6.3}$$

$$\tilde{\rho}^{01}_{qq'}(\boldsymbol{r_2}\sigma_2, \boldsymbol{r_1}\sigma_1) = \frac{-2\sigma_1\langle q|a^\dagger_{\boldsymbol{r_1}-\sigma_1} a^\dagger_{\boldsymbol{r_2}\sigma_2}|q'\rangle}{\langle q|q'\rangle} \tag{6.4}$$

and $\mathcal{H}$ is the nuclear EDF. However, the choice of transitional densities to be used in GCM calculations is not unique and for discussion see, i.e. Ref. [114].

The HFB wave functions are not eigenfunctions of the particle number operator and correspond only to its proper mean value. Consequently, in order for the GCM collective wave function to correspond to the proper particle number, one has to either project HFB wave functions on the proper particle number or solve the Hill-Wheeler equation with an

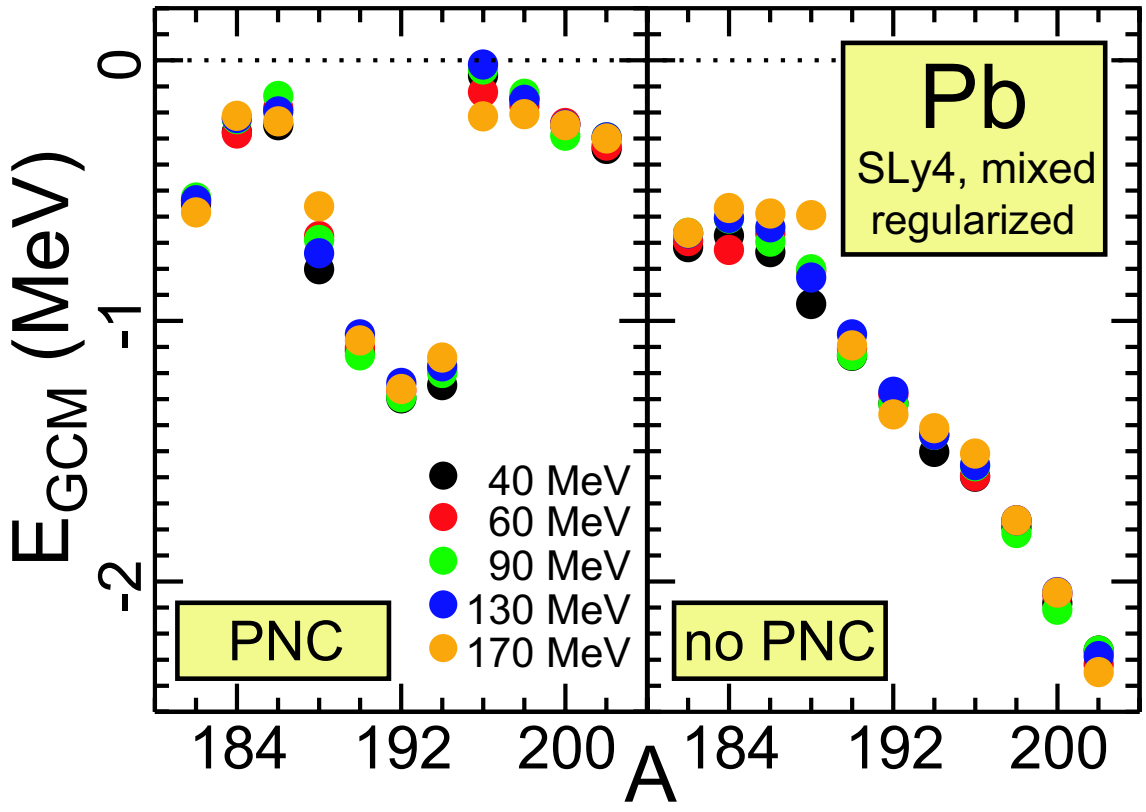

Figure 6.1: Preliminary results: GCM correction energy resulting from configuration mixing of β-deformed HFB states, with $\Delta\beta = 0.075$, for Pb isotopes with (left panel) and without (right panel) particle number constrain used in GCM calculations for various values of the cutoff energy.

additional constrain on the particle number [112]:

$$\sum_{q'} \left[\mathbb{H}_{qq'} - \lambda \mathbb{N}_{qq'}\right] f_{q'} = E_q \sum_{q'} \mathbb{I}_{qq'} f_{q'}, \tag{6.5}$$

where

$$\mathbb{N}_{qq'} = \mathrm{Tr}\langle q|\hat{\rho}|q'\rangle. \tag{6.6}$$

In this work we adopt the former procedure. The importance of keeping the proper mean value of particles (emphasized in Ref. [112]) is illustrated in Fig. 6.1. One can see that without a particle number constrain imposed, the GCM correction energy is much larger than a state for which the constrain is imposed. Moreover, the GCM energy weakly depends on the cutoff, even though the pairing regularization procedure is well-defined in the DFT framework and does not regularize transitional densities. On the other hand, the Hamiltonian kernel (6.1) is calculated as a product of the EDF for transitional densities and the overlap between states. The overlap is sharply peaked for diagonal matrix elements and

becomes negligibly small before the 'regularized' transitional densities significantly depend on the cutoff energy.

However, in order to be able to explain low-energy properties of atomic nuclei within the DFT approach, there are some concerns to be answered first:

- How to construct effective nuclear EDF in the systematic manner? How to constrain its parameters by underlying fundamental theory?
- How to incorporate self-binding effects in the Density Functional Theory?
- What are formal limitations of calculating matrix elements of physical operators in DFT?
- Under what formal approximations and assumptions the low-lying excited states can be calculated within the Density Functional Theory?

These are very important challenges of modern low-energy nuclear structure and we plan to continue our research pursuing them.

6.2 Conclusions and Summary

In this work, we investigated consequences of the energy cutoff in Skyrme-HFB calculations. We concentrated on two aspects of this procedure:

- Ultraviolet divergence in local densities appearing due to the contact character of the effective interaction.
- Non-unitarity of the Bogoliubov transformation in the truncated space.

We analyzed the ultraviolet divergence that appears in various local densities and introduced the regularization scheme, which allows the divergent components to be removed. We showed that for the pairing component of the energy density functional, $\mathcal{H}_{pair} = g\tilde{\rho}^2$, our scheme is equivalent the regularization method introduced earlier by Bulgac *et al.* by regularization of the gap equation. Moreover, we checked our scheme for the model case, $\mathcal{H}_{pair} = g\tilde{\rho}$, and found that it provides results independent of the cutoff energy. The introduced method can be also applied to more involved forms of the pairing ED, such as the abnormal kinetic density dependent terms. In examples, we analyzed numerically the regularization of densities render regularization of mean fields. This is no longer the case for a general ED, so this problem requires further investigation.

Furthermore, we performed numerical investigation of the pairing regularization method and found it to be very suitable for a description of spherical and deformed nuclei. We checked the stability of the method with respect to the cutoff energy and found fluctuations in the total energy below 200 keV. Fluctuations coming from the method itself do not exceed 50 keV for cutoff energies as low as 30 MeV. However, if a still lower cutoff energy is assumed, the Thomas-Fermi approximation to the s.p. Green's function may no longer be valid.

We found that the differences between pairing renormalization and regularization procedures for volume and mixed pairing are rather small. Therefore, physical conclusions previously obtained within the pairing renormalization scheme remain valid. Nevertheless,

we believe that the theoretical motivation and simplicity of the regularization method is preferred to a phenomenological renormalization scheme.

We found that the non-unitarity of the Bogoliubov transformation due to the truncation of the quasiparticle space was one the major reasons for the increase of the total energy for Skyrme-HFB calculations in the coordinate space for low cutoff energy. We proposed a new, two-step method of solving HFB equations in the coordinate space, which ensures the unitarity of the Bogoliubov transformation in the second step. This method can be applied for cutoff energies as low as 20 MeV, in contrast to the minimum of about $\epsilon_{\rm cut} \approx 60\,{\rm MeV}$ in the standard approach. Due to the reduction of the dimension of the quasiparticle space one can speed up the calculation, which is a crucial issue in coordinate mixing calculations employing GCM method. However, in the second step of our method, the cutoff energy concept is not applicable and in order to remove the ultraviolet divergences from local densities one has to employ the renormalization scheme. Formulating the pairing regularization scheme for this method requires further investigations.

Bibliography

Bibliography

[1] *RIA Theory Blue Book*, http://www.orau.org/ria/RIATG/Blue_Book_FINAL.pdf

[2] *The science of the Rare Isotope Accelerator (RIA)*, http://www.orau.org/ria/pdf/RIAFINAL.pdf

[3] M. Lacombe, B. Loiseau, J.M. Richard, R. Vinh Mau, J. Côté, P. Pirés, and R. de Tourreil, Phys. Rev. C **21**, 861 (1980)

[4] R. Machleidt, K. Holinde, and C. Elster, Phys. Rep. **149**, 1 (1987)

[5] V.G. Stoks, R.A. Klomp, C.P. Terheggen, and J.J. de Swar, Phys. Rev. C **49**, 2950 (1994)

[6] C. Ordóñez, L. Ray, and U. van Kolck, Phys. Rev. Lett. **72**, 1982 (1994)

[7] R.B. Wiringa, V.G. Stoks, and R. Schiavilla, Phys. Rev. C **51**, 38 (1995)

[8] R. Machleidt, F. Sammarruca, and Y. Song, Phys. Rev. C **53**, 1483 (1996)

[9] D.R. Entem and R. Machleidt, Phys. Lett. B **524**, 93 (2001)

[10] S.K. Bogner, T.T.S. Kuo, A. Schwenk, D.R. Entem, and R. Machleidt, Phys. Lett. B **576**, 265 (2001)

[11] S.K. Bogner, T.T.S. Kuo, and A. Schwenk, Phys. Rep. **386**, 1 (2003)

[12] P. Navrátil, J.P. Vary, and B.R. Barrett, Phys. Rev. C **62**, 054311 (2000)

[13] P. Navrátil and W.E. Ormand, Phys. Rev. C **68**, 034305 (2003)

[14] C. Forssén, P. Navrátil, W.E. Ormand, and E. Caurier, Phys. Rev. C **71**, 044312 (2005)

[15] S.C. Pieper, R.B. Wiringa, and J. Carlson, Phys. Rev. C **70**, 054325 (2004)

[16] M. Mayer, Phys. Rev. **75**, 1969 (1949)

[17] O. Axel, J.H.D. Jensen, and H.E. Sues, Phys. Rev. **75**, 1766 (1949)

[18] J.P. Elliott and A.M. Lane, *Handbuch der Physik* volume XXXIX. Springer-Verlag, Berlin (1957)

[19] M. Honma, T. Mizusaki, and T. Otsuka, Phys. Rev. Lett. **75**, 1284 (1995)

[20] E. Caurier, G. Martínez-Pinedo, F. Nowacki, A. Poves, and A.P. Zuker, Rev. Mod. Phys **77**, 427 (2004)

[21] C. Lanczos, J. Res. Nat. Bur. Stand. **45**, 252 (1950)

[22] S.R. White, Phys. Rev. Lett. **69**, 2863 (1992)

[23] S.R. White, Phys. Rev. B **48**, 10345 (1993)

[24] T. Papenbrock and D.J. Dean, Phys. Rev. C **67**, 051303(R) (2003)

[25] T. Papenbrock and D.J. Dean, J. Phys. G **31**, S1377 (2005)

[26] S. Koonin, D. Dean, and K. Langanke, Phys. Rep. **278**, 2 (1997)

[27] P.E. Hodgson, Rev. Mod. Phys **34**, 765 (1971)

[28] W.D. Myers and W.J. Swiatecki, Annu. Rev. Nucl. Part. Sci. **32**, 309 (1982)

[29] P. Möller, J.R. Nix, and K.-L. Kratz, At. Data Nucl. Data Tables **66**, 131 (1997)

[30] P. Hohenberg and W. Kohn, Phys. Rev. **136**, B864 (1964)

[31] W. Kohn and L.J. Sham, Phys. Rev. **140**, A1133 (1965)

[32] N.N. Bogoliubov, Sov. Phys. Usp. **2**, 236 (1959)

[33] P.G. de Gennes, *Superconductivity of Metals and Alloys*. Benjamin, New York (1966)

[34] D.L. Hill and J.A. Wheeler, Phys. Rev. **89**, 1102 (1953)

[35] J.J. Griffin and J.A. Wheeler, Phys. Rev. **108**, 311 (1957)

[36] D.M. Brink and A. Weiguny, Nucl. Phys. A **120**, 59 (1968)

[37] F. Villars, Annu. Rev. Nucl. Sci. **7**, 185 (1957)

[38] A. Kamlah, Z. Phys. **216**, 52 (1968)

[39] P.-G. Reinhard, Z. Phys. A **285**, 93 (1978)

[40] P.-G. Reinhard, Nucl. Phys. A **252**, 120 (1975)

[41] M. Bender, G.F. Bertsch, and P.-H. Heenen, Phys. Rev. C **73**, 034322 (2006)

[42] J.L. Egido and P. Ring, Nucl. Phys. A **383**, 189 (1982)

[43] J.A. Sheikh and P. Ring, Nucl. Phys. A **665**, 71 (2000)

[44] J.A. Sheikh, P. Ring, E. Lopes, and R. Rossignoli, Phys. Rev. C **66**, 044318 (2002)

[45] M.V. Stoitsov, J. Dobaczewski, R. Kirchner, W. Nazarewicz, and J. Terasaki, *to be published*

[46] T. Duguet, *to be published*

[47] P. Ring and P. Schuck, *The Nuclear Many-Body Problem.* Springer-Verlag, New York (1980)

[48] S. Marcos, H. Flocard, and P.-H. Heenen, Nucl. Phys. A **410**, 125 (1983)

[49] S. Marcos, H. Flocard, and P.-H. Heenen, Phys. Lett. B **134**, 287 (1984)

[50] I.Zh. Petkov and M.V Stoitsov, *Nuclear Density Functional Theory.* Clarendon Press, Oxford (1991)

[51] C. Speicher, E. Endel, and R.M. Dreizler, Nucl. Phys. A **562**, 569 (1993)

[52] M. Bender, P.-H. Heenen, and P.-G. Reinhard, Rev. Mod. Phys **75**, 121 (2003)

[53] *Extended Density Functionals in Nuclear Structure Physics*, ed. by G.A. Lalazissis, P. Ring, and D. Vretenar (Springer Verlag, 2004).

[54] T.H.R. Skyrme, Phil. Mag. **1**, 1043 (1956)

[55] T.H.R. Skyrme, Nucl. Phys. **9**, 615 (1959)

[56] T.H.R. Skyrme, Nucl. Phys. **9**, 635 (1959)

[57] D. Vauterin and D.M Brink, Phys. Rev. C **5**, 626 (1972)

[58] D. Vauterin, Phys. Rev. C **7**, 296 (1973)

[59] M. Beiner, H. Flocard, Nguyen Van Giai, and P. Quentin, Nucl. Phys. A **238**, 29 (1975)

[60] H. Krivine, J. Treiner, and O. Bohigas, Nucl. Phys. A **336**, 155 (1980)

[61] J. Dobaczewski, H. Flocard, and J. Treiner, Nucl. Phys. A **422**, 103 (1984)

[62] E. Chabanat, P. Bonche, P. Haensel, J. Meyer, and F. Schaeffer, Nucl. Phys. A **635**, 231 (1998)

[63] J.W. Negele and D. Vautherin, Phys. Rev. C **5**, 1472 (1972)

[64] J.W. Negele and D. Vautherin, Phys. Rev. C **11**, 1031 (1975)

[65] K. Huang and C.N. Yang, Phys. Rev. **105**, 767 (1957)

[66] T.D. Lee and C.N. Yang, Phys. Rev. **105**, 1119 (1957)

[67] M.Ya. Amusia and V.N. Efimov, Ann. of Phys. **47**, 377 (1968)

[68] H.-W. Hammer and R.J. Furnstahl, Nucl. Phys. A **678**, 277 (2000)

[69] R.J. Furnstahl and H.-W. Hammer, Ann. of Phys. **302**, 206 (2002)

[70] S.J. Puglia, A. Bhattacharyya, and R.J. Furnstahl, Nucl. Phys. A **723**, 145 (2003)

[71] J. Dobaczewski, W. Nazarewicz, T.R. Werner, J.F. Berger, C.R. Chinn, and J. Dechargé, Phys. Rev. C **53**, 2809 (1996)

[72] J. Bardeen, L.N. Cooper, and J.R. Schrieffer, Phys. Rev. **108**, 1175 (1957)

[73] J. Dechargé and D. Gogny, Phys. Rev. C **21**, 1568 (1980)

[74] R.R. Chasman, Phys. Rev. C **14**, 1935 (1976)

[75] F. Tondeur, Nucl. Phys. A **315**, 353 (1979)

[76] J. Dobaczewski, W. Nazarewicz, and P.-G. Reinhard, Nucl. Phys. A **693**, 361 (2001)

[77] F. Barranco, R.A. Broglia, G. Gori, E. Vigezzi, P.F. Bortignon, and J. Terasaki, Phys. Rev. Lett. **83**, 2147 (1999)

[78] N. Giovanardi, F. Barranco, R.A. Broglia, and E. Vigezzi, Phys. Rev. C **65**, 041304 (2002)

[79] M. Samyn, S. Goriely, P.-H. Heenen, J.M. Pearson, and F. Tondeur, Nucl. Phys. A **700**, 142 (2002)

[80] S. Goriely, M. Samyn, P.-H. Heenen, J.M. Pearson, and F. Tondeur, Phys. Rev. C **66**, 024326–1 (2002)

[81] Y.M. Engel, D.M. Brink, K. Goeke, S.J. Krieger, and D. Vautherin, Nucl. Phys. A **249**, 215 (1975)

[82] D.J. Dean and M. Hjorth-Jensen, Rev. Mod. Phys **75**, 607 (2003)

[83] H. Esbensen, G.F. Bertsch, and K. Hencken, Phys. Rev. C **56**, 3054 (1997)

[84] T. Papenbrock and G.F. Bertsch, Phys. Rev. C **59**, 2052 (1999)

[85] A. Bulgac, nucl-th/9907088

[86] A. Bulgac and Y. Yu, nucl-th/0109083

[87] A. Bulgac and Y. Yu, Phys. Rev. Lett. **88**, 042504 (2002)

[88] A. Bulgac, Phys. Rev. C **65**, 051305(R) (2002)

[89] Y. Yu and A. Bulgac, Phys. Rev. Lett. **90**, 222501 (2003)

[90] A. Bulgac and Y. Yu, Int. J. Mod. Phys. E **13**, 147 (2004)

[91] T. Duguet, Phys. Rev. C **69**, 054317 (2004)

[92] T. Duguet, K. Bennaceur, and P. Bonche, nucl-th/0508054

[93] T. Nikšić, P. Ring, and D. Vretenar, Phys. Rev. C **71**, 044320 (2005)

[94] P.J. Borycki, J. Dobaczewski, W. Nazarewicz, and M.V. Stoitsov, Phys. Rev. C **73**, 044319 (2006)

[95] G. Bruun, Y. Castin, R. Dum, and K. Burnett, Eur. Phys. J. D **7**, 433 (1999)

[96] M. Grasso and M. Urban, Phys. Rev. A **68**, 033610 (2003)

[97] N. Tajima, Phys. Rev. C **69**, 034305 (2004)

[98] J. Dobaczewski, P.J. Borycki, W. Nazarewicz, and M.V. Stoitsov, Eur. Phys. J. A **25, s01**, 541 (2005)

[99] P.J. Borycki, W. Nazarewicz, and M.V. Stoitsov, *to be published*

[100] K.T. Hecht and A. Adler, Nucl. Phys. A **137**, 129 (1969)

[101] A. Arima, M. Harvey, and K. Shimizu, Phys. Lett. **30B**, 517 (1969)

[102] P.J. Borycki, J. Ginocchio, W. Nazarewicz, and M.V. Stoitsov, Phys. Rev. C **68**, 014304 (2003)

[103] J. Dobaczewski, W. Nazarewicz, and M.V. Stoitsov, Eur. Phys. J. A **15**, 21 (2002)

[104] K. Bennaceur and J. Dobaczewski, Comput. Phys. Commun. **168**, 96 (2005)

[105] M.V. Stoitsov, J. Dobaczewski, W. Nazarewicz, and P. Ring, Comput. Phys. Commun. **167**, 43 (2005)

[106] W. Satuła, P.-G., D. Dean, J. Gary, S. Mizutori, and W. Nazarewicz, Phys. Lett. B **407**, 103 (1997)

[107] S. Takahara, N. Onishi, and N. Tajima, Phys. Lett. B **331**, 261 (1994)

[108] E. Perlińska, S.G. Rohozinski, J. Dobaczewski, and W. Nazarewicz, Phys. Rev. C **69**, 014316 (2004)

[109] L.H. Thomas, Proc. Camb. Phil. Soc. **23**, 542 (1927)

[110] E. Fermi, Z. Phys. **48**, 73 (1928)

[111] J. Dobaczewski, P.J. Borycki, W. Nazarewicz, and M.V. Stoitsov, *to be published*

[112] P. Bonche, J. Dobaczewski, H. Flocard, P.-H. Heenen, and J. Meyer, Nucl. Phys. A **510**, 466 (1990)

[113] P.-G. Reinhard and K. Goeke, Rep. Prog. Phys. **50**, 1 (1987)

[114] T. Duguet and P. Bonche, Phys. Rev. C **67**, 054308 (2003)

[115] C. Bloch and A. Messiah, Nucl. Phys. **39**, 95 (1962)

[116] G.C. Wick, Phys. Rev. **80**, 268 (1950)

[117] J. Dobaczewski, *Teoria Układów Jądrowych, to be published*

[118] H.J. Lipkin, Ann. of Phys. **9**, 272 (1960)

Appendices

Appendix A

Matrix Properties

Lemma A.0.1 *For any given matrices A, B, and C*

$$Tr\{A[B,C]\} = Tr\{B[C,A]\} = Tr\{C[A,B]\} \tag{A.1}$$

Theorem A.0.1 (Bloch-Messiah Theorem [47, 115]) *Any unitary matrix, $\mathcal{A}$, of the form*

$$\mathcal{A} = \begin{pmatrix} A & B^* \\ B & A^* \end{pmatrix}, \tag{A.2}$$

can be factorized into three matrices:

$$\mathcal{A} = \begin{pmatrix} D & 0 \\ 0 & D^* \end{pmatrix} \begin{pmatrix} \bar{U} & \bar{V} \\ \bar{V} & \bar{U} \end{pmatrix} \begin{pmatrix} C & 0 \\ 0 & C^* \end{pmatrix}, \tag{A.3}$$

where C, D are unitary and $\bar{U}, \bar{V}$ are real matrices of the form:

$$\bar{U} = \begin{pmatrix} \mathbf{0} & \mathbf{0} & \mathbf{0} \\ \mathbf{0} & \boldsymbol{u_i} & \mathbf{0} \\ \mathbf{0} & \mathbf{0} & \mathbf{1} \end{pmatrix} \tag{A.4}$$

$$\bar{V} = \begin{pmatrix} \mathbf{1} & \mathbf{0} & \mathbf{0} \\ \mathbf{0} & \boldsymbol{v_i} & \mathbf{0} \\ \mathbf{0} & \mathbf{0} & \mathbf{0} \end{pmatrix}, \tag{A.5}$$

and:

$$\boldsymbol{u_i} = \begin{pmatrix} u_i & 0 \\ 0 & u_i \end{pmatrix} \qquad \boldsymbol{v_i} = \begin{pmatrix} 0 & v_i \\ -v_i & 0 \end{pmatrix}. \tag{A.6}$$

Theorem A.0.2 (Singular Value Decomposition) *Every rectangular $M \times N$ matrix A can be factorized:*

$$A = U\Sigma V^T, \tag{A.7}$$

where U is $M \times M$ orthogonal matrix, V is $N \times N$ orthogonal matrix, and Σ is $M \times N$ diagonal matrix:

$$\Sigma_{ij} = s_i \delta_{ij}.$$

Values s_i are positively defined and are called singular values.

Appendix B

HFB Equations

B.1 Product States

Definition B.1.1 (Product state) *Product state is a many-body state, for which contractions of particle creation and annihilation operators are C-numbers.*

Theorem B.1.1 (Wick's Theorem [116]) *If contractions between each pair of operators $C(c_i, c_j)$ in a product are C-numbers, the matrix element value,*

$$\frac{\langle\psi_1|\prod_i c_i|\psi_2\rangle}{\langle\psi_1|\psi_2\rangle}, \tag{B.1}$$

where

$$\boldsymbol{c} = \begin{bmatrix} \boldsymbol{a} \\ \boldsymbol{a}^\dagger \end{bmatrix} \tag{B.2}$$

and $a, a^\dagger$ are particle creation and annihilation operators, respectively, is equal to a sum over all permutations of contractions and self-contractions of operators.

Lemma B.1.1 (Generalized Density Matrix) *The generalized density matrix is a $2M$-dimensional matrix of the expectation values of the generalized density operator*

$$\hat{\mathcal{R}} = C(c^\dagger, c). \tag{B.3}$$

For a product state $|\psi\rangle$

$$\mathcal{R} = C(c^\dagger, c) = \begin{bmatrix} \rho & \kappa \\ -\kappa^* & 1-\rho^* \end{bmatrix}, \tag{B.4}$$

where ρ is the one-body density matrix

$$\rho = \langle\psi|\hat{\rho}|\psi\rangle = \langle\psi|a^\dagger a|\psi\rangle^T \tag{B.5}$$

and κ is the pairing tensor

$$\kappa = \langle\psi|\hat{\kappa}|\psi\rangle = \langle\psi|aa|\psi\rangle^T. \tag{B.6}$$

The density matrix is Hermitian and the pairing tensor is skew-symmetric. The generalized density matrix is projective and Hermitian.

Theorem B.1.2 *Every product state may be written as a vacuum for a set of quasiparticle operators, which are linear combination of particle creation and annihilation operators.*

Definition B.1.2 (Bogoliubov Transformation) *A unitary transformation between particle space and quasiparticle space is called the Bogoliubov transformation*

$$\gamma = \mathcal{A}^\dagger c, \tag{B.7}$$

where

$$\mathcal{A} = \begin{bmatrix} A & B^* \\ B & A^* \end{bmatrix}. \tag{B.8}$$

In terms of Bogoliubov transformation matrices A and B the density matrix and the pairing tensor are

$$\rho = B^* B^T \tag{B.9}$$
$$\kappa = B^* A^T. \tag{B.10}$$

Unitarity of the Bogoliubov transformation gives:

$$A^\dagger A + B^\dagger B = 1 \tag{B.11}$$
$$A^\dagger B^* + B^\dagger A^* = 0 \tag{B.12}$$
$$A A^\dagger + B^* B^T = 1 \tag{B.13}$$
$$A B^\dagger + B^* A^T = 0. \tag{B.14}$$

B.2 Time Reversal Symmetry

Definition B.2.1 (Time Reversal Operator) *The time reversal operator, $\hat{T}$, is the operator defines by its effect on coordinate, momentum, and angular momentum operators:*

$$\hat{T}\hat{\boldsymbol{r}}\hat{T}^\dagger = \hat{\boldsymbol{r}} \tag{B.15}$$
$$\hat{T}\hat{\boldsymbol{p}}\hat{T}^\dagger = -\hat{\boldsymbol{p}} \tag{B.16}$$
$$\hat{T}\hat{\boldsymbol{L}}\hat{T}^\dagger = -\hat{\boldsymbol{L}}. \tag{B.17}$$

Lemma B.2.1 *The time reversal operator for particles with spin is given by expression:*

$$\hat{T} = \exp\left(-i\pi \hat{S}_y/\hbar\right)\hat{K}, \tag{B.18}$$

where $\hat{S}_y$ is y component of the spin operator and $\hat{K}$ is complex conjugation operator in coordinate representation.

The generalized density matrix transforms under the time reversal transformation:

$$\mathcal{R}^t = \langle\psi|\hat{T}\hat{\mathcal{R}}\hat{T}^\dagger|\psi\rangle = \mathcal{U}_t \mathcal{R}^* \mathcal{U}_t^\dagger, \tag{B.19}$$

where in the doubled dimension

$$\mathcal{U}_t = \begin{bmatrix} U_t & 0 \\ 0 & U_t^* \end{bmatrix}. \tag{B.20}$$

As a consequence, under the time reversal transformation the upper and the lower component of the generalized density transform differently. However, one can redefine the generalized density, so that both components transform according to the same tranformation under the time reversal symmetry:

$$\tilde{\mathcal{R}} = \mathcal{W}\mathcal{R}\mathcal{W}^{\dagger}, \tag{B.21}$$

where

$$\mathcal{W} = \begin{bmatrix} 1 & 0 \\ 0 & U_t \end{bmatrix}. \tag{B.22}$$

Definition B.2.2 (Abnormal Density) *The abnormal density is given by expression:*

$$\tilde{\rho} = \langle\psi|\hat{\tilde{\rho}}|\psi\rangle = \langle\psi|\hat{T}a\hat{T}^{\dagger}a|\psi\rangle^{T}. \tag{B.23}$$

In terms of the paring tensor it can be written as:

$$\tilde{\rho} = \kappa U_t^{\dagger}. \tag{B.24}$$

In this new representation the generalized density matrix can be written as

$$\tilde{\mathcal{R}} = \begin{bmatrix} \rho & \tilde{\rho} \\ \tilde{\rho}^{\dagger} & 1-\rho^{t} \end{bmatrix}, \tag{B.25}$$

where $\tilde{\rho}$ is called the abnormal density.

For the Hermitian generalized density matrix, $\mathcal{R}$, the generalized density matrix, $\tilde{\mathcal{R}}$, (B.21) and the abnormal density must be also Hermitian.

Bogoliubov transformation matrix, $\tilde{\mathcal{A}}$, in this new representation reads

$$\tilde{\mathcal{A}} = \begin{bmatrix} \varphi_1 & \varphi_2 \\ \varphi_2 & -\varphi_1 \end{bmatrix}, \tag{B.26}$$

where matrices φ_1, φ_2 are

$$\varphi_1 = B^{*} \tag{B.27}$$

$$\varphi_2 = U_t^{T} A^{*}. \tag{B.28}$$

B.3 Hartree-Fock-Bogoliubov Equations

Consider EDF

$$E = \mathrm{Tr}\left\{\mathcal{H}[\mathcal{R}]\right\}, \tag{B.29}$$

where $\mathcal{H}$ is a functional of the generalized density matrix $\mathcal{R}$.

Variation of E yields

$$\delta E = \frac{1}{2}\mathrm{Tr}\left\{\frac{\partial\mathcal{H}[\mathcal{R}]}{\partial\mathcal{R}^{T}}\delta\mathcal{R}\right\}. \tag{B.30}$$

Since the generalized density matrix is projective (Lemma B.1.1), one can write:

$$\delta E = \frac{1}{2}\mathrm{Tr}\left\{\frac{\partial\mathcal{H}[\mathcal{R}]}{\partial\mathcal{R}^{T}}\left[[\delta\mathcal{R},\mathcal{R}],\mathcal{R}\right]\right\}, \tag{B.31}$$

and Lemma A.0.1 gives:

$$\delta E = \frac{1}{2}\mathrm{Tr}\left\{[\delta\mathcal{R},\mathcal{R}]\left[\frac{\partial\mathcal{H}[\mathcal{R}]}{\partial\mathcal{R}^T},\mathcal{R}\right]\right\}. \tag{B.32}$$

Since the variation of the generalized density matrix is arbitrary, the condition of energy minimum results with Hartree-Fock-Bogoliubov (HFB) equations [32, 47, 117]

$$\left[\frac{\partial\mathcal{H}[\mathcal{R}]}{\partial\mathcal{R}^T},\mathcal{R}\right] = 0. \tag{B.33}$$

As a consequence, the generalized density matrix and the single particle HFB Hamiltonian,

$$H[\mathcal{R}] = \frac{\partial\mathcal{H}[\mathcal{R}]}{\partial\mathcal{R}^T}, \tag{B.34}$$

can be diagonalized simultanously.

However, as discussed above, a product state that is described by the generalized density matrix with non-vanishing pairing tensor does not belong to a single subspace $\mathscr{H}_N$ of the Fock space. Therefore, variational minimalization of energy would result in a product state corresponding to the highest binding energy, rather than a minimum energy state corresponding to a given number of particles. In order to constrain the number of particles in the system, minimization of Routhian,

$$E_\mu[\mathcal{R}] = \mathrm{Tr}\left\{\mathcal{H}[\mathcal{R}]\right\} - \mu N[\mathcal{R}], \tag{B.35}$$

where

$$N[\mathcal{R}] = \mathrm{Tr}\left\{\rho\right\}, \tag{B.36}$$

is in order. Consequently, HFB equations [32, 47, 117] read

$$[H_\mu[\mathcal{R}],\mathcal{R}] = 0, \tag{B.37}$$

where

$$H_\mu[\mathcal{R}] = \frac{\partial}{\partial\mathcal{R}^T}\left\{\mathcal{H}[\mathcal{R}] - \mu\rho\right\}. \tag{B.38}$$

Using the $\{A,B\}$ representation, the HFB equations in matrix form can be written as:

$$\begin{bmatrix} h_\mu & \Delta \\ -\Delta^* & -h_\mu^* \end{bmatrix}\begin{bmatrix} B_i^* \\ A_i^* \end{bmatrix} = E_i\begin{bmatrix} B_i^* \\ A_i^* \end{bmatrix}, \tag{B.39}$$

where E_i is quasiparticle energy and

$$h_\mu = h - \mu = \frac{\partial}{\partial\rho^T}\mathcal{H} - \mu \tag{B.40}$$

$$\Delta = \frac{\partial}{\partial\kappa^T}\mathcal{H}. \tag{B.41}$$

On the other hand, using the $\{\varphi_1,\varphi_2\}$ representation, the HFB equations are [61]:

$$\begin{bmatrix} h_\mu & \tilde{h} \\ \tilde{h} & -h_\mu \end{bmatrix}\begin{bmatrix} \varphi_{1i} \\ \varphi_{2i} \end{bmatrix} = E_i\begin{bmatrix} \varphi_{1i} \\ \varphi_{2i} \end{bmatrix}, \tag{B.42}$$

where

$$\tilde{h} \;=\; \frac{\partial}{\partial \tilde{\rho}^T}\mathcal{H}. \tag{B.43}$$

Variational minimization of Ruthian (B.35) results in a state with a given mean value of particles, $\langle\psi|\hat{N}|\psi\rangle = N$. However, this is still not an eigenstate of the particle number operator and since atomic nuclei are few body systems, even a small component of the wave function belonging to $\mathscr{H}_{N'}$, so that $N' \neq N$ may significantly change the result. Therefore, different particle number projection techniques are being used and developed [43, 44, 118].

Appendix C

Pairing Regularization

C.1 Ultraviolet Divergence in Local Densities

By multiplying HFB equations (4.4) by vector $[\varphi^*_{2i}, -\varphi^*_{1i}]$, integrating over coordinates and summing over all positive energy HFB solutions, one obtains:

$$\begin{aligned}
&\sum_{i>0,\sigma_1} E_i \int d^3\boldsymbol{r_1} \left[\ \varphi^*_{2i}(\boldsymbol{r_1}\sigma_1),\quad -\varphi^*_{1i}(\boldsymbol{r_1}\sigma_1)\ \right] \left[\begin{array}{c} \varphi_{1i}(\boldsymbol{r_1}\sigma_1) \\ \varphi_{2i}(\boldsymbol{r_1}\sigma_1) \end{array}\right] = \\
&\quad = \sum_{i>0,\sigma_1\sigma_2} \iint d^3\boldsymbol{r_1} d^3\boldsymbol{r_2} \left[\ \varphi^*_{2i}(\boldsymbol{r_2}\sigma_2),\quad -\varphi^*_{1i}(\boldsymbol{r_2}\sigma_2)\ \right] \times \\
&\quad \times \left[\begin{array}{cc} h_\mu(\boldsymbol{r_2}\sigma_2, \boldsymbol{r_1}\sigma_1) & \tilde{h}(\boldsymbol{r_2}\sigma_2, \boldsymbol{r_1}\sigma_1) \\ \tilde{h}(\boldsymbol{r_2}\sigma_2, \boldsymbol{r_1}\sigma_1) & -h_\mu(\boldsymbol{r_2}\sigma_2, \boldsymbol{r_1}\sigma_1) \end{array}\right] \left[\begin{array}{c} \varphi_{1i}(\boldsymbol{r_1}\sigma_1) \\ \varphi_{2i}(\boldsymbol{r_1}\sigma_1) \end{array}\right], \qquad \text{(C.1)} \\
&\sum_{i>0,\sigma_1} E_i \int d^3\boldsymbol{r_1} \left\{\varphi^*_{2i}(\boldsymbol{r_1}\sigma_1)\varphi_{1i}(\boldsymbol{r_1}\sigma_1) - \varphi^*_{1i}(\boldsymbol{r_1}\sigma_1)\varphi_{2i}(\boldsymbol{r_1}\sigma_1)\right\} = \\
&\quad = \sum_{i>0,\sigma_1\sigma_2} \iint d^3\boldsymbol{r_1} d^3\boldsymbol{r_2} \Big\{ \varphi^*_{2i}(\boldsymbol{r_2}\sigma_2) h_\mu(\boldsymbol{r_2}\sigma_2, \boldsymbol{r_1}\sigma_1)\varphi_{1i}(\boldsymbol{r_1}\sigma_1) + \\
&\quad + \varphi^*_{2i}(\boldsymbol{r_2}\sigma_2)\tilde{h}(\boldsymbol{r_2}\sigma_2, \boldsymbol{r_1}\sigma_1)\varphi_{2i}(\boldsymbol{r_1}\sigma_1) + \varphi^*_{1i}(\boldsymbol{r_2}\sigma_2) h_\mu(\boldsymbol{r_2}\sigma_2, \boldsymbol{r_1}\sigma_1)\varphi_{2i}(\boldsymbol{r_1}\sigma_1) - \\
&\quad - \varphi^*_{1i}(\boldsymbol{r_2}\sigma_2)\tilde{h}(\boldsymbol{r_2}\sigma_2, \boldsymbol{r_1}\sigma_1)\varphi_{1i}(\boldsymbol{r_1}\sigma_1) \Big\}. \qquad \text{(C.2)}
\end{aligned}$$

Since for every HFB solution $([\varphi_{1i}, \varphi_{2i}], E_i)$ there exists also a coupled orthogonal solution $([\varphi_{2i}, -\varphi_{1i}], -E_i)$, the left side of Eq. (C.2) vanishes as a sum over products of orthogonal vectors.

Due to the energy cutoff applied, the completeness relation is not satisfied. One has to introduce function $\mathcal{F}_{\epsilon_{\rm cut}}$

$$\sum_{\epsilon<\epsilon_{\rm cut}, i>0} [\varphi_{1i}(\boldsymbol{r_2}\sigma_2)\varphi^*_{1i}(\boldsymbol{r_1}\sigma_1) + \varphi_{2i}(\boldsymbol{r_2}\sigma_2)\varphi^*_{2i}(\boldsymbol{r_1}\sigma_1)] = \mathcal{F}_{\epsilon_{\rm cut}}(\boldsymbol{r_2}\sigma_2, \boldsymbol{r_1}\sigma_1), \qquad \text{(C.3)}$$

where

$$\lim_{\epsilon_{\rm cut}\to\infty} \mathcal{F}_{\epsilon_{\rm cut}}(\boldsymbol{r_2}\sigma_2, \boldsymbol{r_1}\sigma_1) = \delta(\boldsymbol{r_2} - \boldsymbol{r_1})\delta_{\sigma_2\sigma_1}. \qquad \text{(C.4)}$$

For a local spin-independent EDF

$$\mathcal{F}_{\epsilon_{\rm cut}}(\boldsymbol{r_2}\sigma_2,\boldsymbol{r_1}\sigma_1)=\mathcal{F}_{\epsilon_{\rm cut}}(\boldsymbol{r_2},\boldsymbol{r_1})\delta_{\sigma_2\sigma_1}. \tag{C.5}$$

Using completeness relation (C.3) and the definition of the abnormal density, one obtains:

$$\begin{aligned}
0 &= \int d^3\boldsymbol{r_1}d^3\boldsymbol{r_2}\delta(\boldsymbol{r_2}-\boldsymbol{r_1})\Bigg[\left(\tilde{B}(\boldsymbol{r_2})\boldsymbol{\nabla}_{\boldsymbol{r_2}}\boldsymbol{\nabla}_{\boldsymbol{r_1}}+\tilde{U}(\boldsymbol{r_2})\right)\left[\mathcal{F}_{\epsilon_{\rm cut}}(\boldsymbol{r_2},\boldsymbol{r_1})-\rho(\boldsymbol{r_2},\boldsymbol{r_1})\right]+\\
&\quad+\left(B(\boldsymbol{r_2})\boldsymbol{\nabla}_{\boldsymbol{r_2}}\boldsymbol{\nabla}_{\boldsymbol{r_1}}+U(\boldsymbol{r_2})-\mu\right)\left[\tilde{\rho}_r(\boldsymbol{r_2},\boldsymbol{r_1})-F_{\tilde{\rho}}(\boldsymbol{r_2},\boldsymbol{r_1})\right]\Bigg]=\\
&= \int d^3\boldsymbol{r}d^3\boldsymbol{x}\delta(\boldsymbol{x})\Bigg\{\left[\tilde{B}(\boldsymbol{r})\left(\frac{1}{4}\nabla^2_{\boldsymbol{r}}-\nabla^2_{\boldsymbol{x}}\right)+\tilde{U}(\boldsymbol{r})\right]\left[\mathcal{F}_{\epsilon_{\rm cut}}(\boldsymbol{r},\boldsymbol{x})-\rho(\boldsymbol{r},\boldsymbol{x})\right]+\\
&\quad+\left[B(\boldsymbol{r})\left(\frac{1}{4}\nabla^2_{\boldsymbol{r}}-\nabla^2_{\boldsymbol{x}}\right)+U(\boldsymbol{r})-\mu\right]\left[\tilde{\rho}_r(\boldsymbol{r},\boldsymbol{x})-F_{\tilde{\rho}}(\boldsymbol{r},\boldsymbol{x})\right]\Bigg\},
\end{aligned} \tag{C.6}$$

where

$$\boldsymbol{r} = \frac{\boldsymbol{r_1}+\boldsymbol{r_2}}{2}, \tag{C.7}$$

$$\boldsymbol{x} = \boldsymbol{r_2}-\boldsymbol{r_1}, \tag{C.8}$$

and

$$\rho(\boldsymbol{r_2},\boldsymbol{r_1}) = \sum_\sigma \rho(\boldsymbol{r_2}\sigma,\boldsymbol{r_1}\sigma), \tag{C.9}$$

$$\tilde{\rho}(\boldsymbol{r_2},\boldsymbol{r_1}) = \sum_\sigma \tilde{\rho}(\boldsymbol{r_2}\sigma,\boldsymbol{r_1}\sigma), \tag{C.10}$$

and the notation used is

$$F(\boldsymbol{r},\boldsymbol{x}) := F(\boldsymbol{r_1},\boldsymbol{r_2}). \tag{C.11}$$

In Eq. (C.6) the completeness function, $\mathcal{F}_{\epsilon_{\rm cut}}$, gives divergence in integral over $\boldsymbol{x}$ with an increase of the cutoff energy (see Eq. (C.4)). Therefore, at $\boldsymbol{x}=0$:

$$\begin{aligned}
&\left[\tilde{B}(\boldsymbol{r})\left(\frac{1}{4}\nabla^2_{\boldsymbol{r}}-\nabla^2_{\boldsymbol{x}}\right)+\tilde{U}(\boldsymbol{r})\right]\left[\mathcal{F}_{\epsilon_{\rm cut}}(\boldsymbol{r},\boldsymbol{x})-\rho(\boldsymbol{r},\boldsymbol{x})\right]\Big|_{\boldsymbol{x}=0}=\\
&=-\left[B(\boldsymbol{r})\left(\frac{1}{4}\nabla^2_{\boldsymbol{r}}-\nabla^2_{\boldsymbol{x}}\right)+U(\boldsymbol{r})-\mu\right]\tilde{\rho}(\boldsymbol{r},\boldsymbol{x})\Big|_{\boldsymbol{x}=0}.
\end{aligned} \tag{C.12}$$

C.2 Rearrangement Terms

Applying chain rule:

$$\frac{\delta}{\delta\rho}g_{eff} = \frac{\partial g_{eff}}{\partial U}\frac{\delta U}{\delta\rho}+\frac{\partial g_{eff}}{\partial M^*}\frac{\delta M^*}{\delta\rho}+\frac{\partial g_{eff}}{\partial g}\frac{\delta g}{\delta\rho}. \tag{C.13}$$

The derivatives in Eq. (C.13) are given by:

$$\frac{\partial g_{eff}}{\partial g} = \left(\frac{g_{eff}}{g}\right)^2, \tag{C.14}$$

$$\frac{\delta g}{\delta \rho} = -V_0 \beta \gamma \frac{\rho^{\beta-1}}{\rho_0^\beta}, \tag{C.15}$$

$$\frac{\partial g_{eff}^{(i)}}{\partial M^*} = g_{eff}^{(i)2} \frac{3}{4\pi^2\hbar^2} \left(k_{\rm cut} + |k_F| \arctan \frac{|k_F|}{k_{\rm cut}}\right), \tag{C.16}$$

$$\frac{\partial g_{eff}^{(r)}}{\partial M^*} = g_{eff}^{(r)2} \frac{3}{4\pi^2\hbar^2} \left(k_{\rm cut} - \frac{k_F}{2} \ln \frac{k_{\rm cut}+k_F}{k_{\rm cut}-k_F}\right), \tag{C.17}$$

$$\frac{\partial g_{eff}^{(i)}}{\partial U} = g_{eff}^{(i)2} \frac{M^{*2}}{2\pi^2\hbar^4} \frac{1}{|k_F|} \arctan \frac{|k_F|}{k_{\rm cut}}, \tag{C.18}$$

$$\frac{\partial g_{eff}^{(r)}}{\partial U} = g_{eff}^{(r)2} \frac{M^{*2}}{4\pi^2\hbar^4} \frac{1}{k_F} \ln \frac{k_{\rm cut}+k_F}{k_{\rm cut}-k_F}. \tag{C.19}$$

The variation of U and m, assuming the variation of rearrangement term to be small, is:

$$\frac{\delta U}{\delta \rho} = \frac{3t_0}{2}(1+x_0) + \frac{t_3}{12}\rho^\alpha \left((1+\frac{x_3}{2})(\alpha+2)(\alpha+1) - \right.$$
$$\left. - (x_3+\frac{1}{2}) \left(\frac{\alpha(\alpha-1)}{\rho^2}\sum_q \rho_q^2 + \frac{4\alpha}{\rho}\rho_q + 2\right)\right) - \frac{1}{2}\left(\frac{g_{eff}}{g}\right)^2 \gamma\beta(\beta-1)\frac{\rho^{\beta-2}}{\rho_0^\beta}\sum_q \tilde{\rho}_q^2, \tag{C.20}$$

$$\frac{\delta M^*}{\delta \rho} = -\frac{M^{*2}}{4\hbar^2}\left(t_1(1-x_1) + 3t_2(1+x_2)\right). \tag{C.21}$$

Finally, the rearangement terms are:

$$\begin{aligned}
\delta^{(i)}U = {} & g_{eff}^{(i)2}\left[-\frac{3}{4\pi^2\hbar^2}\left(k_{\rm cut} + |k_F|\arctan\frac{|k_F|}{k_{\rm cut}}\right)\frac{M^{*2}}{4\hbar^2}\left(t_1(1-x_1)+3t_2(1+x_2)\right) - \right. \\
& - \frac{M^{*2}}{2\pi^2\hbar^4}\frac{1}{|k_F|}\arctan\frac{|k_F|}{k_{\rm cut}}\left\{\frac{3t_0}{2}(1+x_0) + \frac{t_3}{12}\rho^\alpha\left[(1+\frac{x_3}{2})(\alpha+2)(\alpha+1) - \right.\right. \\
& - \left.\left.(x_3+\frac{1}{2})\left(\frac{\alpha(\alpha-1)}{\rho^2}\sum_q\rho_q^2 + \frac{4\alpha}{\rho}\rho_q + 2\right)\right] - \right. \\
& \left. - \frac{1}{2}\left(\frac{g_{eff}^{(i)}}{g}\right)^2\gamma\beta(\beta-1)\frac{\rho^{\beta-2}}{\rho_0^\beta}\sum_q\tilde{\rho}_q^2\right\} - V_0\,\gamma\beta\frac{\rho^{\beta-1}}{\rho_0^\beta g^2}\Bigg]\frac{1}{2}\sum_q\tilde{\rho}_q^2,
\end{aligned} \tag{C.22}$$

$$
\begin{aligned}
\delta^{(r)}U &= g_{eff}^{(r)2}\left[-\frac{3}{4\pi^2\hbar^2}\left(k_{\rm cut}-\frac{k_F}{2}\ln\frac{k_{\rm cut}+k_F}{k_{\rm cut}-k_F}\right)\frac{M^{*2}}{4\hbar^2}\left(t_1(1-x_1)+3t_2(1+x_2)\right)+\right.\\
&+ \frac{M^{*2}}{4\pi^2\hbar^4}\frac{1}{k_F}\ln\frac{k_{\rm cut}+k_F}{k_{\rm cut}-k_F}\left\{\frac{3t_0}{2}(1+x_0)+\frac{t_3}{12}\rho^\alpha\left[(1+\frac{x_3}{2})(\alpha+2)(\alpha+1)-\right.\right.\\
&- \left.\left.(x_3+\frac{1}{2})\left(\frac{\alpha(\alpha-1)}{\rho^2}\sum_q\rho_q^2+\frac{4\alpha}{\rho}\rho_q+2\right)\right]-\right.\\
&- \left.\frac{1}{2}\left(\frac{g_{eff}^{(r)}}{g}\right)^2\gamma\beta(\beta-1)\frac{\rho^{\beta-2}}{\rho_0^\beta}\sum_q\tilde{\rho}_q^2\right\}-V_0\gamma\beta\frac{\rho^{\beta-1}}{\rho_0^\beta g^2}\left]\frac{1}{2}\sum_q\tilde{\rho}_q^2.\right. \qquad \text{(C.23)}
\end{aligned}
$$

Vita

Piotr Jerzy Borycki was born a very beautiful and promising child on April 8, 1978 in Warsaw, Poland. He quickly proved to be among the most lively and bright in daycare, then kindergarten and schools. As his incompetency in humanities became apparent in high school, he eagerly got interested in science, by taking part and winning or reaching final level in regional and Polish national competitions for high school students in the areas of mathematics, physics, chemistry, and technical knowledge. His passion continued during studies of physics in years 1996-2001 at the Warsaw University of Technology, where he received his MS degree after five years of scientific and Polish Ministry of National Education scholarships. He collaborated there with his scientific advisor, Prof. Witold Nazarewicz, and was the coauthor of four journal articles and numerous conference presentations. In August 2001 he joined the Department of Physics and Astronomy at the University of Tennessee. In December 2006 he received the degree of Doctor of Philosophy with a major in Physics.